

2

NAVAL POSTGRADUATE SCHOOL

Monterey, California

AD-A205 696



THESIS

FLOWFIELD MEASUREMENTS IN THE VORTEX WAKE OF A
MISSILE AT HIGH ANGLE OF ATTACK IN TURBULENCE

by

Lung, Ming-Hung

December 1988

Advisor:

Richard M. Howard

Approved for public release; distribution is unlimited.

DTIC
ELECTE
MAR 28 1989
S a H D

89 3 27 003

Unclassified

Security Classification of this page

REPORT DOCUMENTATION PAGE

1a Report Security Classification Unclassified		1b Restrictive Markings	
2a Security Classification Authority		3 Distribution Availability of Report Approved for public release; distribution is unlimited.	
2b Declassification/Downgrading Schedule		5 Monitoring Organization Report Number(s)	
4 Performing Organization Report Number(s)		7a Name of Monitoring Organization Naval Postgraduate School	
6a Name of Performing Organization Naval Postgraduate School	6b Office Symbol (If Applicable) Code 67	7b Address (city, state, and ZIP code) Monterey, CA 93943-5000	
6c Address (city, state, and ZIP code) Monterey, CA 93943-5000		9 Procurement Instrument Identification Number	
8a Name of Funding/Sponsoring Organization	8b Office Symbol (If Applicable)	10 Source of Funding Numbers	
8c Address (city, state, and ZIP code)		Program Element Number	Project No
		Task No	Work Unit Accession No
11 Title (Include Security Classification) Flowfield Measurements in the Vortex Wake of a Missile at High Angle of Attack in Turbulence.			
12 Personal Author(s) Lung, Ming-Hung			
13a Type of Report Master's Thesis	13b Time Covered From To	14 Date of Report (year, month, day) December 1988	15 Page Count 143
16 Supplementary Notation			
17 Cosati Codes		18 Subject Terms (continue on reverse if necessary and identify by block number)	
Field	Group	Vortex Asymmetry, Turbulence, Vortex, High Angle of Attack, Missile, Vertical Launch	
	Subgroup		
19 Abstract (continue on reverse if necessary and identify by block number)			
<p>The flowfield downstream of a vertically-launched surface-to-air missile model at an angle of attack of 50° and a Reynolds number of 1.1×10^5 was investigated in a wind tunnel of the Naval Postgraduate School. The goal of this thesis is to experimentally validate the pressure measurement system for flowfield variables with elevated levels of turbulence; to determine the location and intensity of the asymmetric vortices in the wake of the VLSAM model at a raised level of freestream turbulence; and to display the asymmetric vortices by velocity mapping and pressure contours. The purpose is to correlate the results with the force measurements of Rabang to provide a greater understanding of the vortex flowfield.</p> <p>The body-only configuration was tested. Two flowfield conditions were treated: the nominal ambient wind tunnel condition, and a condition with grid-generated turbulence of 3.8% turbulence intensity and a dissipation length scale of 1.7 inches. The following conclusions were reached: 1) The relative strengths of the asymmetric vortices can be noted by the sharp spike shape in the ambient condition; this condition becomes diffused and becomes fatter in the turbulent condition; 2) The right side vortex has greater strength than the left side one as seen by the diffusion in the total pressure coefficient and static pressure coefficient contours with and without a turbulent condition; 3) an increase in turbulence intensity tends to reduce the strength of the asymmetric nose-generated vortices and pushes the two asymmetric vortices closer together; 4) and crossflow velocities were examined and were found to indicate the behavior denoted by the pressure contours.</p>			
20 Distribution/Availability of Abstract		21 Abstract Security Classification	
<input checked="" type="checkbox"/> unclassified/unlimited <input type="checkbox"/> same as report <input type="checkbox"/> DTIC users		Unclassified	
22a Name of Responsible Individual Richard M. Howard		22b Telephone (Include Area code) (408) 646-2870	22c Office Symbol Code 67HO

DD FORM 1473, 84 MAR

83 APR edition may be used until exhausted

Security Classification of this page

All other editions are obsolete

Unclassified

Approved for public release; distribution is unlimited.

Flowfield Measurements in the Vortex Wake of a Missile
at High Angle of Attack in Turbulence

by

Lung, Ming-Hung
Lieutenant, Republic of China Navy
B.S., Chinese Naval Academy, 1984

Submitted in partial fulfillment of the requirements for
the degree of

MASTER OF SCIENCE IN ENGINEERING SCIENCE

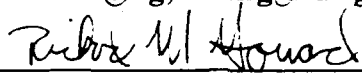
from the

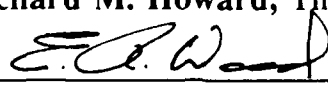
NAVAL POSTGRADUATE SCHOOL
December 1988

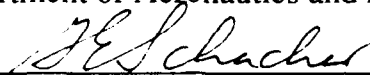
Author:


Lung, Ming-Hung

Approved by:


Richard M. Howard, Thesis Advisor


E. R. Wood, Chairman
Department of Aeronautics and Astronautics


Gordon E. Schacher,
Dean of Science and Engineering

ABSTRACT

The flowfield downstream of a vertically-launched surface-to-air missile model at an angle of attack of 50° and a Reynolds number of 1.1×10^5 was investigated in a wind tunnel of the Naval Postgraduate School. The goal of this thesis is to experimentally validate the pressure measurement system for flowfield variables with elevated levels of turbulence; to determine the location and intensity of the asymmetric vortices in the wake of the VLSAM model at a raised level of freestream turbulence; and to display the asymmetric vortices by velocity mapping and pressure contours. The purpose is to correlate the results with the force measurements of Rabang to provide a greater understanding of the vortex flowfield. The body-only configuration was tested. Two flowfield conditions were treated: the nominal ambient wind tunnel condition, and a condition with grid-generated turbulence of 3.8% turbulence intensity and a dissipation length scale of 1.7 inches. The following conclusions were reached: 1) The relative strengths of the asymmetric vortices can be noted by the sharp spike shape in the ambient condition; this condition becomes diffused and becomes fatter in the turbulent condition; 2) The right side vortex has greater strength than the left side one as seen by the diffusion in the total pressure coefficient and static pressure coefficient contours with and without a turbulent condition; 3) an increase in turbulence intensity tends to reduce the strength of the asymmetric nose-generated vortices; also pushes the two asymmetric vortices closer together; 4) and crossflow velocities were examined and were found to indicate the behavior denoted by the pressure contours.

on For	<input checked="checked" type="checkbox"/>
A&I	<input type="checkbox"/>
ed	<input type="checkbox"/>
Justification	
By	
Distribution/	
Availability Codes	
Avail and/or	
Not	Special
A-1	

TABLE OF CONTENTS

I. INTRODUCTION.....	1
A. BACKGROUND.....	1
B. THEORY.....	3
1. Asymmetric Vortex Theory.....	3
2. Two Dimensional Crossflow.....	8
3. Three Dimensional Vortices	12
4. Turbulence	15
5. Effects of Body, Wing, Strakes and Tail	18
C. EFFECT ON VERTICALLY-LAUNCHED SURFACE TO AIR MISSILE.....	19
1. Marine Environment.....	19
2. Launch and Crosswind Velocities.	20
3. Other Launch Considerations	21
II. EXPERIMENT APPARATUS	23
A. EXPERIMENTAL HARDWARE	23
1. Wind Tunnel.....	23
2. VLSAM and Support Equipment	26
3. Velmex 8300 3-D Traverser.....	30
4. Scanivalve.....	33
5. Turbulence-Generating Grids	35
6. 5-Hole Pressure Probe.....	41
7. HP Data Acquisition System.....	43
B. EXPERIMENT SOFTWARE	45
1. PPROBE Program	45
2. CALP Program.....	51
3. CONVERT Program	51
4. REVX Program.....	58

5. XPLANE Program.....	58
6. ARROW Program.....	58
C. EXPERIMENTAL CONDITIONS.....	59
D. EXPERIMENT PROCEDURE.....	61
1. Dynamic Pressure Calibration.....	61
2. Scanivalve Transducer Calibration.....	61
3. Pressure Probe Calibration.....	63
4. Preliminary Run and Data Collection.....	64
5. Actual Run.....	65
E. EXPERIMENTAL CORRECTIONS.....	66
III. RESULTS.....	68
A. DYNAMIC PRESSURE CALIBRATION.....	68
B. TRANSDUCER CALIBRATION.....	71
C. PRELIMINARY RUN.....	75
D. BODY ONLY WITHOUT TURBULENCE.....	81
E. BODY-ONLY WITH TURBULENCE.....	87
IV. CONCLUSION AND RECOMMENDATIONS.....	95
LIST OF REFERENCES.....	97
APPENDIX A. PPROBE PROGRAM.....	100
APPENDIX B. CALP PROGRAM.....	113
APPENDIX C. CONVERT PROGRAM.....	119
APPENDIX D. PRESSURE PROBE CALIBRATION CHART.....	122
APPENDIX E. REVX PROGRAM.....	123
APPENDIX F. XPLANE PROGRAM.....	124
APPENDIX G. ARROW PROGRAM.....	126
APPENDIX H. RUN MATRIX.....	128
INITIAL DISTRIBUTION LIST.....	129

LIST OF FIGURES

Figure 1.	Vortex Flow About an Blunt-Nosed Cylinder. [Ref. 2].....	4
Figure 2.	Vortex Flow About a Slender-Nose Cylinder [Ref. 2].....	5
Figure 3.	Vortex Generation Regimes [Ref. 8].....	7
Figure 4.	Two Dimensional Crossflow about a Cylinder [Ref. 9].....	9
Figure 5.	Side Force to Normal Force Ratio [Ref. 9]	11
Figure 6.	Side Force Variations with Nose Roll Angle: Runs WOA102 to WOA802 [Ref. 3].....	14
Figure 7.	Vortex Shedding on a Missile at High Angle of Attack [Ref. 18.].....	17
Figure 8.	Naval Postgraduate School Low Speed Wind Tunnel [Ref. 26;p. 3-7]	24
Figure 9.	Turnable Assembly and VLSAM in Wind Tunnel	25
Figure 10.	Drawing of VLSAM Model and the Specification [Ref. 3]	28
Figure 11.	The Planar Survey Grid.	29
Figure 12.	VLSAM Model with Support Equipment and Pressure Probe in the Test Section (without Wing)	30
Figure 13(a).	Velmex 8300 #-D Traverser-- Motor Controller Assembly	31
Figure 13(b).	Velmex 8300 3-D Traverser-- Traversing Assembly	32
Figure 14.	48-Port Scanivalve	34
Figure 15.	Scanivalve Control	35
Figure 16.	Turbulence Grids 2, 3, and 4, Clockwise from the Left Grid 2, 3, and 4.....	36
Figure 17.	Planview of VLSAM Model and Pressure Probe in the Test Section (not to scale).....	37
Figure 18.	Square-Mesh Turbulence-Generating Grid.....	38
Figure 19.	Grid Turbulence Intensity.....	39
Figure 20.	Grid Turbulence Length Scales	40
Figure 21.	5-Hole Probe and its Measuring Tip [Ref. 29].....	42
Figure 22.	HP Data Acquisition System.....	44

Figure 23.	Digital Multimeter (DMM) Soft Front Panel. [Ref. 30]	44
Figure 24.	Whole Hardware Setting.....	46
Figure 25.	Program Procedures.....	47
Figure 26.	PPROBE Program Flow Chart.....	50
Figure 27(a).	CONVERT Program Flow Chart.....	52
Figure 27(b).	CONVERT Program Flow Chart.....	53
Figure 28.	ROB802: Side Force Coefficient [Ref. 3].....	59
Figure 29.	Body Configurations and Reference System [Ref. 3].....	60
Figure 30.	Calibration Manometer.....	63
Figure 31.	Digital Panel Meter (DPM).....	64
Figure 32.	Blockage Factors [Ref. 3].....	67
Figure 33(a).	Dynamic Pressure Calibration at no Grid	69
Figure 33(b).	Dynamic Pressure Calibration at Grid #1	69
Figure 33(c).	Dynamic Pressure Calibration at Grid #2	70
Figure 33(d).	Dynamic Pressure Calibration for Grid #3.....	70
Figure 33(e).	Dynamic Pressure Calibration at Grid #4	71
Figure 34(a).	Transducer Calibration at no Grid Condition for the Preliminary Run.....	73
Figure 34(b).	Transducer Calibration at no Grid Condition.....	74
Figure 34(c).	Transducer Calibration at Grid #1 Condition.....	75
Figure 35.	Preliminary Crossflow Velocity Vector Superimposed on the Grid.....	77
Figure 36(a).	Total Pressure Coefficient Contour.....	78
Figure 36(b).	Local Static Pressure Coefficient Contour.....	79
Figure 37 (a).	3D Surface Plot. Local Total Pressure Coefficient.....	80
Figure 37 (b).	3D Surface Plot. Local Static Pressure Coefficient.....	81
Figure 38.	Crossflow Velocity Vector Superimposed on the Grid for no Grid Condition	83
Figure 39(a).	Total Pressure Coefficient Contour at no Grid Condition.....	84
Figure 39(b).	Local Static Pressure Coefficient Contour at no Grid Condition.....	85

Figure 40(a).	3D Surface Plot. Local Total Pressure Coefficient at no Grid Condition.....	86
Figure 40(b).	3D Surface Plot. Local Static Pressure Coefficient at no Grid Condition.....	87
Figure 41.	R1B801. Side Force Coefficient. [Ref. 3].....	88
Figure 42.	Crossflow Velocity Vector Superimposed on the Grid for Grid 1 Condition.....	90
Figure 43(a).	Total Pressure Coefficient Contour at Grid 1 Condition.....	91
Figure 43(b).	Local Static Pressure Coefficient Contour at Grid 1 Condition ...	92
Figure 44(a).	3D Surface Plot. Local Total Pressure Coefficient at Grid 1 Condition.....	93
Figure 44(b).	3D Surface Plot. Local Static Pressure Coefficient at Grid 1 Condition.....	94

NOMENCLATURE

α :	angle of attack
α_{av} :	the AOA at which steady asymmetric vortices are formed
AOA:	angle of attack
α_{sv} :	the AOA at which steady symmetric vortices are formed
α_{uv} :	the AOA at which unsteady vortices are formed
C_{ps} :	Static pressure coefficient
C_{pt} :	Total pressure coefficient
C_y :	side force coefficient
d :	base diameter of the missile body
ϵ :	blockage correction
K :	wind tunnel calibration factor
L_1 :	missile length scale
L_d :	missile diameter
L_e :	turbulent scale
l_n/d :	missile's nose fineness ratio
l_n :	nose length
M :	mach number
N :	normal force
P_1 :	indicated total pressure
P_2 :	indicated static pressure
P_3 :	indicated static pressure
P_4 :	pitch angle pressure
P_5 :	pitch angle pressure

P_{atm} : ambient pressure
 P_s : static pressure
 P_t : total pressure
 P_{tc} : total pressure coefficient of pressure probe calibration
 θ : pitch angle
 Q : free stream dynamic pressure
 q : local dynamic pressure
 θ_A : nose semi-vortex angle
 θ_c : pitch angle coefficient
 q_m : measured dynamic pressure
 θ_R : roll angle
 R : air constant - 1718
 ρ : air density
 Re : Reynolds number $C = (\rho U d / \mu)$
 T : temperature
 t : time
 T_{av} : average temperature
 T_0 : ambient temperature
 Γ_u : turbulence intensity - (u/U)
 U : longitudinal mean velocity
 u : longitudinal velocity function
 U_m : Test section velocity
 v : lateral velocity function
 V_c : velocity coefficient of pressure probe calibration
 V_v : vertical velocity

Y: side force

μ : absolute viscosity

ACKNOWLEDGMENTS

First of all, I would like to thank the Republic of China Navy General Headquarters for providing me the opportunity to study here.

I would like to express my sincere appreciation to Professor Richard Howard, my thesis advisor, for his dedicated assistance and guidance during the study. Without his encouragement, patience and enthusiasm this thesis could not have come to a successful completion.

I would also like to thank Mr. Jack King and Mr. Alan McGuire for their technical instruction and assistance in the wind tunnel apparatus and data acquisition system.

I would like to thank Lt. Ao Chia-Ning, Republic of China Navy, Mr. Li Shang-Wu and Miss Wang Ching-Hua for their assistance in plotting the figures; Miss Jeng Shan-Jung and Mrs. Hania La Born for their assistance in typing and formatting the thesis.

Finally, I would like to thank my mother Lung Chen-yu-chu, my sister and my brothers for their love and encouragement.

I. INTRODUCTION

A. BACKGROUND

In the past there has been a need for trainable launchers, both in azimuth and in elevation, so that the anti-aircraft missiles could be fired into gathering and guidance beams which direct them toward their targets. By way of contrast, a missile fired from a vertical launcher has to guide itself into the appropriate direction and heading. [Ref.1]

Vertical launchers are part of a general evolution in anti-aircraft missile systems towards a higher rate of target engagement, which has three complementary aspects. The first aspect is the number of targets arriving simultaneously or nearly simultaneously. The ship must attempt to overcome the usual limitation of one engagement per fire control radar. Having overcome this limitation, the ship must keep enough defensive missiles in the air at any one time to fully exploit fire control capacity. The US AEGIS class ships are equipped with the US Mark 26 trainable launcher which fires about twice as fast as its predecessor, the Mark 13. The new Martin Mark 41 vertical launcher fires about five times faster than the US Mark 13 trainable launcher, i.e., at about one missile per second. [Ref. 1]

The second aspect is the number of targets which appear over an extended length of time. Current point defense systems, such as SEA SPARROW and SEA WOLF, generally employ box launchers containing six or eight rounds. Once they have been fired off, the launcher must be reloaded by hand, a relatively laborious process. To provide automatic reloading would require considerable below deck

space, which is in short supply on most ships. A ship with a vertical launcher and with each missile stored in and launched from its own canister, offers a significant improvement in magazine handling within the usual constraints of above-deck space.

The third aspect is the ability to carry out sustained operation in the face of air opposition. Missiles are voracious consumers of magazine space, hence the number of missiles per ship is always very limited. A Magazine/Launch system, then, has to be adapted to rapid replenishment if ships are to operate for a protracted period. The adoption of a vertical launcher greatly simplifies replenishment since each missile is reloaded while still inside its shipping container.

Perhaps the single greatest advantage of the vertical launching system over more conventional systems is that they save valuable space--a trainable launcher needs clear space not only for its own rotation but also for its blast in different directions, which is why such launchers are so widely spaced aboard modern warships. In a vertical system, by way of contrast, the missile blast is concentrated in the immediate area of the launcher (and, to a greater extent, can be vented down into the launching cell), and there is no need for allowing a clear arc of fire. [Ref. 1]

However, in a vertical launch surface-to-air missile (VLSAM) system, the aerodynamic surfaces do not suffice to control the missile at take-off, since it takes off at a very low initial speed. Rather, the missile generally relies on movable vanes set into its rocket motor exhaust. Any early failure of the booster motor will drop the missile directly back on its launcher. In addition, when it enters the open ocean environment at low velocity, the missile is subject to potentially significant crosswinds. The resultant of the missile and crosswind velocities is a potential high

angle of attack flow around the missile. This high angle of attack flow may cause asymmetric vortices to form on the missile nose and afterbody (to be discussed later) which induce side forces that might give flight control problems to the VLSAM at launch. The launch environment may contain some degree of turbulence, both from the atmospheric boundary layer, and from the airflow about the ship superstructure. Understanding the effect of this turbulence on the aerodynamic characteristics of a VLSAM during launch is the goal of a continuing effort of research and experiments conducted at the Naval Postgraduate School (NPS). In an earlier work, Roane [Ref. 2] developed a system of modelling flowfield turbulence by a series of four grids to generate turbulence in the NPS low speed wind tunnel. Rabang [Ref. 3] examined the effect of this turbulence on the asymmetric vortex induced forces generated on a VLSAM model. The goal of this thesis is to experimentally validate a flowfield technique to determine the location and intensity of the asymmetric vortices in the wake of the VLSAM model at various levels of freestream turbulence. The purpose is to understand better the asymmetric vortex behavior as effected by turbulence, and to provide flowfield information for correlation with numerical predictions. This study involves flowfield measurements at a high angle of attack about a body-only configuration with and without freestream turbulence.

B. THEORY

1. Asymmetric Vortex Theory

The progressive development of the wake along the blunt-nosed slender cylindrical body when viewed in cross-flow planes is similar to the growth with time of the flow behind a two dimensional cylinder at an angle of attack. As shown

in Figure 1 from Ref. 2, a separation "bubble" exists and prevents the formation of the vortices in the area immediately aft the nose. Further downstream, two symmetrical vortices are disposed from the lee side. These vortices are fed by vortex sheets containing boundary layer fluid which has separated from the body. Further along the body these vortices alternately detach and move downstream one by one at an angle to the freestream. Other vortices form on the lee side of the body at an increasing distance and behave in a similar manner. This process continues along the body length. The result is a side force on the body, relatively small in magnitude, that appears as a consequence of the steady asymmetric vortices. [Ref. 4 & 5]

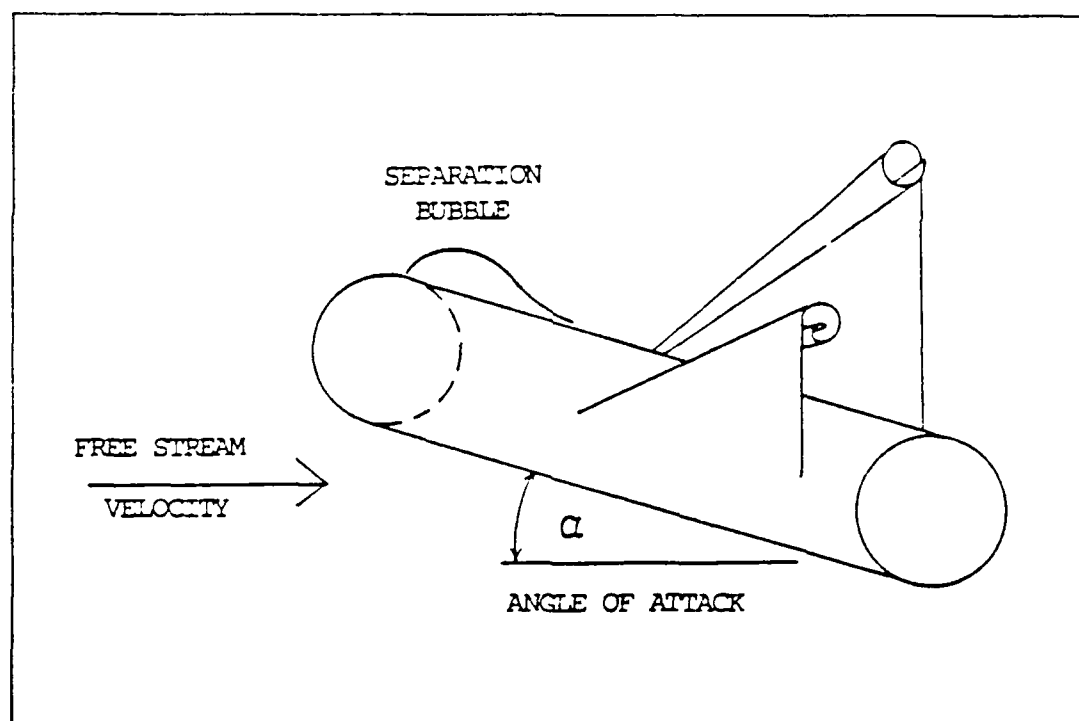


Figure 1. Vortex Flow About an Blunt-Nosed Cylinder. [Ref. 2]

On a slender ogive nose tip, the nose-induced separation phenomenon on a blunt-nosed cylinder does not occur, and consequently, nose-generated asymmetric

vortices generate much a greater proportion of the overall side force. The net effect of a slender body with vortex formation occurs along the entire length of the body, as shown in Figure 2. [Ref. 5]

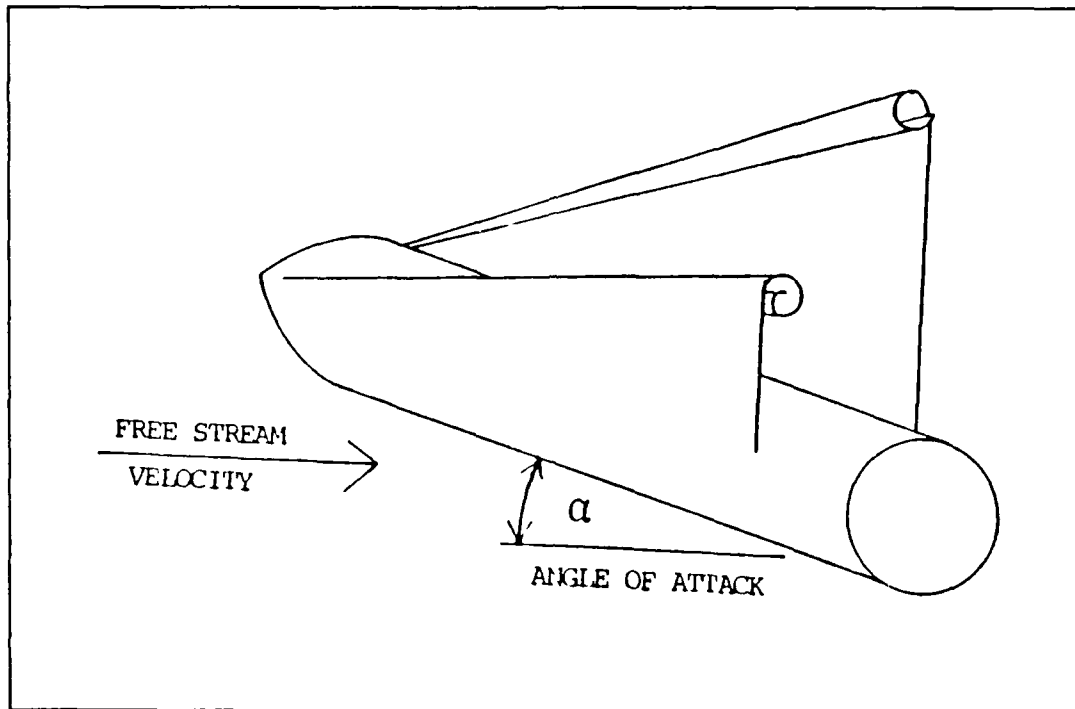


Figure 2. Vortex Flow About a Slender-Nose Cylinder [Ref. 2]

In recent years, there has been considerable interest in the development of reliable techniques for the prediction of aerodynamic characteristics of missiles and of aircraft at high angles of attack. These research efforts have revealed that the flow on the leeside of these bodies is characterized by a vortex system which mainly depends on the angle of attack, nose shape, overall fineness ratio, crossflow Mach number and Reynolds number. Other secondary factors may include roll angle, freestream turbulence, surface roughness, acoustic environment and vibration. [Ref. 6, 7]. In later sections we will discuss the effects of the factors mentioned above.

a.. Vortex Regions

As a slender body is being pitched through the angle of attack range $0 \leq \alpha \leq 90^\circ$, it experiences four distinct flow patterns (see Figure 3) that reflect the diminishing influence of the axial flow component as described by Ericsson and Reding [Ref. 8]. The flow regimes are characterized as follows:

Regime I ($0^\circ \leq \alpha \leq \alpha_{sv}$): At low angles of attack the axial flow dominates and the flow is attached.

Regime II ($\alpha_{sv} \leq \alpha < \alpha_{av}$): At intermediate angles of attack, the crossflow sweeps the boundary layer to the leeward side where it is separated and rolls up into a symmetric vortex pair. The vortices are steady with time.

Regime III ($\alpha_{av} \leq \alpha < \alpha_{uv}$): At high angles of attack crossflow effects start to dominate and the vortices become asymmetric, thereby producing side forces at zero sideslip. These asymmetrical vortices gives rise to significant side forces and yawing moments. Nelson observed a random switching from a nearly symmetrical attached pair of vortices to a separated multi-vortex system occurring at 35° angle of attack. [Ref. 7]. The position on the slender body of asymmetrical vortex shedding moves forward with increased angle of attack and with Reynolds number and moves rearward with increasing Mach number [Ref. 6]. At the higher end of this angle of attack range, there are some random flow switching and flow instabilities.

Regime IV ($\alpha_{uv} \leq \alpha \leq 90^\circ$): At a very high angle of attack, the crossflow dominates completely and the boundary layer is shed in the form of a von Karman vortex sheet or a random wake depending upon Reynolds number, Mach number and geometric details.

Of particular interest is Regime III where the side forces, yawing and rolling moments can be affected due to the asymmetrical nature of the separated flow field. Since these changing patterns are significant, the side forces and moments produced can be larger than the control moments produced by the deflection of the conventional control devices. And the effectiveness of aft control surface or fins can be greatly reduced by the vortex wake produced by forward separation.

2. Two Dimensional Crossflow

Airflow over the slender body can be divided into normal and axial components. The axial flow component follows along the slender body length and the crossflow is essentially a two dimensional flow normal to a cylinder.

At angles of attack above 30° , in Regime III, the effective Reynolds number on a cylinder essentially equals the crossflow Reynolds number [Ref. 9]. Thus, the sectional characteristics for the slender body should be similar to those of a 2D cylinder. The crossflow Reynolds number is the primary factor which influences the separation point of the boundary layer. Viscous flow, surface roughness, and turbulence are other factors which influence boundary layer separation. Following Achenbach's terminology, a cylinder in incompressible crossflow experience four distinct flow regimes, each with a different type of flow separation, as shown in Figure 4. [Ref. 9]

At subcritical Reynolds number, the boundary layer is laminar, and flow separation occurs near the lateral meridian where ϕ , is defined as the angle from the direction of the crossflow, varies 80° to 90° .

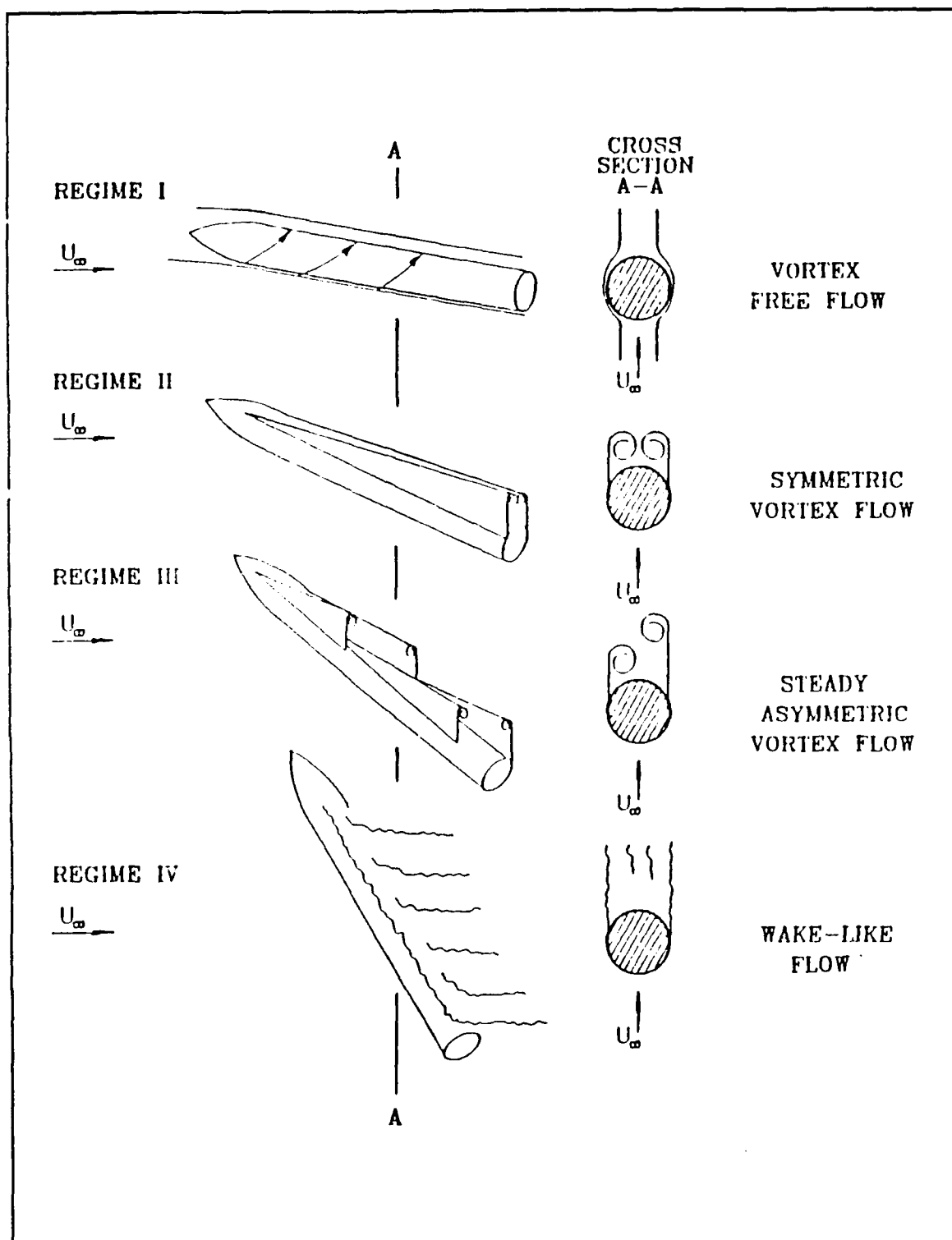


Figure 3. Vortex Generation Regimes [Ref. 8]

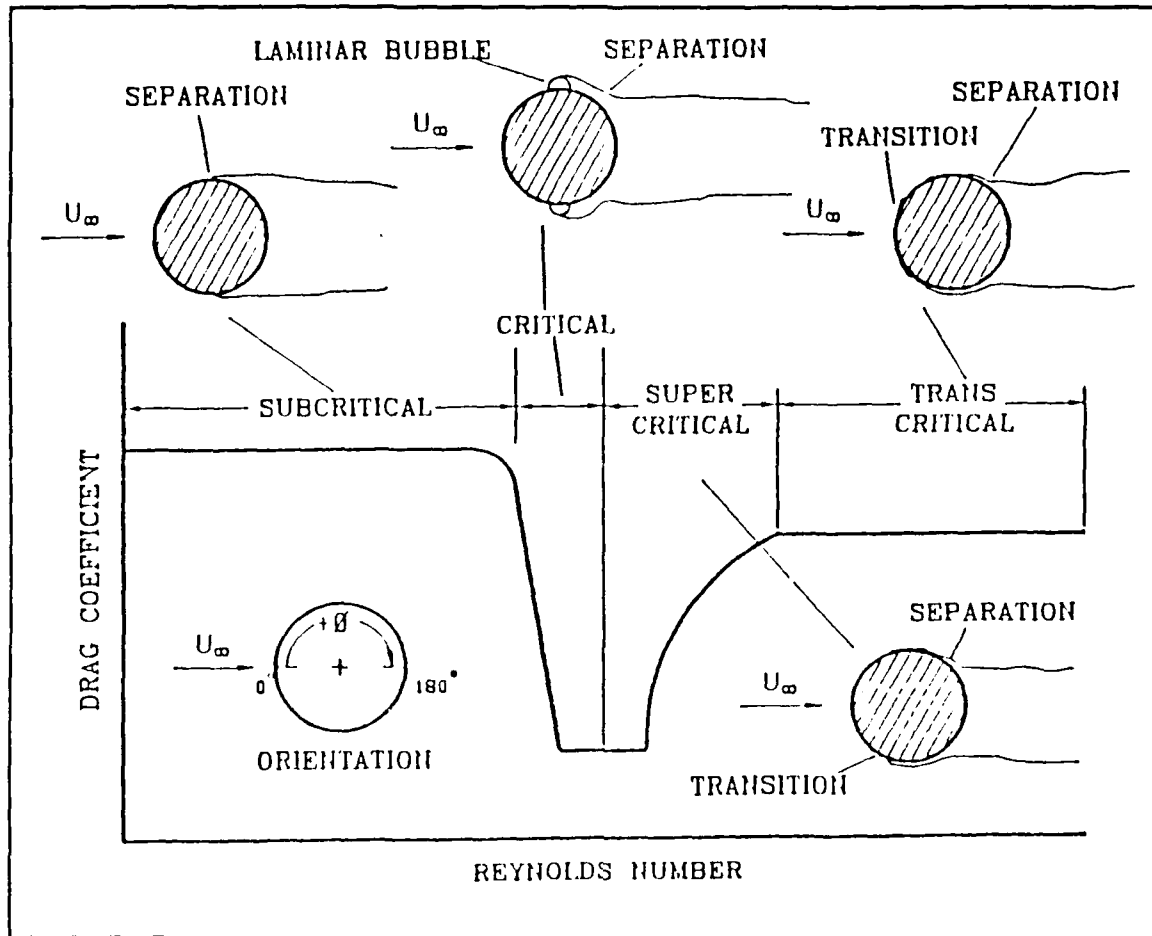


Figure 4. Two Dimensional Crossflow about a Cylinder [Ref. 9]

In the critical Reynolds number range, a laminar separation bubble develops near the lateral meridian at $\phi \approx 90^\circ$, followed by transition in the detached laminar shear layer and turbulent reattachment. The reattached turbulent boundary layer is more energetic than the laminar boundary layer and separation is delayed to $\phi \approx 140^\circ$, resulting in a dramatic reduction of the drag. Thus, a drag-bucket is produced in the critical Reynolds number region.

As the Reynolds number is increased, transition moves forward of the lateral meridian and the laminar bubble is lost. Thus, separation moves forward of

$\phi \approx 100^\circ$ as the turbulent boundary layer thickness grows with increasing Reynolds number. A drag increase accompanies the wake growth.

For asymmetric behavior in this Reynolds number regime, both supercritical and critical separations allow large suction peaks to be realized on one side of the body, whereas on the other side, subcritical separation cuts off the peak suction pressures, producing a large pressure differential across the body. The pressure drops sharply as the separation moves rearward in the critical Reynolds number range, resulting in a pronounced maximizing of the 2D lift to drag ratio. [Ref. 9]

Figure 5 presents a logical progression of asymmetric vortex separation with increasing Reynolds number that explains how both a maximum and a minimum $|C_{y}|_{\max}/C_n$ can occur in the critical Reynolds number range. At subcritical effective Reynolds numbers, asymmetric subcritical separation occurs near the 80° meridian to produce a moderate normalized side force.

As the critical Reynolds number range is entered, critical/subcritical separation can occur. This provides the maximum differential in the separation location on opposite sides of the body and the maximum suction pressure differential in the vicinity of the lateral meridian where it is the most effective in producing a side force. The peak is sharp because a relatively small increase in Reynolds number results in asymmetric critical separation where nearly equal suction pressures occur at the lateral meridians and the separation asymmetry affects the pressure only at $\phi \approx 140^\circ$, where they are relatively ineffective in producing the side force. Thus, both the normalized side force and the side force itself will be very small. [Ref. 9]

Finally, as effective Reynolds number increases through the supercritical regime on to the transcritical region, the flow separation asymmetry moves toward the lateral meridian where it is once again efficient in generating a side force. [Ref. 9]

The Reynolds number dictates the greatest influence on the normal force and drag characteristics, especially within the critical range where the maximum side force and the maximum vortex asymmetry occur. [Ref. 9]

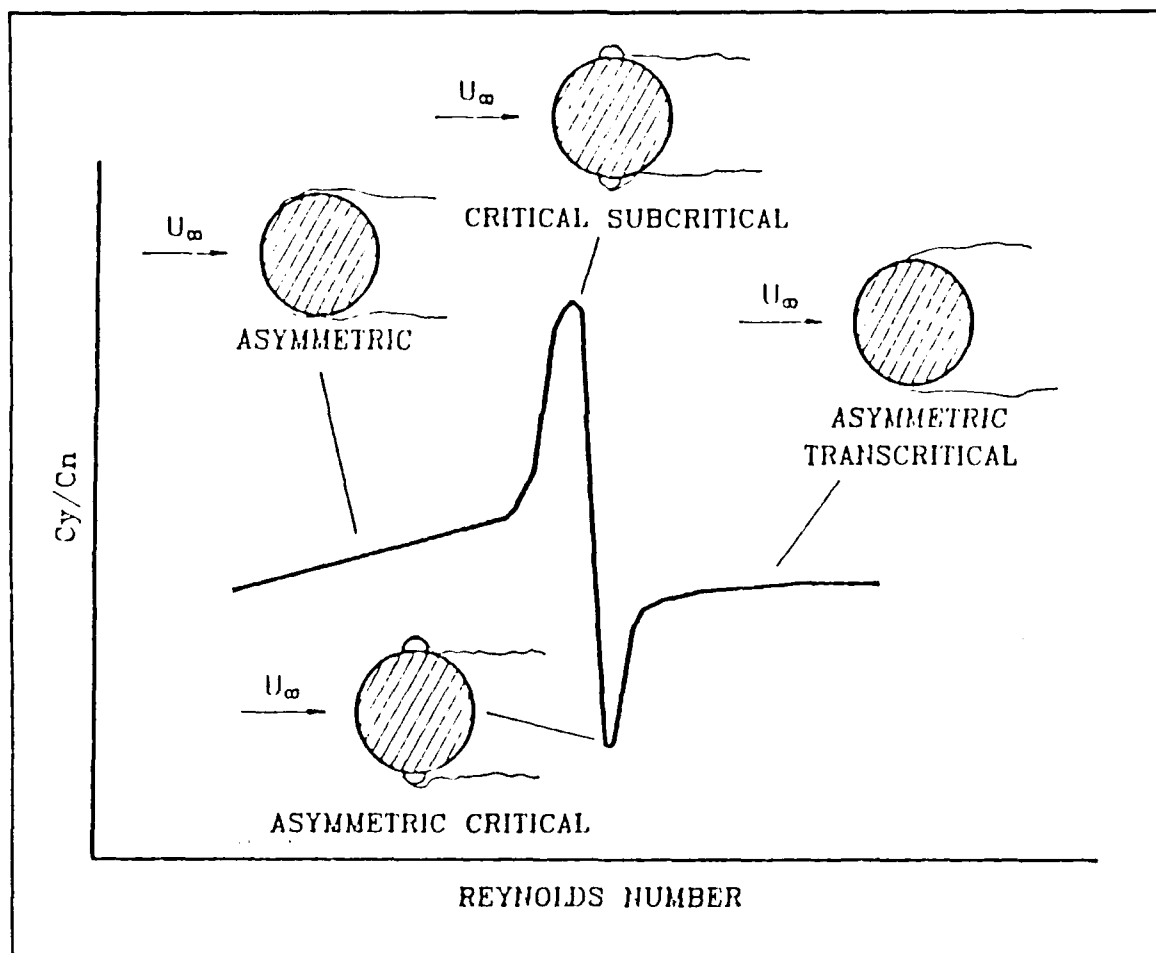


Figure 5. Side Force to Normal Force Ratio [Ref. 9]

3. Three Dimensional Vortices

The nose geometry of a missile is an important factor in vortex generation and disposition. [Refs. 7, 10, 11, & 12] Missile nose geometry falls into two shapes: cones and ogives, both pointed and blunt. Noses are dimensionalized for comparison by their length to base diameter ratio or fineness ratio (l_n/d). There are two kinds of asymmetric vortex shedding on slender bodies. [Ref. 13] On pointed bodies, the vortex asymmetry, and thus the side force, usually begins at the nose, and vortices are shed at a relatively rapid rate to give alternating side-force cells on long-slender bodies. A slight amount of nose bluntness can cause the second type of vortex shedding to occur. Here asymmetric vortices develop first at the rear of the body, and the alternating vortex shedding does not occur as rapidly. Thus the side force cells are much larger and can cover the entire cylindrical aft body. When initially generated by a slender-forebody, they are not affected by the aft-body vortices, though the afterbody forces will contribute to the overall magnitude of induced forces from the nose-body combination. [Refs. 7 & 9]

For pointed conical and ogive noses, observations indicate that α_{AV} occurs as a function of the semi-vertex angle θ_A . At all Mach numbers, asymmetric vortex shedding starts when the angle of attack exceeds the total induced angle at the apex $\alpha_{AV} \approx 2\theta_A$. For a conical nose:

$$\theta_{AC} = \theta_C \quad (1)$$

For a tangent ogive nose:

$$\theta_A = \tan^{-1} \left[\frac{\frac{l_n}{d}}{\frac{l_n}{d} - 0.25} \right] \quad (2)$$

For slender noses Equation 2 can be approximated by:

$$\theta_A \approx \frac{l_n}{d} \quad (3)$$

Nose fineness ratio has been shown to have an effect on the asymmetric vortex induced side force [Refs. 7, 10, 11, 12 & 14]

The magnitude of the maximum side force generally increases with an increase in the nose fineness ratio and decreases with an increasing Mach number to nearly zero at supersonic speeds. [Refs. 15 & 16].

As the nose fineness ratio increases, the nose apex angle decreases and the angle of attack for the onset of asymmetric vortices will decrease. Thus, a missile with high nose fineness ratio may become more susceptible to induced side forces at a lower angle of attack than a missile having a lower nose fineness ratio. Jorgensen demonstrated that decreasing the nose fineness ratio is more beneficial in reducing side forces than blunting the nose [Ref. 7].

In addition to the nose fineness ratio, the nose-generated vortical flow is extremely sensitive to the nose roll angle. This phenomenon results from surface imperfections and deviations in the nose axisymmetric geometry. Figure 6 shows the work by Rabang investigating the resulting side force coefficient for nose roll angles varied in 45° increments. [Ref. 3]

Should the afterbody roll angle change with nose roll angle remaining constant, the afterbody vortices will change the side force magnitude and direction as noted by Kruse [Ref. 17]. Since the nose and body of a missile do not rotate

independently of each other, the vortex system generated by the nose should still dominate afterbody vortices on an axisymmetric missile configuration.

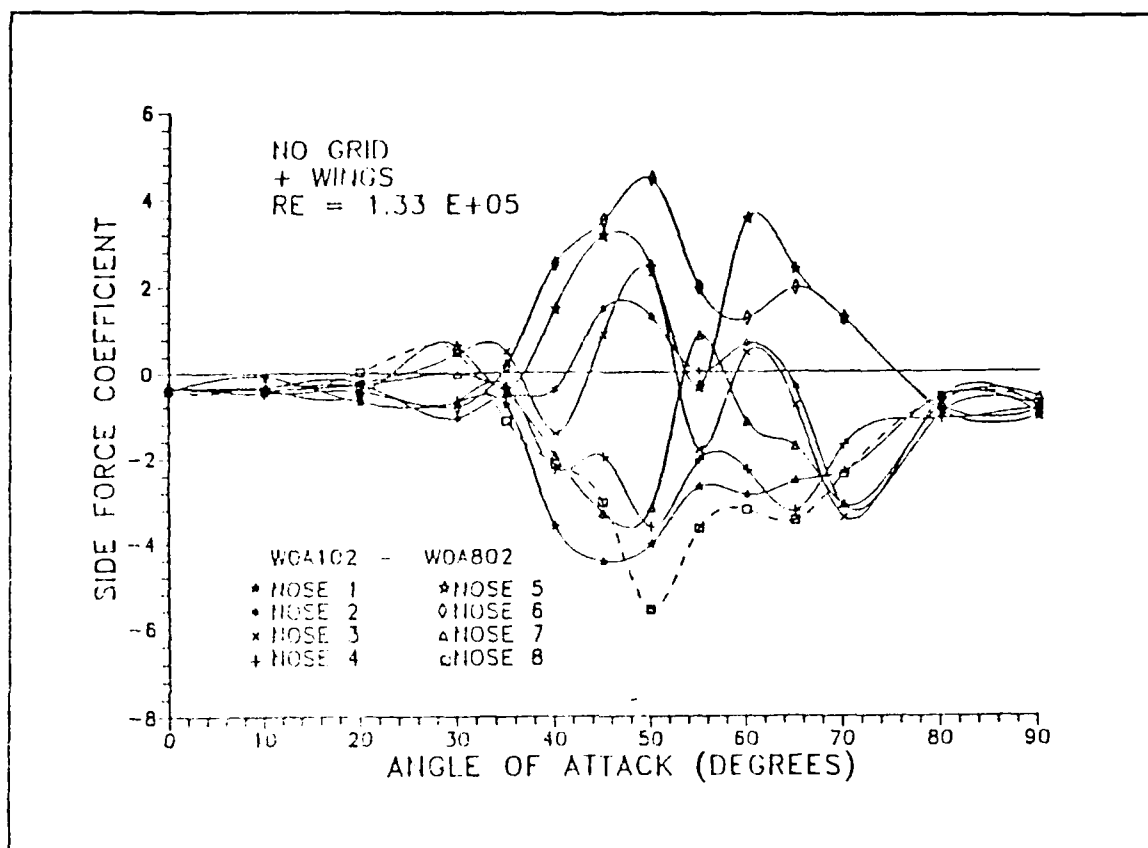


Figure 6. Side Force Variations with Nose Roll Angle: Runs WOA102 to WOA802 [Ref. 3]

The behavior of the asymmetric vortices is well documented for a vast number of models and shapes, yet their cause is still not well understood. The general consensus among the high angle of attack researchers is that vortex asymmetry is induced by the location of boundary layer separation [Refs. 13 & 18]. But Keener and Chapman consider the principal effect to be a hydrodynamic (inviscid) instability in the initially symmetric vortex formation and the interaction of the vortices (which increases in strength with incidence) with the

surrounding potential flow field. In addition to the hydrodynamic instability, the vortex asymmetry is also strongly affected by boundary-layer (viscous) asymmetries resulting from transition and separation differences on each side of the body. [Ref. 19]

4. Turbulence

a. Turbulence Intensity and Length Scale

Flow in which there are random, small-scale velocity fluctuations about the mean freestream flow velocity is said to be turbulent. In calculating the effect of turbulence on a body in the flowfield, a comparison must be made between the scale of the body and that of the turbulence. In addition, consideration must be given to the energy contained in the turbulence flowfield.

Turbulence intensity is the measure of the relative magnitude of velocity fluctuations in the flowfield. Mathematically, for a horizontal flowfield or crosswind, the turbulence intensity T_u is the ratio of the root-mean-square (rms) velocity fluctuation u' , to the mean velocity component in the flowfield, U_∞

$$T_u = u'/U_\infty \quad (4)$$

Since the turbulence intensity measures the magnitude of velocity fluctuation, a higher intensity indicates higher kinetic energy and correlates to more turbulent flow.

The length scale of the turbulence, L_e , is a measure of the dimension of the velocity fluctuation. The effect of the length scale on a body is a function of the relative dimensions of the turbulent eddies and the body itself. The length scale, despite the inference of a purely spatial measure, also represents the temporal character of the turbulent fluctuations. An increase in the spatial length of the

turbulence corresponds to an increase in the time the body is exposed to the fluctuation.

Turbulence length scale to body size ratio may dictate the manner in which turbulence affects the VLSAM flowfield. The turbulence length scale can be compared to missile length, $L_e:L_1$, or missile diameter, $L_e:L_d$. When the turbulence length scale is many times larger than the missile length, $L_e \gg L_1$, the effect on the missile is somewhat like a uniform steady-state flowfield independent from the time, especially at low turbulence intensities. The effects of the flowfield on vortex development are largely dictated by those conditions and factors discussed earlier for a two dimensional cylinder.

When the turbulence length scale is comparable to the body length, $L_e \approx L_1$, the flowfield is distinctly non-uniform and may cause unwanted rolling, pitching and yawing motion. [Ref. 20] In both cases, the missile body motion results from the actual flowfield conditions about the missile body.

When the turbulence length scale is smaller than the body, $L_e \ll L_1$, the result has a distinctly different effect. Most importantly, when it is comparable or smaller than the missile diameter, $L_e \leq L_d$, the small scale turbulence present in the flowfield may change the boundary layer and flow separation present on the missile surface, particularly when the turbulence length scale is the same size or smaller than the boundary layer thickness. The results of Rabang show an increase in turbulence intensity with length scale on the order of the nose-generated vortex scale tends to delay the onset of induced side force, to steady the asymmetric vortex formation, and to leave the maximum value C_y more or less unaltered. [Ref. 3]. The results of Rabang show an increase in turbulence intensity with a length scale

on the order of the boundary-layer scale tends to reduce the magnitude of the induced side forces. [Ref. 3]

Both large and small scale turbulence length scales actually coexist in the flowfield since the turbulence length is the mean of the disturbances in the flowfield. The combination of different length scales may add complexity to the qualitative analysis of the flowfield. As the disturbances in the flowfield experience strain, the disturbances will break up into finer disturbances of smaller scale and decreasing energy. The process repeats itself or cascades until the small disturbances eventually disappear owing to viscosity. When the disturbances decrease in size and energy, their individual intensities will decrease at a faster rate. Thus, the turbulence length scale average will be biased towards the larger turbulence scales in the flowfield and gives an accurate quantitative representation of all the length scales within the flowfield, since the energy and intensity of the larger scale turbulence is dominant [Ref. 21.].

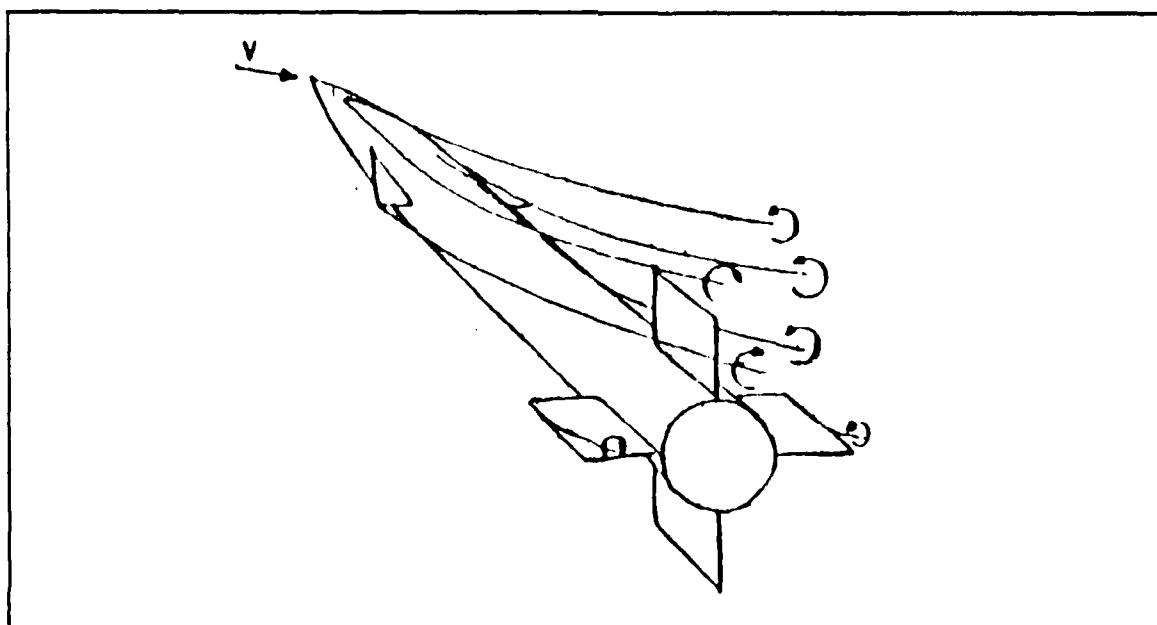


Figure 7. Vortex Shedding on a Missile at High Angle of Attack
[Ref. 18.].

5. Effects of Body, Wing, Strakes and Tail

The vortex structure of the complete missile can be constructed by superimposing those of the body, wing strakes, and tail. This results in a vortex system as shown in Figure 7. [Ref. 18] Body vortices interact with wings and tails, and wing or canard vortices interact with tails. The interaction can be very strong if a vortex passes very close to a tail surface. The addition of wings causes the nose vortices to move closer to the body. As the vortices move closer to the body, the result is comparable to increasing the effective angle of attack causing unsteady asymmetric vortices. The net effect of the wing-body combination seems to be a reduction in the effective angle of attack for the onset of asymmetric vortices and side forces. [Ref. 22]

For the body-only case, from the previous research by Rabang, an increase in turbulent intensity and scale tend to reduce the induced side forces and to shift the range of action to slightly higher incidence angles. [Ref. 3]

The addition of strakes will generate additional vortices, improving the interaction between body vortices and airflow over the wings. The placement of long strakes along the missile body and nose was found by some researchers to reduce the forces and moments generated by asymmetric vortices. [Ref. 18]. Rabang demonstrated the addition of wings and strakes typical of a VLSAM tended to preserve the induced side force for all levels of turbulence intensities and length scales. [Ref. 3]

The adding of a tail has, in general, relatively little influence on the maximum side forces. With the application of wings of high aspect ratio, the tail loses its efficiency at a small angle of attack, but gains in efficiency with the growing angle of attack. [Ref. 18]

The use of small nose bluntness, nose booms and boundary layer trips has proven effective in reducing asymmetric vortex-induced loads. [Ref. 23]

C. EFFECT ON VERTICALLY-LAUNCHED SURFACE TO AIR MISSILE

1. Marine Environment

Conditions in the marine atmospheric environment may have a significant effect on the VLSAM. The atmospheric boundary layer (ABL) is the result of the interaction of the atmospheric flow over the underlying land or sea surface. This layer is characterized by a turbulent transfer of momentum, heat and mass (water vapor) and their associated gradients.

The surface layer, approximately the lowest 10% of the A.B.L., is characterized by the mechanically produced turbulence from the surface roughness and friction with nearly constant vertical fluxes of momentum, heat and mass. The height of this layer may vary over a wide range but is typically of the order of 50 meters. In the lower most part of the surface layer, commonly referred to as the roughness layer, the surface has the greatest effect on generating turbulence and influencing fluid motion. Mean flow in the roughness layer is nonhomogeneous and three-dimensional in nature. In the marine roughness layer, the traveling surface waves affect the flow which result in various properties of the sea surface. However, the observation of these wave effects has been hindered by the motion of the instrument platform induced by the wind and waves as well as by the presence of the platforms (towers, buoys, ships) in the flow field. Furthermore, the majority of the flow in the surface layer itself can be considered horizontally homogeneous. [Ref. 20]

A measure of the general roughness of the surface is given by Z_0 , the roughness length. Its value is determined as a function of the mean wind velocity at various elevations above the surface of interest. Surface layer turbulence length scale and intensity can be empirically determined by combining the roughness length with the elevation and windspeed. [Ref. 24]

For a typical open ocean roughness length in the range $10^{-3} < Z_0 < 10^{-2}$ meters, turbulence intensities are on the order of 13 to 17 percent at a 10 meter elevation and mean wind speed of approximately 25 m/sec. [Ref. 24:p. 11]

Apparently, the turbulence intensity in the marine surface layer can be significant. However, the effect of such turbulence fluctuations is highly dependent upon the length scales present. For the conditions stated in the preceding paragraph, the longitudinal turbulence length scales are in the range $80 < L_e < 90$ meters. For a typical missile with a 1.1 foot diameter, the turbulence length scale to missile body scale ratio is about $L_e: L_d = 280:1$, and would have little effect on its boundary layer development. Yet, the cascade effect presented above allows for a decrease in the length scale until viscous forces dissipate the energy. Therefore, it is possible that the initial large scale turbulence and crosswind interaction with the ship superstructure would decrease, or "cascade," to scales where they could affect the development of the missile boundary layer.

2. Launch and Crosswind Velocities.

A typical VLSAM launching with a 10g acceleration reaches an altitude of approximately 56 feet traveling at a vertical velocity of $V_v = 164$ ft/sec. The VLSAM is still well within the surface layer environment (50 meters) and is subject to crosswind and turbulence effects. As an example, if a ship travels at 20 knots and a mean wind speed of 20 m/sec are combined with the VLSAM launch

velocity, the resultant vector is at 191 ft/sec at an angle of 31° from the missile flight direction. The result represents the VLSAM flying at an effective angle of attack of 31° at 191 ft/sec. This places the VLSAM in Regime III, the asymmetric vortex region, as it travels through the surface layer. [Ref. 2]

Gregoriou also states that an effective angle of attack up to $\alpha = 50^\circ$ may be reached by a VLSAM while it pitches over towards a target. [Ref. 25] These examples illustrate the distinct possibility of asymmetric vortex induced side forces on a VLSAM during launch phase.

3. Other Launch Considerations

There are many factors which affect the aerodynamics of VLSAM during the launch phase of its flight. They can be divided into two categories. One category of factors are inherent to the design of the missile, such as the plume (or jet) effect of the missile's engine, blast effects of the vented exhaust gases and activation of the flight control system. The other category of factors includes shipboard roll, pitch, and yaw, and ship airwake turbulence. [Ref. 2]

Plume and blast effects can affect the VLSAM while the propulsion system gases or exhaust gases impinge on the aerodynamic surfaces of the missile. In addition, the exhaust gases can directly impact the flowfield into which the missile is launched, especially if the gases are vented upward into the vicinity of the accelerating missile.

The VLSAM itself may impose some form of flight control, aerodynamic or thrust vector, to maintain flight attitude during the launch phase. [Ref. 25] Should the missile change flight attitude, the flowfield around it will be altered.

The ship undergoes constant roll, pitch and yaw motion and transmits this motion to the launch platform of VLSAM--the canister, since the canister used for

storage is also the launcher. This increases the complexity to the initial velocity vector as the VLSAM leaves the guide.

In addition to the turbulence generated in the marine atmospheric boundary layer, turbulence may be produced by the ship's hull and superstructure. This flowfield or ship airwake may increase turbulence intensities while decreasing turbulence length scales.

The above considerations, while not forming a complete description, emphasize the numerous factors which may influence the flight behavior of the VLSAM during the launch phase. Except for the limited discussion in the preceding paragraphs, these additional effects are beyond the scope of the present investigation.

II. EXPERIMENT APPARATUS

A. EXPERIMENTAL HARDWARE

The experimental hardware for this experiment can be divided into 7 major subdivisions. There are the wind tunnel, the VLSAM model with associated support structures, the 3-D traverser, the scanivalve mechanism, the turbulence generating grids, the 5-hole pressure probe and the data acquisition system. Each of these will be individually discussed in the following sections.

1. Wind Tunnel

The horizontal-flow, low-speed wind tunnel that was used during this research is located at the Naval Postgraduate School and is shown in Figure 8. [Ref. 26:pp. 3-7]

It is a single return tunnel measuring 64 feet in length and between 21.5 and 25.5 feet in width. The power section of the tunnel comprises a hundred horsepower electric motor coupled to a three-blade variable pitch fan by a four-speed Dodge truck transmission. Immediately following the propeller blades are a set of stator blades to help straighten the flow. Turning vanes are installed at all four corners, with two small-mesh wire screens installed upstream of the settling chambers, to smooth the airflow and reduce turbulence. A heavy wire screen is also installed downstream of the test section to prevent damage to the fan blades or turning vanes in the event of model failure during operation. The test section of the tunnel measures 45 inches by 32 inches, with corner fillets which house the test section lighting; the cross sectional area is 9.88 square feet. The contraction ratio of settling chamber area to test section area is approximately ten. The walls of the

test section diverge slightly to allow for boundary layer growth without a reduction in the freestream pressure along the test section.

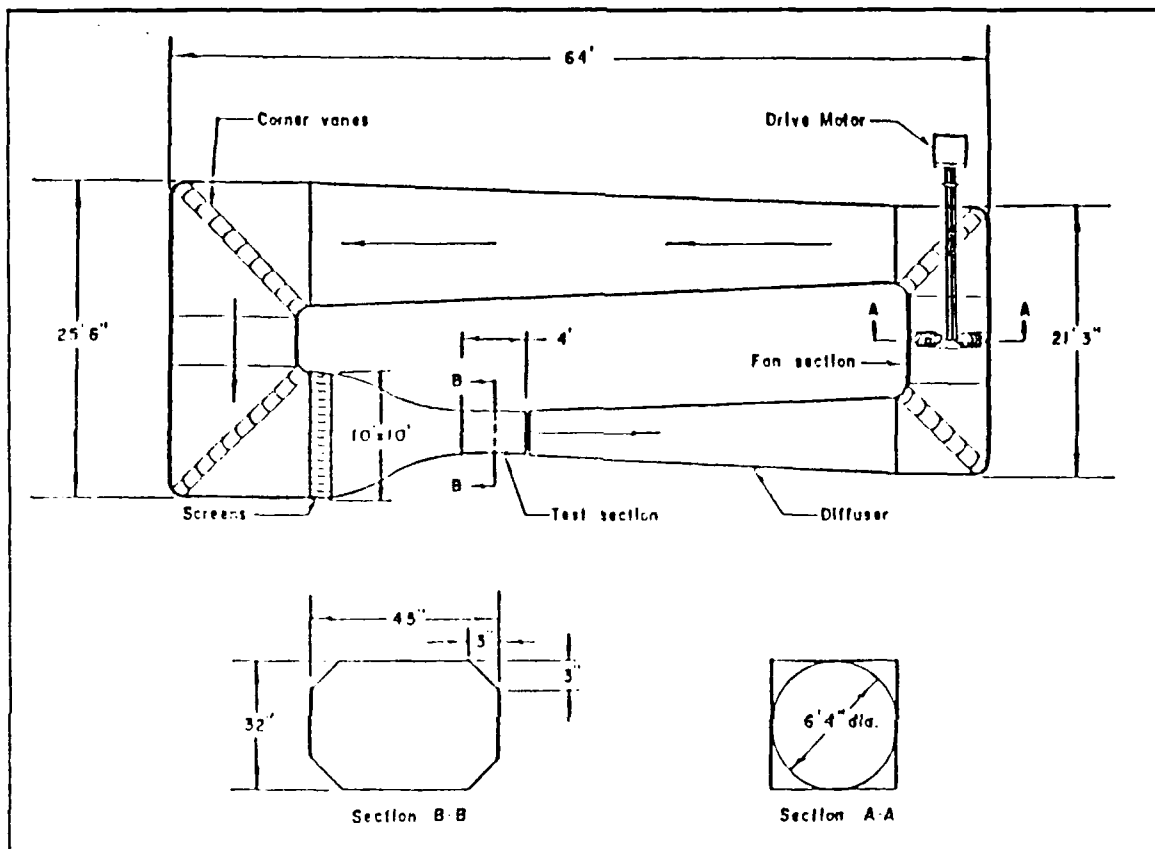


Figure 8. Naval Postgraduate School Low Speed Wind Tunnel
[Ref. 26:p. 3-7]

As the test section is designed to operate at atmospheric pressure, a circumferential breather slot is installed downstream of the test section to replenish air lost through leaks in the tunnel walls. The tunnel was designed to provide velocity up to 290 feet per second in the test section. [Ref. 26]

A reflection plane is installed in the floor of the test section, which decreases the vertical dimension to 28 inches. In the center of the reflection plane is a flush-mounted turnable for adjustments in pitch angle. The angle of the turnable is

remotely controlled with an electric motor installed beneath the tunnel.
[Ref. 26:pp. 3-3,3-4] See Figure 9.

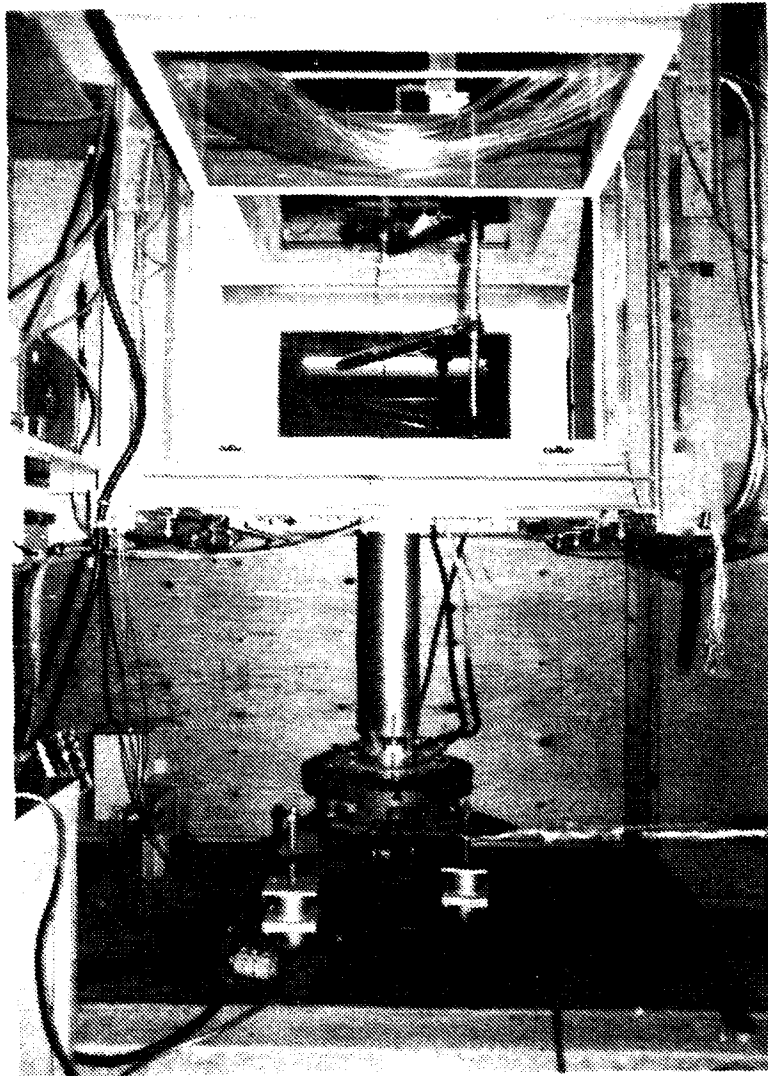


Figure 9. Turnable Assembly and VLSAM in Wind Tunnel

Flow measurement components utilized with the wind tunnel are a dial thermometer, manometer, and pitot static tube. Temperature in the wind tunnel is measured by a dial thermometer extending into the setting chamber. Dynamic pressure in the wind tunnel is measured by the calibrated static pressure difference

between the test section and the settling chamber using a water filled manometer. Static pressure in the settling chamber is measured by four static pressure taps, one on each wall , upstream of the test section to preclude interference from the model. The pressure taps at each section are connected via a common manifold prior to feeding into the manometer. The manometer measures pressure differences in centimeters of water, which is the test section dynamic pressure, and is converted to the actual wind tunnel velocity by Equation (5).

$$U_m = \sqrt{\frac{2 * 2.0475 * P_{cm \ H_2O}}{K * \rho}} \quad (5)$$

where

- U_m = measure velocity (ft/sec)
- 2.0475 = conversion factor.
- $P_{cm \ H_2O}$ = manometer reading in cm of H_2O
- K = Calibration factor¹ , 0.889 for no grid, 1.5084 for Grid #1.
- ρ = air density(lb/ft³)

A pressure transducer circuit connected to the manometer displays test section dynamic pressure on a digital readout.

2. VLSAM and Support Equipment

The VLSAM model was constructed of 6061 and 2024 aluminum alloy oy Naval Postgraduate School personnel. It is intended to model a cruciform tail-control missile with very low aspect ratio long dorsal fins. It is designed to permit force and moment measurements while operating in a subsonic wind tunnel.

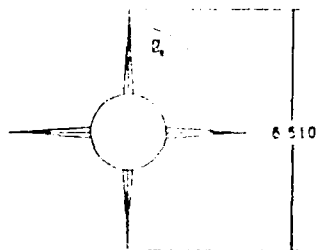
¹New calibration factor.

The body section is a hollow cylinder with locating pin attachment points for the balance gage, sleeve, wings and tails. The machined sleeve provides a close tolerance fit between the balance gage and the interior of the VLSAM model. The model is seated to the balance gage by locating pins. Body roll angle can be varied in 45° increments. Nose roll angle may be varied in 45° increments independent of the body. The nose is a pointed ogive shape. Four very low aspect ratio wings with strakes comprise the cruciform wing section and four tail control fins are mounted equilaterally in fixed position along the model axis. All parts are rigidly connected to the model body by countersunk machine screws. The surface of the VLSAM model is buffed to a polished finish and is free from protuberances. The dimensions of the model are summarized below as shown in Figure 10.

The VLSAM model support is rigidly fixed in the wind tunnel test section by the reflection plane turntable at the base and an aluminum reinforced clear plexiglass section at the top. The plexiglass sheet has slots cut to the width of $5/4$ inches and the length of 7, 8, and 10 inches. These slots correspond to the positions of length/diameter ratios of 3, 6, and 9 of the missile model, i.e., 5.25, 10.5 and 15.75 inches from the nose, respectively.

A planar survey grid, the Y-Z plane, is perpendicular to the freestream velocity and down stream 10.5 inches from the nose of the missile. The magnitude of the Z dimension is divided evenly with respect to the center line of the missile body (see Figure 11). The Y-Z dimensions for the preliminary run and the actual runs are 6.5×8 and 3×5.5 inches respectively. The step distance s are 0.5 inch and 0.25 inch for the preliminary run and for the actual runs respectively. Because of the probe measuring volume, the grid mesh could not be finer than 0.25 inch.

Total length = 22.85 in.
 Base diameter = 1.75 in.
 Length/diameter ratio = 13.06
 Ogive nose length = 4.0 in.
 Ogive/diameter ratio = 2.29
 Wing span/root chord = 3.13 in./13.55 in.
 Tail span root chord = 5.50 in./1.70 in.
 Center of pressure = 13.5 inches aft of nose tip (approx.)



NAVAL POSTGRADUATE SCHOOL
 SURFACE-TO-AIR
 MISSILE MODEL

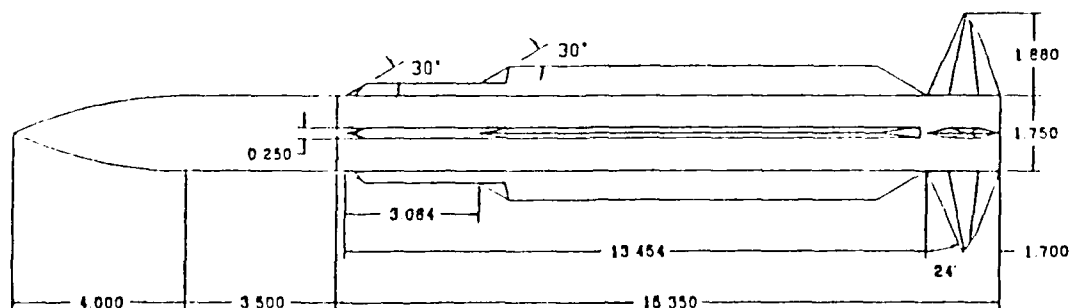
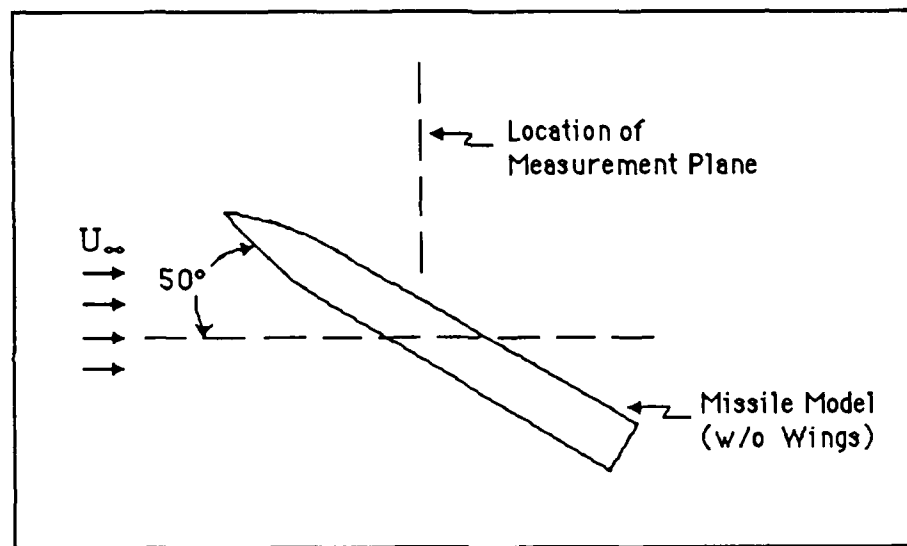
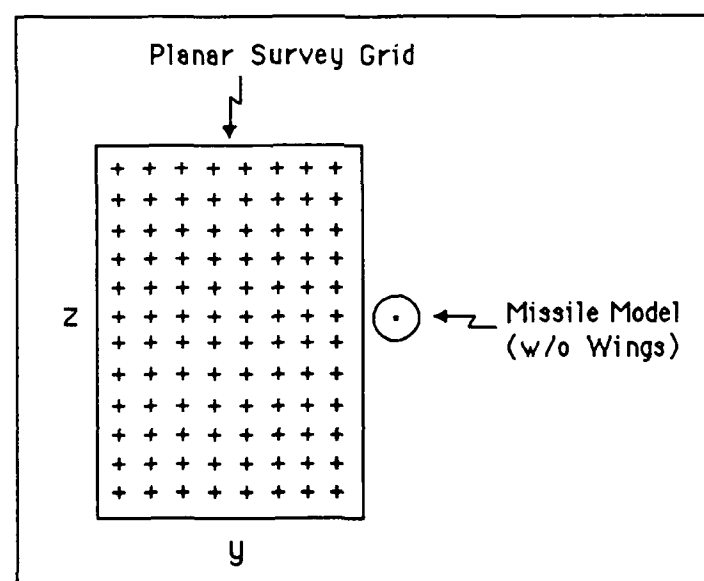


Figure 10. Drawing of VLSAM Model and the Specification [Ref. 3]



(a) Top View



(b) Front View

Figure 11. The Planar Survey Grid.

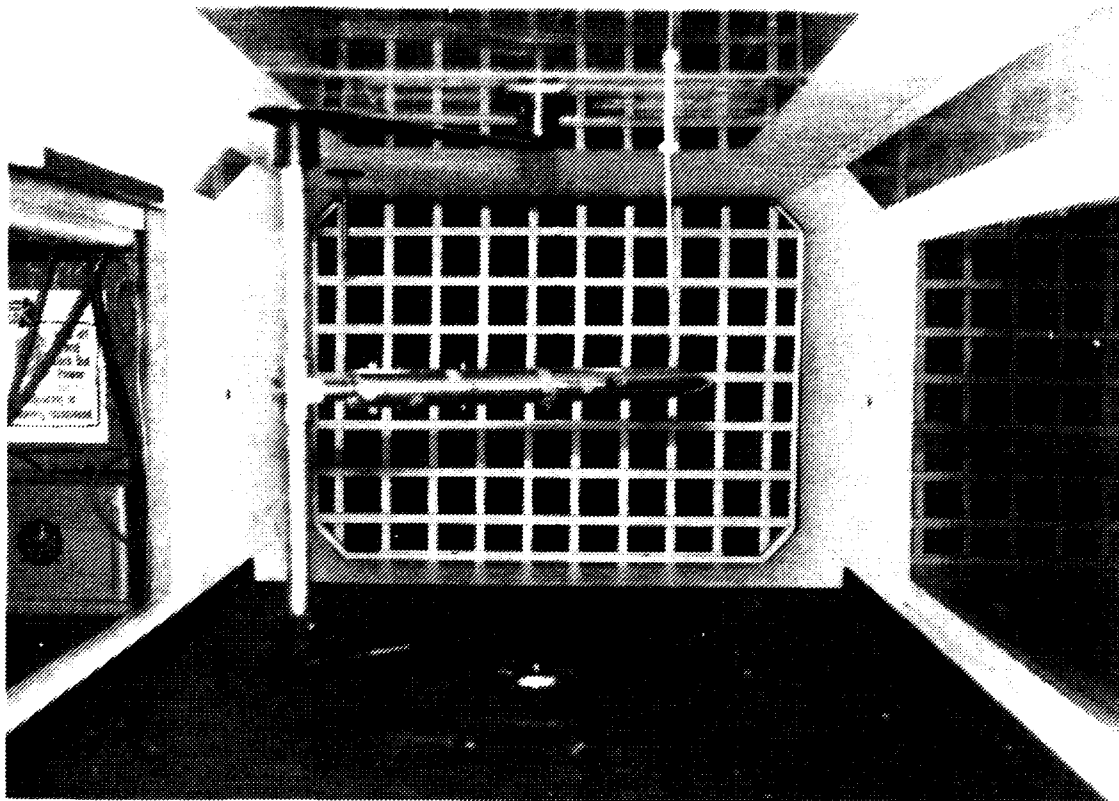


Figure 12. VLSAM Model with Support Equipment and Pressure Probe in the Test Section (without Wing)

The sting model support changes model pitch angle via a chain gear drive powered by an electric motor in the horizontal direction with the pivot point coinciding with the approximate center of the VLSAM model (see Figure 12).

3. Velmex 8300 3-D Traverser

The Velmex 8300 is a 3-D traversing system using three microcomputer-controlled stepping motors (one for each axis of movement). The system is composed of the motor controller assembly and the traversing assembly as shown in Figure 13(a),(b).

A 5-hole pressure probe was attached to the 8300 control drive. It can accurately and effectively move the pressure probe through the test section. The

motor controller assembly is the interface unit between the operator and the motors. The controller is capable of interpreting motor movement commands from a host computer, programmable control, or terminal. Data communication between a terminal and the controller assembly is made through a full-duplex RS-232C port located on the front of the controller assembly. Manual motor movements are input via switches also located on the front panel.

The resident BASIC interpreter software program contains the necessary motor movement subroutines and is responsible for monitoring motor status. Fault

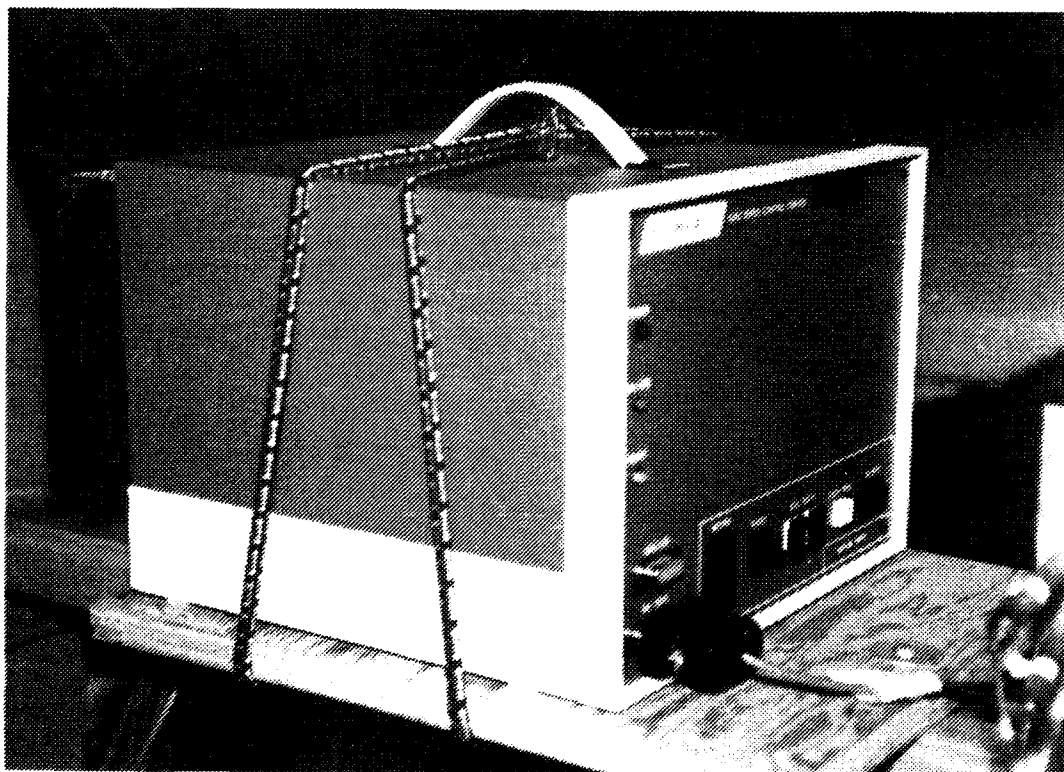


Figure 13(a). Velmex 8300 3-D Traverser -- Motor Controller Assembly

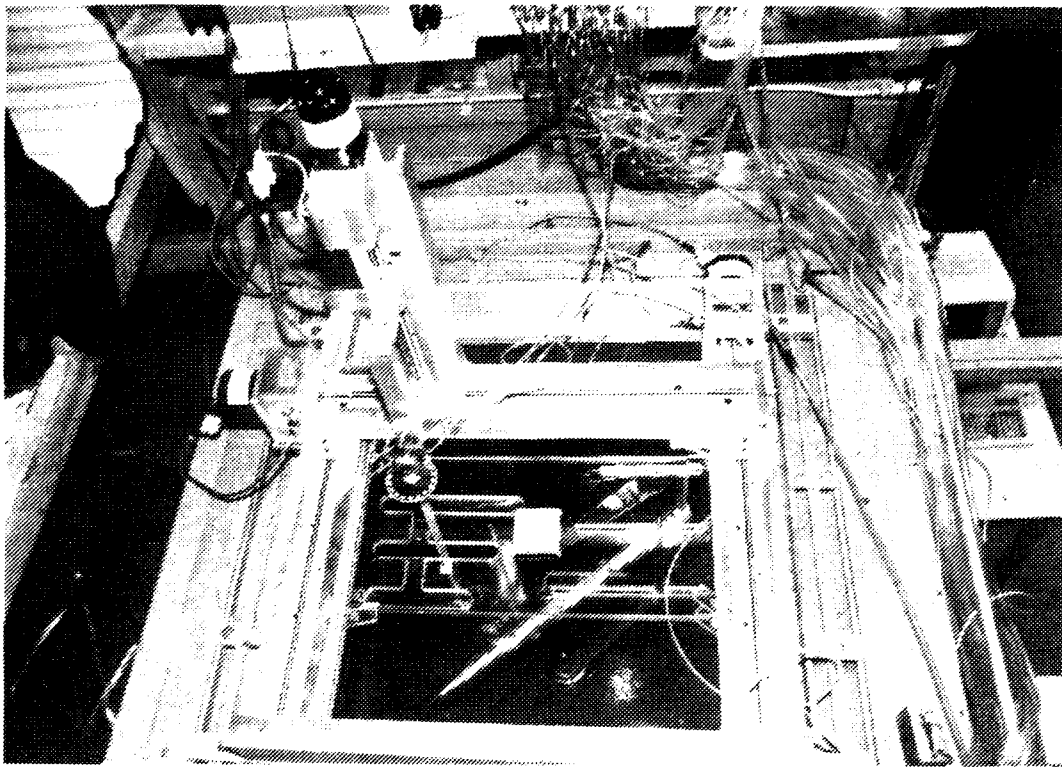


Figure 13(b). Velmex 8300 3-D Traverser -- Traversing Assembly lights on the front panel indicate parity or data bus errors and a ready light indicates the previous motor movement is completed and the controller is ready to accept the next input. Additionally, the controller has 12k of custom firmware for interactive motor control. The combined 20k of ROM is contained on a 6502 based microcomputer along with 4k of RAM. Operator-selectable motor variables, accessible through software commands, include motor velocity, motor acceleration, increment distance, and incremental unit (motor steps or inches) [Ref. 27].

The traverser assembly is a stainless steel and aluminum assembly consisting of three separate motor / jackscrew assemblies. Each motor/jackscrew

moves the traverser along one of the axes depending on the connections made to the controller. Each motor is a 200 step per revolution, 10 amp stepper motor with a maximum velocity of 3000 steps/sec. Minimum motor movement is one motor step (1/200 of a revolution) which equates to approximately 0.000125 inch. [Ref. 27]

An extension aluminum bar was attached to the base of the traverser and mounted to existing hardware located on top of the tunnel. The assembly was mounted in a position such that tunnel-induced vibrations on the traverser were minimized. Additionally, a thin vertical extension bar was inserted behind the probe tubing to reduce the pressure probe vibrations due to the high dynamic loading in the high velocity airstream.

Motor movement were controlled via the controller assembly from an IBM PC/AT computer located adjacent to the tunnel. The program for traverser movement will be discussed in detail in the software section.

4. Scanivalve

One 48-port scanivalve was used to measure each of the 5-hole pressure probe pressures.(See Figure 14.) The scanivalve was used because it provides an economical means of sensing the pressures of a multiple number of sources. It also simplifies calibration procedures in that only one transducer needs to be calibrated.

The scanivalve mechanism puts out a 7-bit binary coded decimal (BCD) signal that corresponds to the port (1-48) currently connected to the scanivalve transducer. This arrangement allows remote, electronic monitoring of the configuration of the port assembly of the scanivalve.

The scanivalve consists of two separate units. One unit contains the transducer, motor drive, and port assembly. The second unit houses the solenoid controller. Control of the scanivalve is accomplished through the solenoid

controller. The solenoid controller allows two commands, STEP and HOME. STEP "steps" the scanivalve one port location. HOME command sends the scanivalve to port number 48. (See Figure 15.)

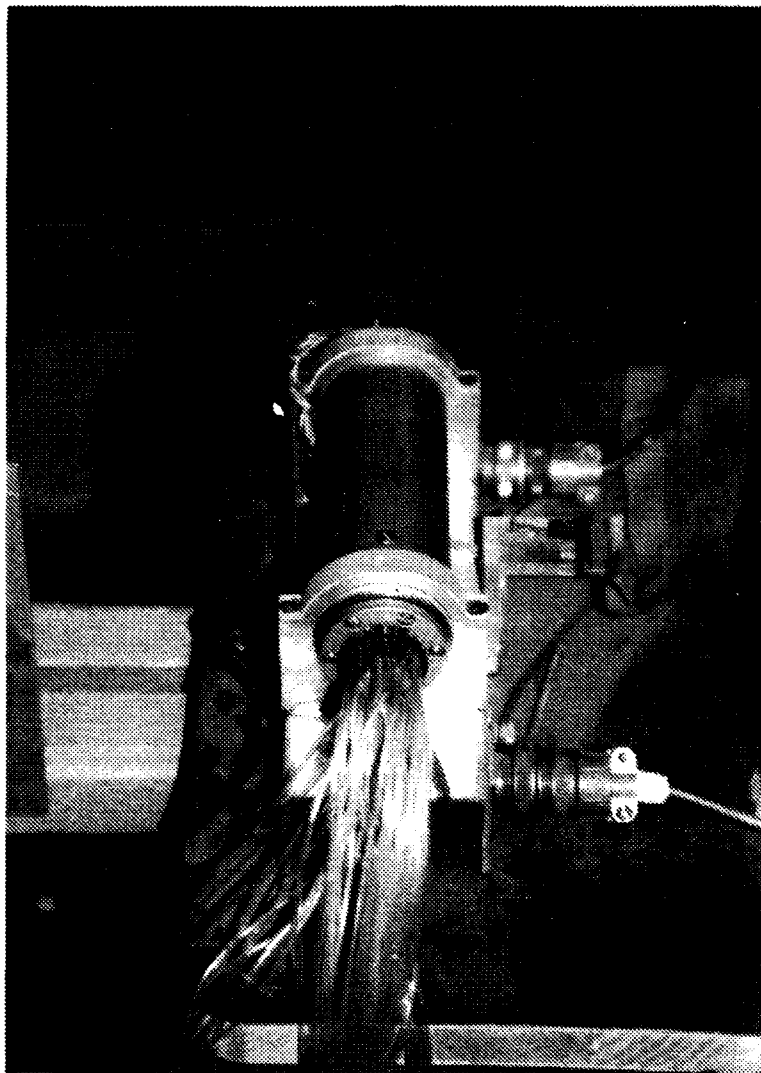


Figure 14. 48-Port Scanivalve

Computer control is accomplished through the solenoid controller by means of the Hewlett-Packard (HP) Relay Actuator. It will accept a 15 voltage pulse to either STOP or HOME.

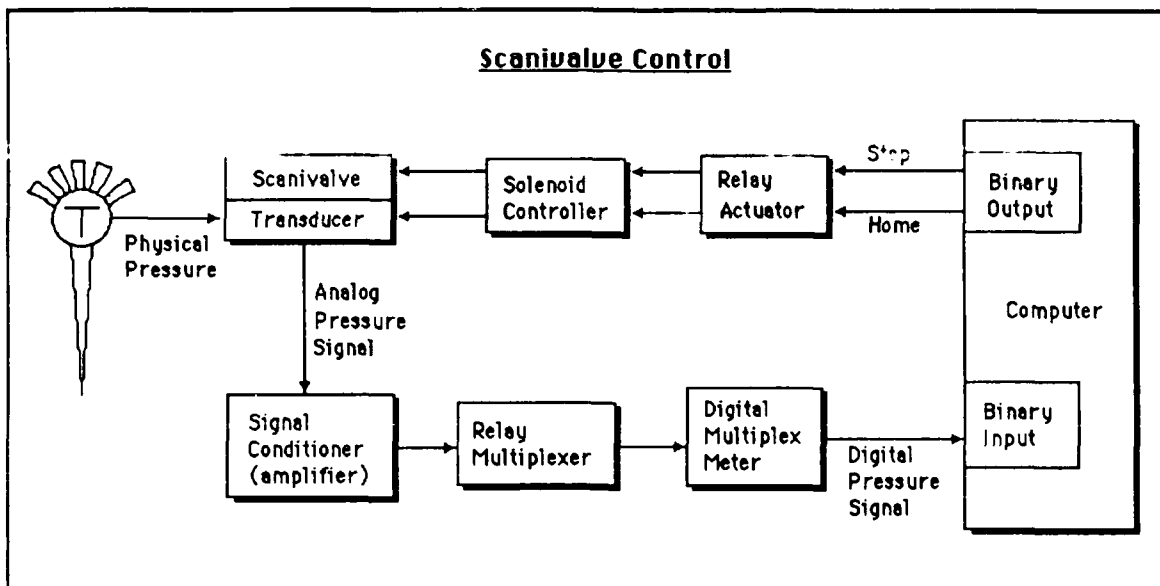


Figure 15. Scanivalve Control

The signal path for the scanivalve, containing information about the 5-hole probe port pressure, passes through the signal conditioner/amplifier to the Relay Multiplexer; then the values measured by the HP Digital Multiplexer are sent to the computer. The signal is conditioned by a low pass filter with a cut off of 10Hz. This removes most of the noise, including power line interference, prior to being measured of the HP Digital Multiplexer. The transducer signal is fed through a 1000 gain low noise amplifier to improve resolution for small magnitude signals. The HP Digital Multimeter converts the analog voltage signal into a digital signal for use by the data acquisition program named "PPROBE." An IBM-AT microcomputer executes the the PPROBE software and stores the collected data in the consecutive files.

5. Turbulence-Generating Grids

The turbulence grids were designed for use in the low speed wind tunnel to generate turbulence in varying intensities and length scales [Ref. 2]. (See

Figure 16). Each grid was mounted in a wood frame, which was placed 73 inches ahead of the pivot axis of the model support system (see Figures 17).

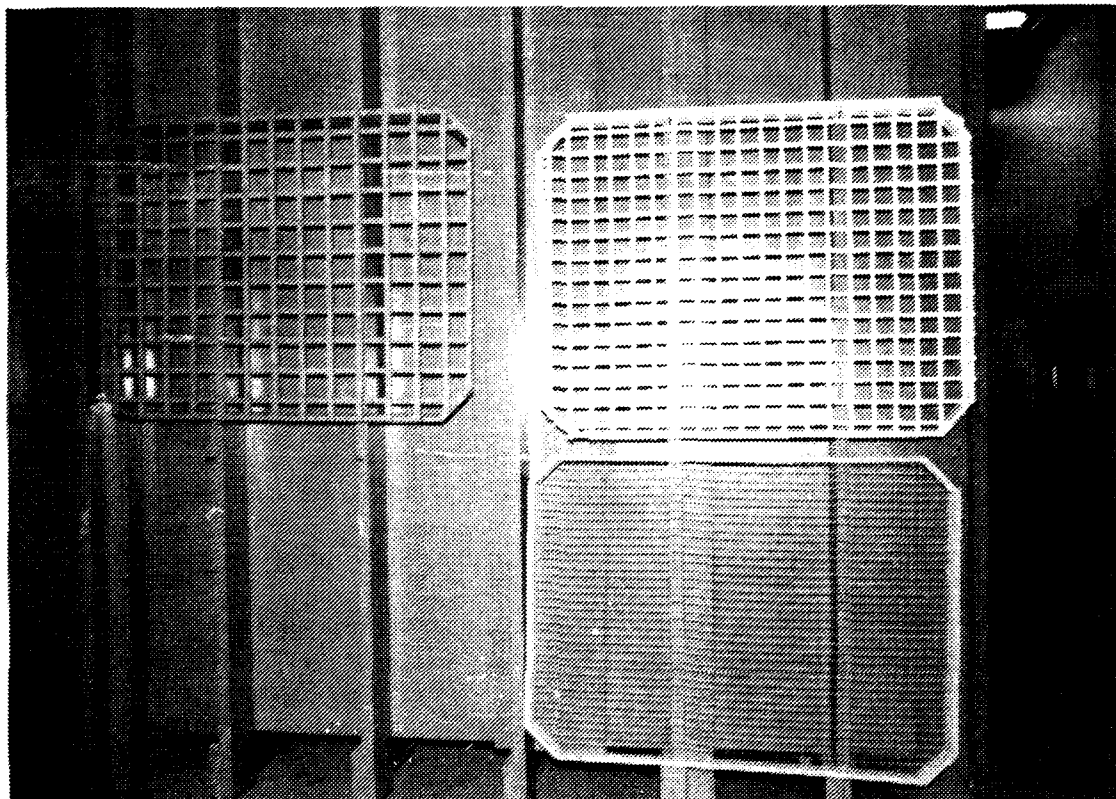


**Figure 16. Turbulence Grids 2, 3, and 4, Clockwise from the Left
Grid 2, 3, and 4**

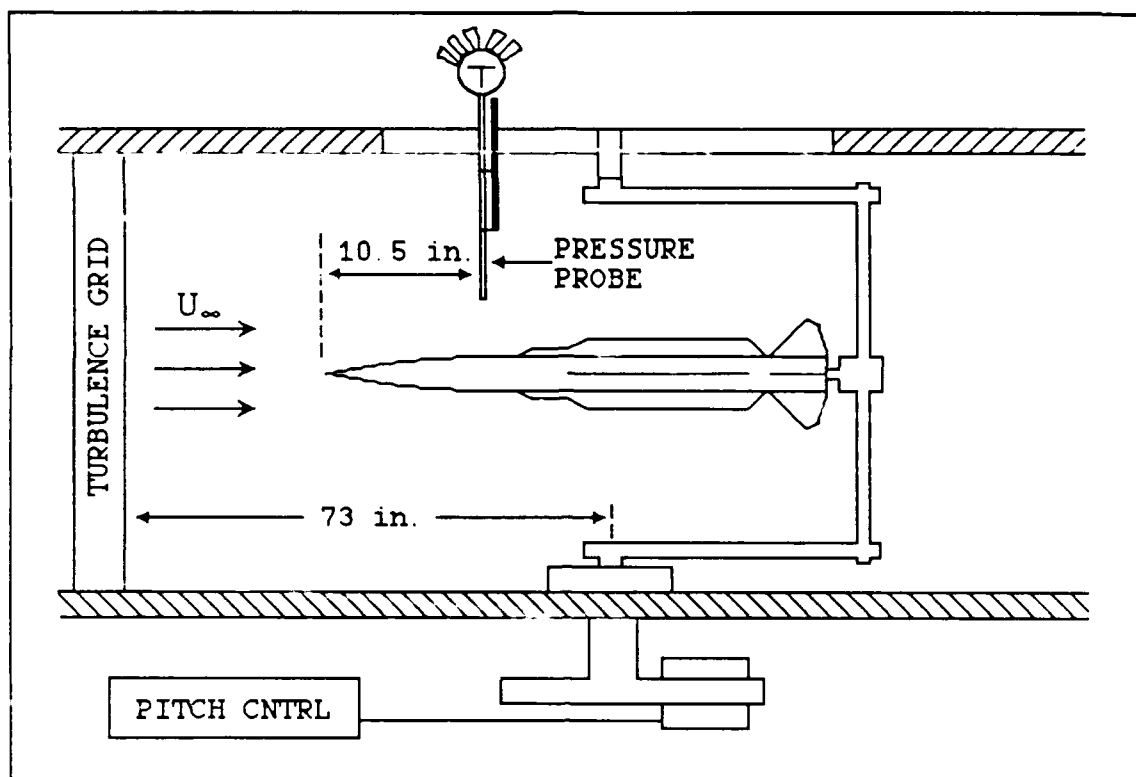


Figure 17. Planview of VLSAM Model and Pressure Probe in the Test Section (not to scale)

TABLE 1. GRID SPECIFICATIONS¹

Grid	Mesh Width (in.)	Bar Diameter (in.)	Mesh/Diameter	Material
One	5.00	1.00	5	Wood
Two	3.75	0.75	5	Wood
Three	2.50	0.50	5	Wood
Four	1.00	0.0625	16	Wire

The specifications for the four grids are listed in Table 1 and Figure 18. Three of the four grids are square-mesh square-bar and fabricated from wood.

¹[Ref. 2:p. 28]

They employ bi-plane construction which generates nearly isotropic homogeneous turbulence. The fourth grid is also square-mesh, but was fabricated from round wire. Turbulence intensities and length scales for each of the grids were determined by Roane [Ref. 2] and are shown in Figures 19 and 20.

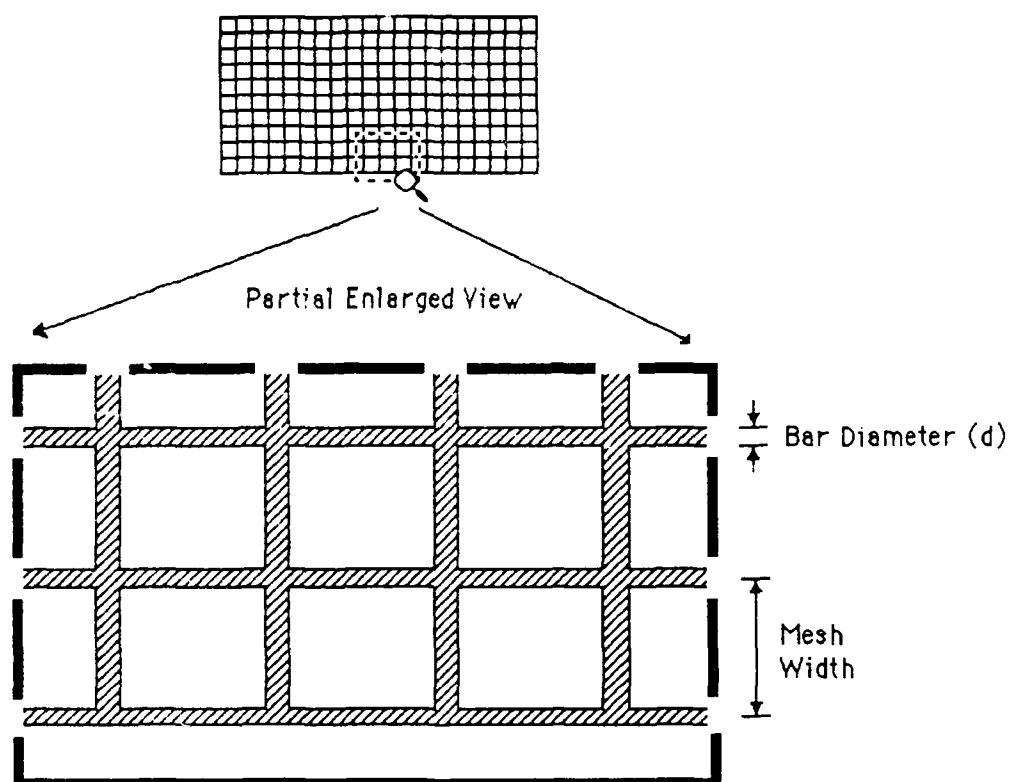


Figure 18. Square-Mesh Turbulence-Generating Grid

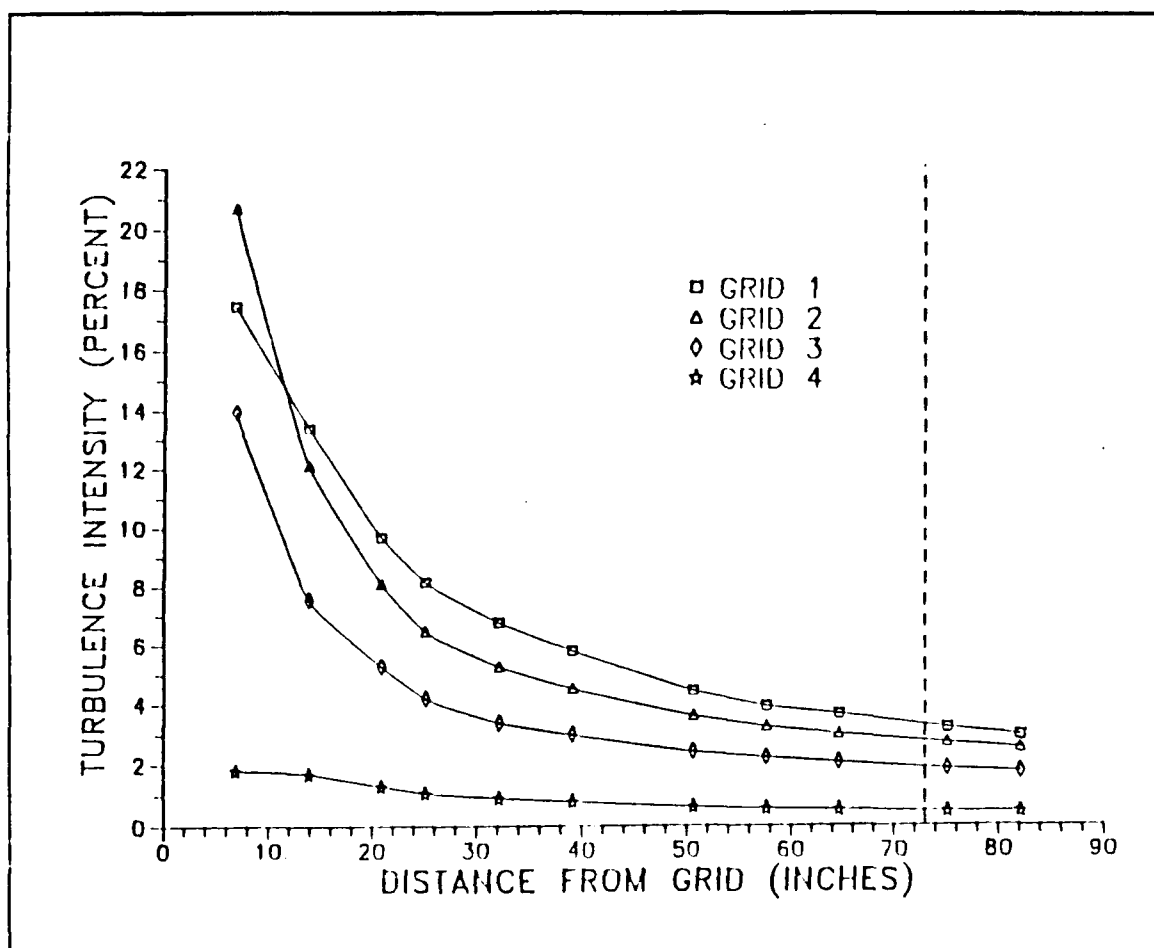


Figure 19. Grid Turbulence Intensity²

²The dashed line indicates the model pivot axis. [Ref. 2:p. 45]

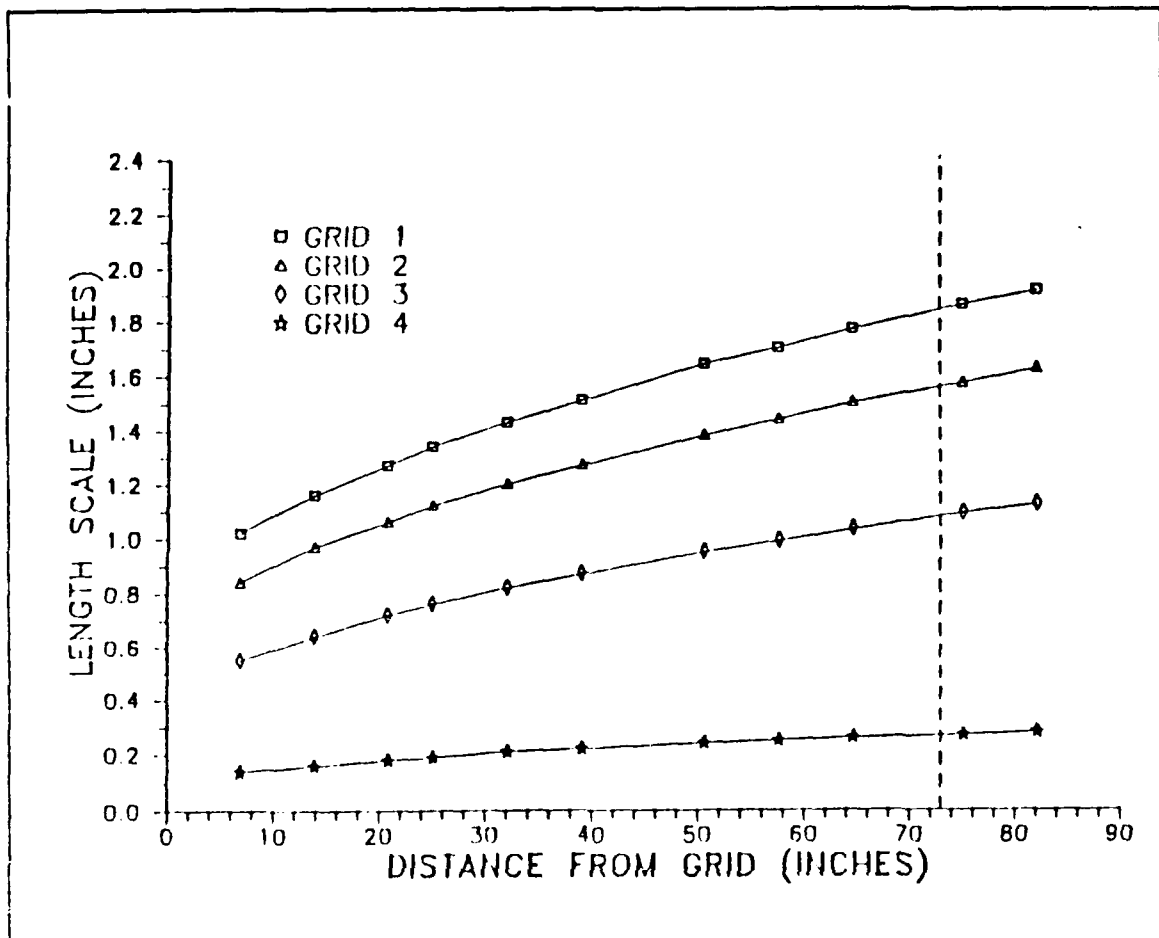


Figure 20. Grid Turbulence Length Scales³

The dynamic pressures shown in Table 2 are the actual dynamic pressures in the test section from Roane [Ref. 2, p. 44-49]. The conclusion from Rabang [Ref. 3] was that the effects of the grid generated turbulence with regards to changing length scales at constant intensity or changing intensities with constant length scale could not be investigated with the present grid turbulence parameters.

³The dashed line indicates the model pivot axis [Ref. 2:p. 48]

**TABLE 2. GRID TURBULENCE PARAMETERS: AT THE MODEL
PIVOT AXIS⁴**

Grid	Intensity (percent)	Length Scale (in.)	Turbulence/ Model Dia.	Dynamic Pressure (lb./ft ²)
One	3.31	1.84	1.05	15.35
Two	2.78	1.56	0.89	14.88
Three	1.88	1.08	0.62	16.38
Four	0.47	0.27	0.15	15.61
None	0.23	-	-	15.85

6. 5-Hole Pressure Probe

Since the local flow angles are high just outside of the vortex core, and the 3-sensor hot wire probe is limited to flow angularities of no more than 45°, from the results of experiments by Naik it was shown that a pressure probe is useful to measure the flowfield where the flow angularity is high (typically greater than 35°) [Ref. 28]. The data from the pressure probe can be reduced to obtain the distributions of local total pressure, static pressure and velocity vectors simultaneously. The wide measurement range is the chief advantage the pressure probe has over other measuring devices. A 5-hole pressure probe is used in this experiment. The disadvantage is the limitation of time-averaged measurements.

The 5-hole pressure probe is made of corrosion resistant non-magnetic stainless steel silver bragged. It is 0.125 inch in diameter and 24 inches in total length with 22 inches of reinforcement tubing. There are five take-off tubes with a reinforcement block on the top. At the measuring tip is a five hole prism shaped

⁴[Ref. 2:pp. 44-49]

measuring section. (See Figure 21) The pressure probe gives the data of pitch angle, yaw angle and velocity. More details can be found in Ref. 29. The pressure data was reduced to obtain isobars of total pressure coefficient and static pressure coefficient, and to map the crossflow velocity vectors.

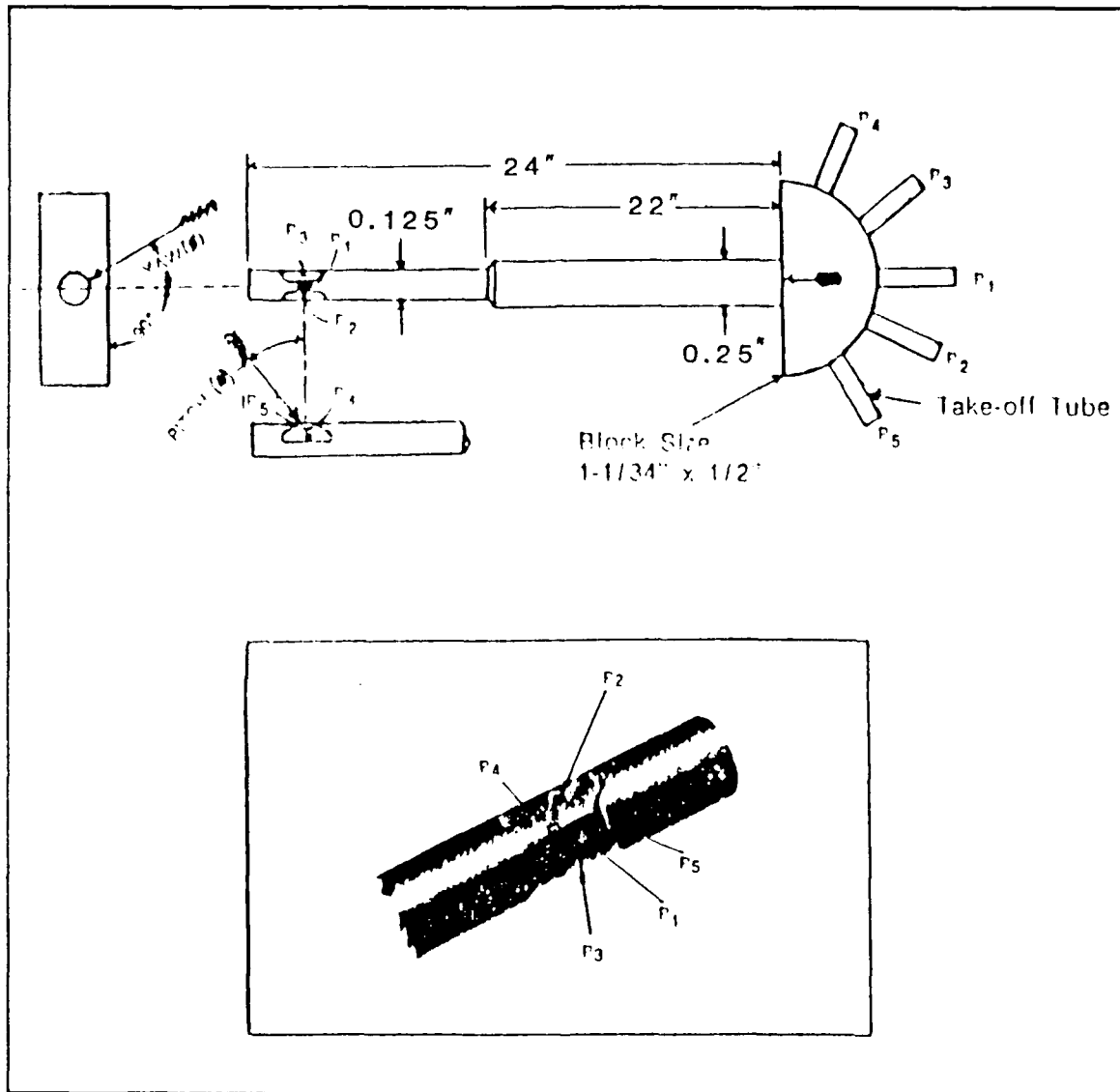


Figure 21. 5-Hole Probe and its Measuring Tip [Ref. 29]

The speed of reading depends on the length and diameter of the pressure passage inside the probe, the size of the pressure tubes to the manometer, and the displacement volume of the manometer. The time constant increases rapidly for smaller diameter tubes. The diameter of tube used in this experiment is 1/4 inch O.D. and the length of the tubes are three feet, so the time delay is about 0.15~0.26 second.

7. HP Data Acquisition System

The HP data acquisition system consists of a combination of hardware and software that allows the IBM PC-AT computer to act as a fully automated instrumentation system. [Ref. 29] The individual HP instruments used in this thesis include the Relay Multiplexer, Digital Multimeter and Relay Actuator. (See Figure 22.) Each of the instruments can be operated manually at the computer screen by means of the mouse control.

In this mode the instrument's operating controls and functions, as well as digital displays, are relayed to the computer screen. Instead of user interaction with the instrument's controls and indicators, each unit is manipulated by the computer mouse controller.

In addition to the manual mode, the HP data acquisition system can be operated in the program (Basic) mode. This method is employed in this thesis. A program was written in the advance Basic language (BASICA) that called up each instruments and its function as necessary. All data acquisition related to the VLSAM wind tunnel experiment was accomplished by the use of the BASICA program.

The Relay Multiplexer provides one common output channel which in turn can be read by the Digital Multimeter.

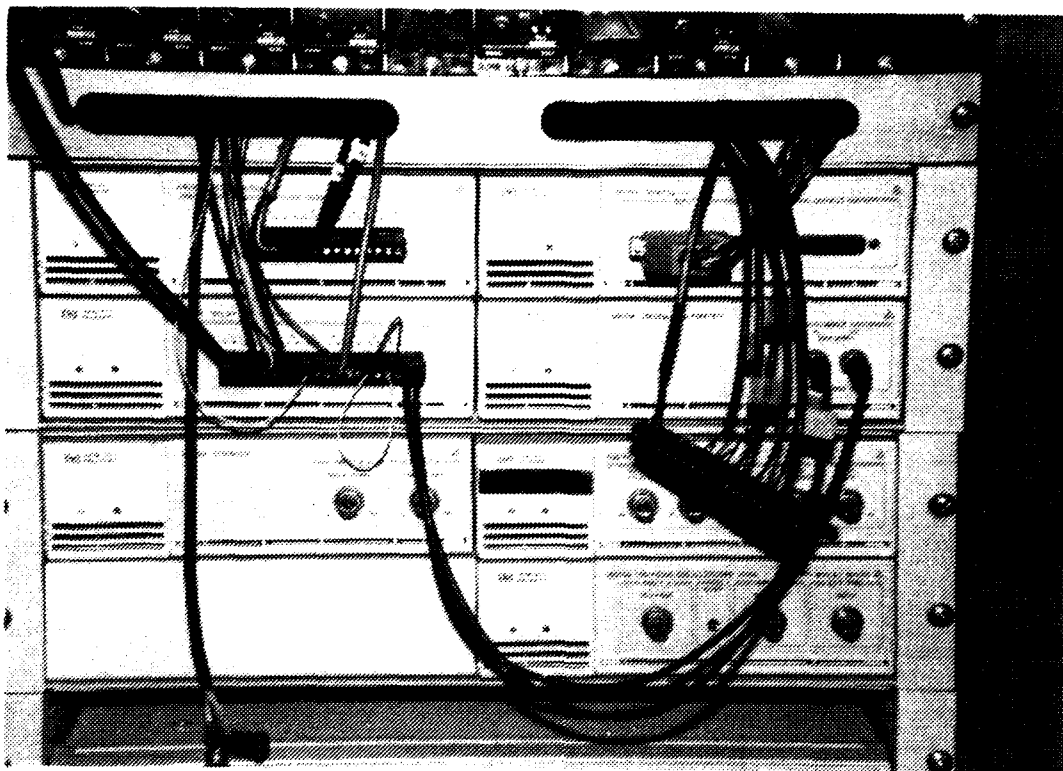


Figure 22. HP Data Acquisition System

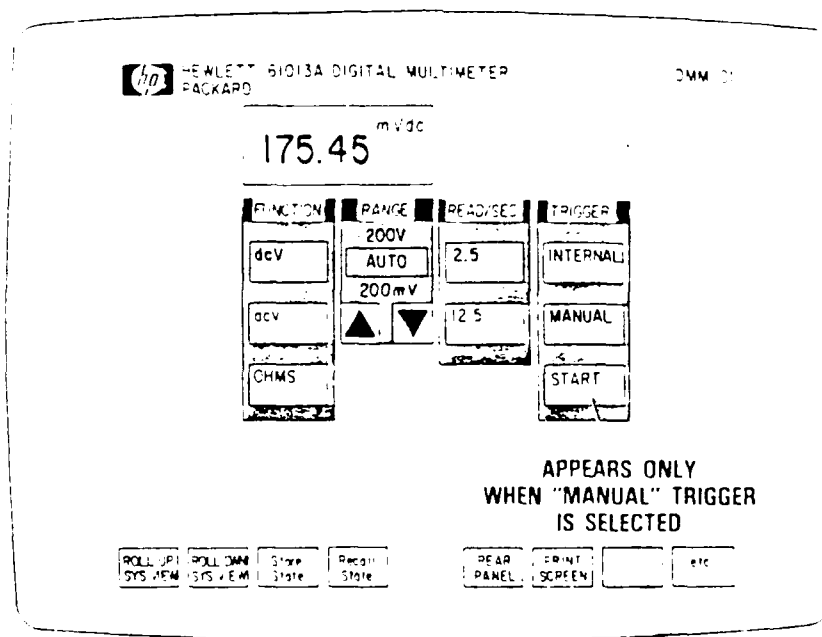


Figure 23. Digital Multimeter (DMM) Soft Front Panel. [Ref. 30]

The Digital Multimeter (DMM) can measure + or - DC voltages, AC voltages and Ohms. In this thesis only the DC voltage measurement function is used. An auto range is used in which the DMM selects the optimal range for the signal that is being measured. The DMM automatically converts input analog voltage signals into a digital (or binary) form which can be read by the computer. The DMM has a continuous data sampling rate of 2.5 or 12.5 readings per second and the higher sampling rate, 12.5 readings per second, with a accuracy of $\pm 0.05\%$ of the input voltage, is used throughout the experiments. (See Figure 23.)

The Relay Actuator is used solely in controlling the scanivalve to STEP or HOME.

The whole setting combined with the 3D-traverser, scanivalve, 5-hole pressure probe, HP data acquisition system and IBM PC AT is shown in Figure 24.

B. EXPERIMENT SOFTWARE

Several programs were used for data acquisition, data reduction and plotting in this experiment. The relation between those programs is shown in Figure 25. Each of them is discussed as follows.

1. PPROBE Program

The BASICA application program that runs the VLSAM experiment is composed of three parts.

a. STATE.FILE

The first is called a STATE.FILE. The statefile is a program automatically compiled by the HP Soft Front Panel software. It tells the computer what configuration each unit was left in when the instruments were last used (i.e., Relay Multiplexer was set for channel one as the input and the output device was

enabled etc.) The statefile in use in the VLSAM laboratory is named PGMSHEL.HPC and is located in the Lung sub-directory on the computer's fixed C-disk. [Ref. 30]

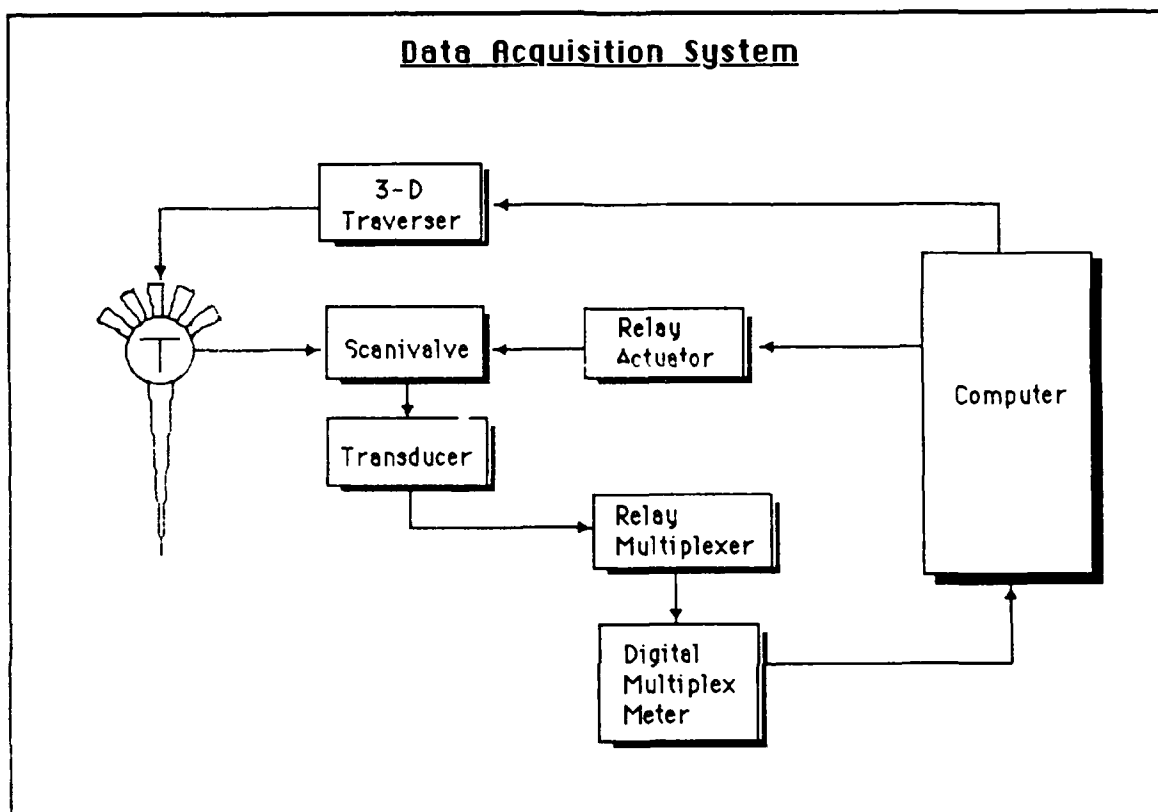


Figure 24. Whole Hardware Setting

b. PGMSHEL

The second part of the BASICA application program is called PGMSHEL. PGMSHEL consists of BASICA program lines that perform initialization chores to allow communication between the HP instruments and the IBM computer. In essence, the PGMSHEL allows the computer to know every function available at each of the data acquisition instruments. When one of these functions is called up in the BASICA application program the computer already

"knows" that function exists and where to find it. PGMSHEL, like the STATE.FILE, is, created by the HP system soft Front Panel Software.[Ref. 30].

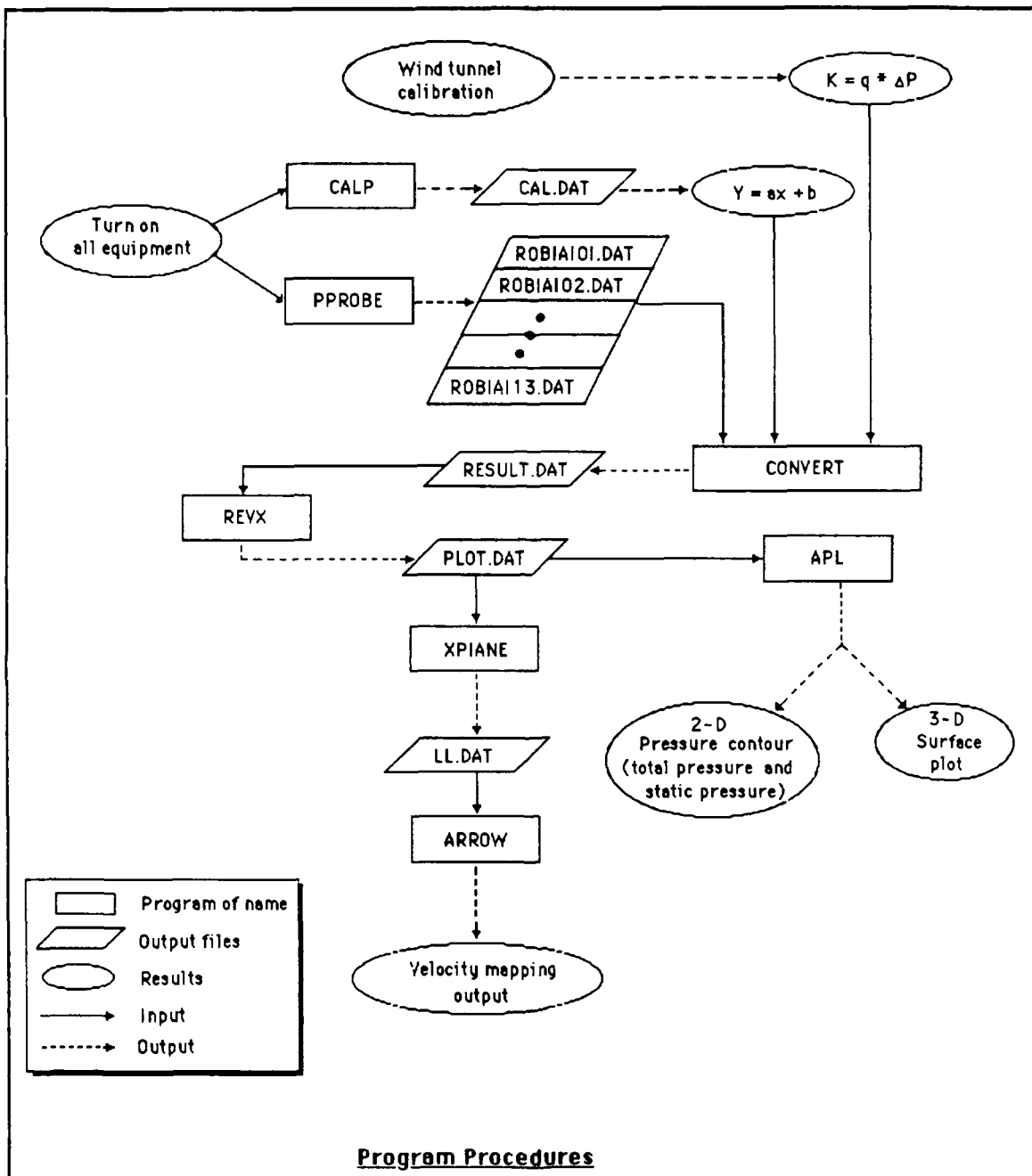


Figure 25. Program Procedures

c. Traverser

The third part of the BASICA application program is the actual application code. PGMSHEL occupies lines 1 through 999. The application code starts at line 1000 and begins to run only after all system initialization is completed. The application code consists of a combination of HP instruments statements with BASICA keywords, the scanivalve control program and the traverser program.

The traverser program was originally written by Kindelspire [Ref. 31] in Advanced Basic (BASICA) language to serve as the interface between the operator and the motor controller assembly. It allows the operator to control precisely the pressure probe movement via the 3-D traverser controller unit. It consists of manual input (meaning one motor movement for each operator input) and computer-controlled movement. It was minimally modified by the author in manual input and the author developed a new computer-controlled movement. The algorithm flow chart is shown in Figure 26 for this experiment. The PPROBE program is shown in Appendix A.

The manual movements were used to pre-position the pressure probe prior to the data collection run through the whole measured plane.

The operator first uses manual input to move the total pressure hole (P_1) of the pressure probe as near as possible in the horizontal direction to the center axis of the VLSAM model, then he moves the probe vertical down to the position where he desires to measure. This point is called the original point, which is used for the reference at each run. After pre-positioning the pressure probe to the original point, the operator selects the computer-controlled movement option. At this option, the operator is prompted to input the dimension measurement in (Y,Z) format and the step distance. All units are in inches. The program will

automatically calculate and display the number of points in the Y-direction and Z-direction and the total number of points to be measured. If the operation is satisfied, then the operator is prompted to input the name of the data file to be stored; otherwise, the program goes back to prompt the operator to re-input the dimension measurement. After the operator inputs the name of the data file, the program displays the name of the data file which automatically increases by the point number in the Y-direction with a extension, DAT. One column of data is written to a single file.⁵ The program prompts the operator to have a final check on the dimension measurement, the number of points and the name of the data file before the data can be acquired. Before the data acquisition, the operator must rotate the pressure probe until the pressure for the ports P_2 and P_3 are equal (nulling); then he inputs the yaw angle indicated by the traverser scale wheel. The first step was to move the scanivalve from port 1 to port 4⁶ via the Relay Actuator with a one second delay time which permits the pressures to equalize before the DDM samples the output voltage from the scanivalve transducer via the Relay Multiplexer.

After ten samples are taken, the Relay Actuator steps the scanivalve to the next port and the process is repeated until all the five channel pressures are

⁵If there are total $16 \times 10 = 160$ points to be measured and the input the name of the data file is TEST, then the date file will automatically increase from TEST 01. DAT to TEST 16. DAT through the whole measurement.

⁶Scanivalve port 4 is consistent with P_1 of the pressure probe and port 5 is consistent with P_2 and so on.

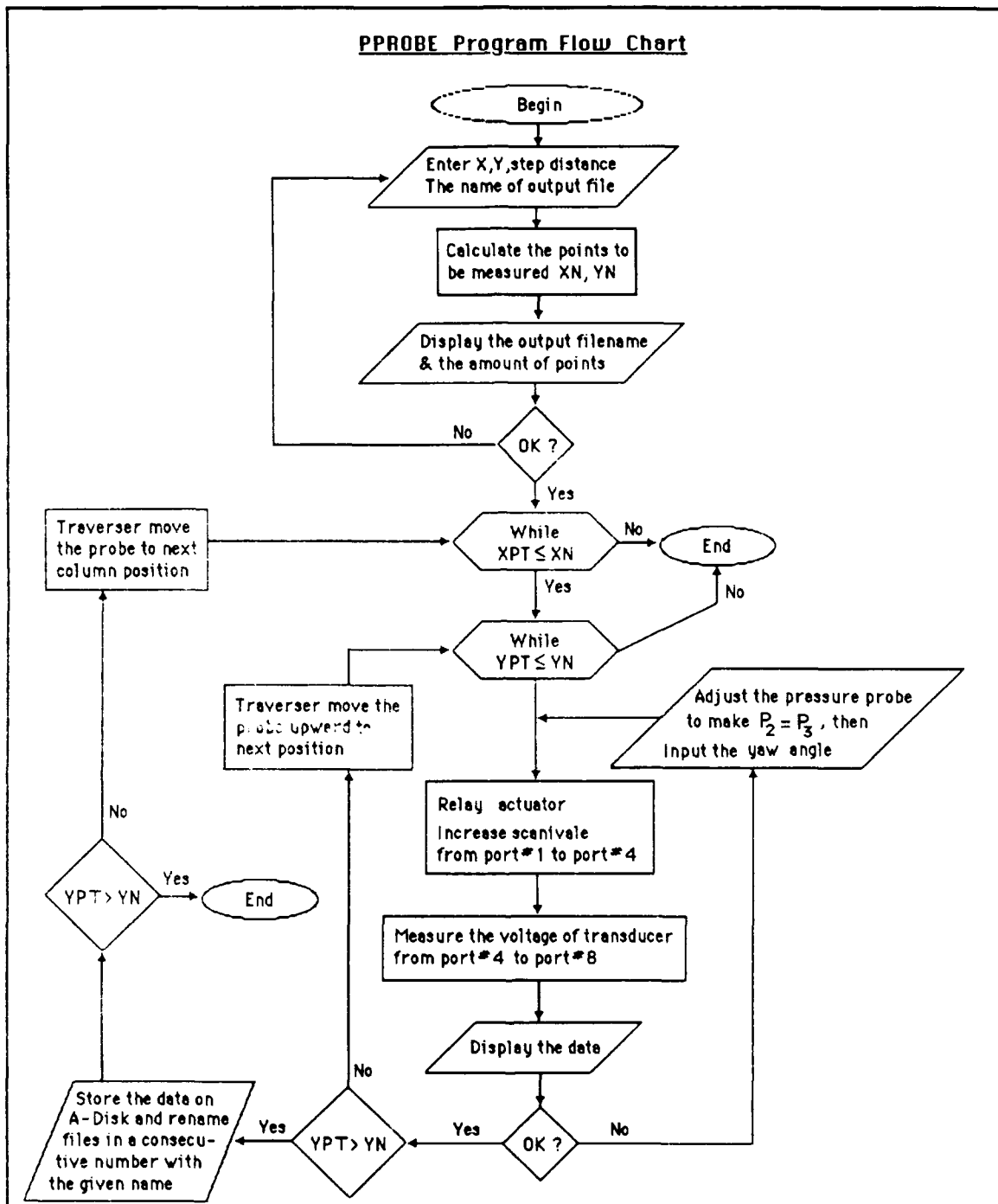


Figure 26 PPROBE Program Flow Chart

measured (i.e., from port 4 to port 8). Then the Relay Actuator homes the scanivalve to port 48. The program will show all the readings and the average

values for each channel. The program prompts the operator to check whether the data is valid or not. If not, it will remeasure; otherwise, the program will move the pressure probe upward one step automatically. It then repeats the data acquisition procedure. After the program finishes the one column data acquisition, it stores all the averaged data of each sample point in a data file, then moves the traverser to the next column position. The program repeats the data acquisition process until all the columns are finished.

2. CALP Program

Before and after each time the CALP program is executed, the transducer voltage output is calibrated by applying a known pressure source. From the output voltage and pressure data, the slope equation is calculated by curve fitting. The slope equation is used by the PPROBE program to convert the transducer voltage to physical pressure. The CALP program is shown in Appendix B.

3. CONVERT Program

The program is written by the author in Fortran. It opens a consecutive file created by program PPROBE and reads the contained data in each row and then converts the data into the Y-Z coordinates, velocity, yaw angle, pitch angle, total local pressure, the total local pressure coefficient, local static pressure and the local static pressure coefficient which is stored into a file named "RESULT.DAT" for later use by the REVX program. The CONVERT program is shown in Appendix C and the pressure probe calibration chart is shown in Appendix D. The data reduction can be divided into 5 parts for interpretation and the flow chart is shown in Figure 27.

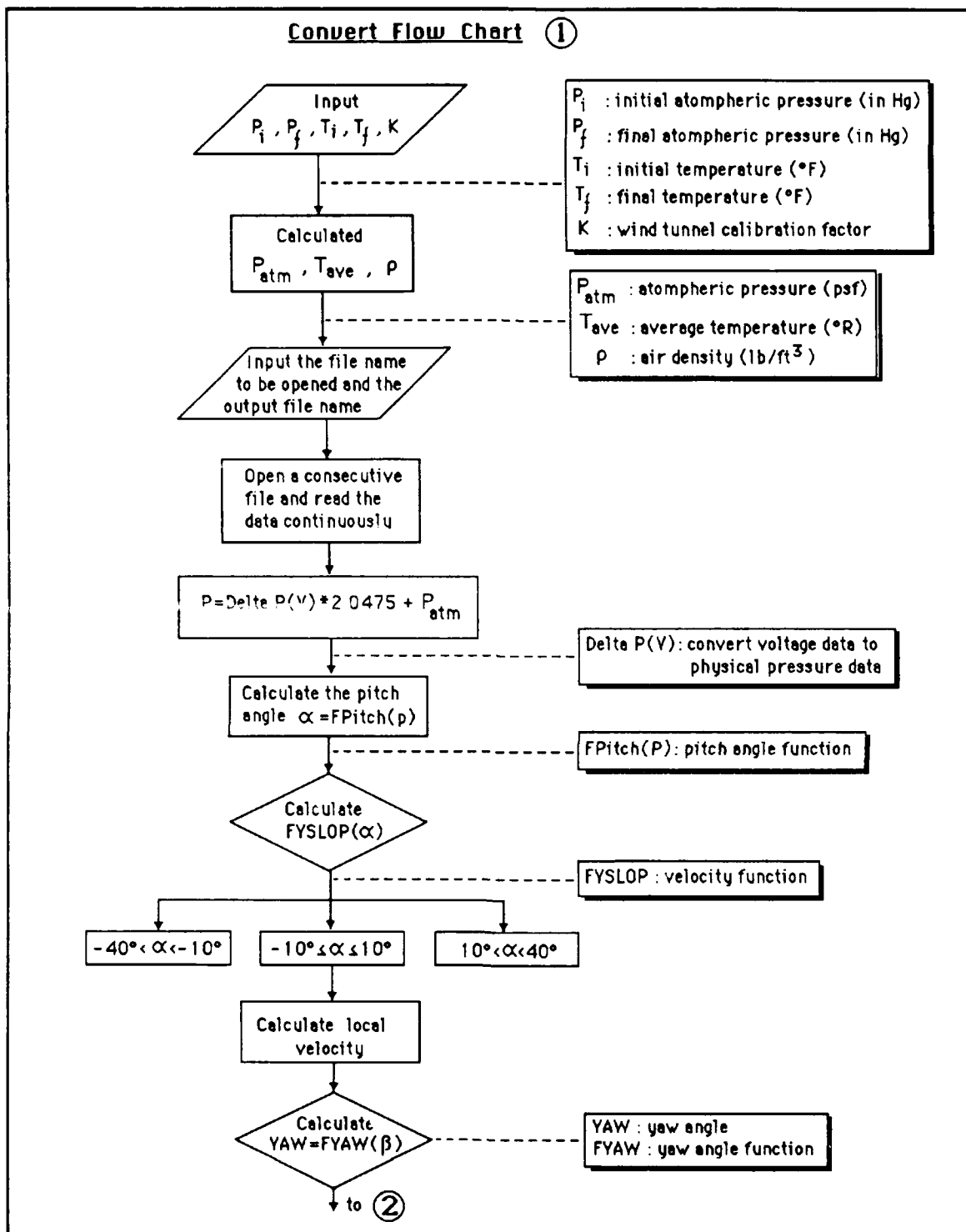


Figure 27(a) CONVERT Program Flow Chart

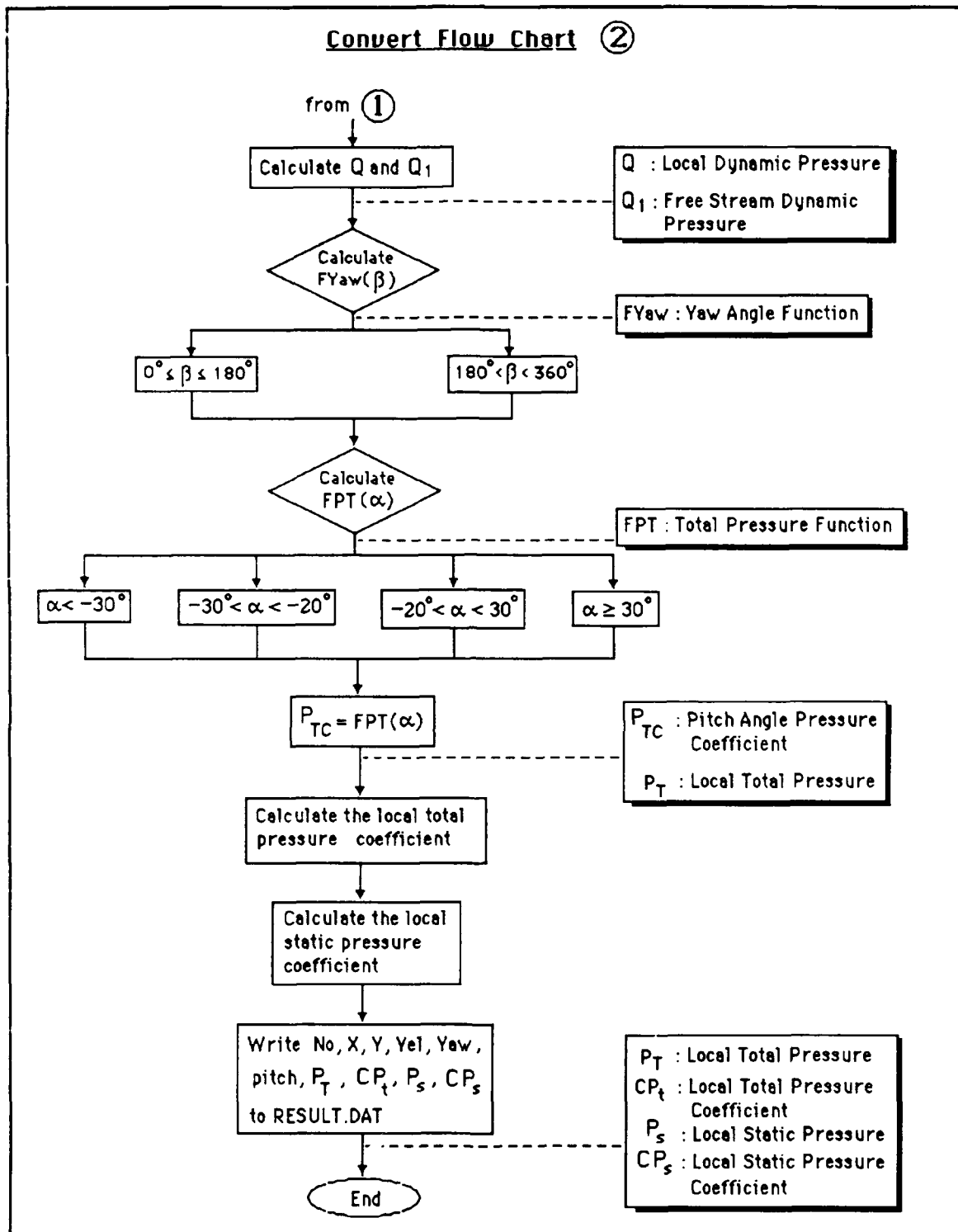


Figure 27(b) CONVERT Program Flow Chart

a. The Coordinate

The Y-Z coordinate is the same as in the original files.

b. The Pitch Angle

The pitch angle coefficient θ_c is determined by calculating Equation

6.

$$\theta_c = \frac{P_4 - P_5}{P_1 - P_2} \quad (6)$$

where θ_c = pitch angle coefficient

- P_1 = indicated total pressure
- P_2 = indicated static pressure
- P_4 = pitch angle pressure
- P_5 = pitch angle pressure

After the pitch angle coefficient is obtained, the corresponding pitch angle must be found. It is calculated by using Equation 7 which was developed by the author by using commercial curve-fitting software to fit the provided calibration chart.

$$\theta = 3.759 + 53.7568\theta_c - 1.3085\theta_c^2 - 1.6583\theta_c^3 - 0.8061\theta_c^4 - 16.5115\theta_c^5 \quad (7)$$

where

- θ = pitch angle (degree)
- θ_c = pitch angle coefficient

c. Velocity:

At any particular pitch angle, θ , the velocity pressure coefficient can be read from the velocity pressure coefficient curve on the calibration chart. The velocity pressure coefficient curve can be represented by Equations 8, 9, and 10 at

different pitch angle regions. They were also developed by the author by using commercial curve-fitting software.

At $\theta < -10^\circ$

$$V_c = 0.981 - 0.0102\theta - 3.0 \times 10^{-4}\theta^2 - 2.5 \times 10^{-6}\theta^3 \quad (8)$$

At $-10^\circ < \theta < 10^\circ$

$$V_c = 0.98 - 0.006\theta + 2.0 \times 10^{-4}\theta^2 \quad (9)$$

At $\theta > 10^\circ$

$$V_c = 0.981 - 0.0035\theta - 1.143 \times 10^{-4}\theta^2 - 5.833 \times 10^{-6}\theta^3 \quad (10)$$

where

- θ = pitch angle (degree)
- V_c = velocity coefficient

And the velocity pressure coefficient is represented by Equation 11.

$$V_c = \frac{P_t - P_s}{P_1 - P_2} = \frac{q}{P_1 - P_2} = \frac{\frac{1}{2} \rho V^2}{P_1 - P_2} \quad (11)$$

where P_t = total pressure (psf)

- P_s = static pressure (psf)
- ρ = gas density ((lb/ft³))
- P_1 = indicated pressure (psf)
- P_2 = indicated static pressure (psf)
- V = velocity (ft/sec)
- q = local dynamic pressure

Recall that

$$P_{atm} = \rho RT$$

$$\rho = \frac{P_{atm}}{R * T} \quad (12)$$

where

- P_{aum} = ambient pressure (psf)
- R = gas constant = 1718 (ft-lb/slug*R)
- T = temperature (°R)
- ρ = density (lb/ft³)

Combine Equations 11 and 12. The velocity is calculated by Equation 13

$$V = \sqrt{\frac{2V_c(P_1 - P_2)}{\rho}} \quad (13)$$

and adding the wind tunnel calibration factor, K , and the conversion factor gives the local velocity in the wind tunnel:

$$U_m = \sqrt{\frac{2 * 2.0475 * V_c * (P_1 - P_2)}{\rho * K}} \quad (14)$$

d. Pressure Coefficient

At a particular pitch angle, θ , the total pressure coefficient, P_{tc} , can also be read from the total pressure coefficient calibrate curve. At different pitch angle regions, it can be represented by Equation 15.

$$\text{At } \left\{ \begin{array}{ll} \theta < -30^\circ & P_{tc} = 0.1 \\ -30^\circ < \theta < -20^\circ & P_{tc} = 0.02 + 1 * 10^{-3} \theta \\ -20^\circ < \theta < 30^\circ & P_{tc} = 0 \\ 30^\circ < \theta < 40^\circ & P_{tc} = 0.03 - 1 * 10^{-3} \theta \end{array} \right. \quad (15)$$

where

- P_{tc} = the total pressure coefficient of pressure probe calibration
- θ = pitch angle

and

$$P_{tc} = \frac{P_t - P_{tL}}{P_{tL} - P_{sL}} \quad (16)$$

where

- P_t = indicated total pressure
- P_{tL} = Local total pressure
- P_{sL} = Local static pressure

$$P_{tL} - P_{sL} = \frac{1}{2} \rho U_m^2 \quad (17)$$

where U_m is from Equation 14. From Equations 16 and 17, both P_{tL} and P_{sL} are calculated.

Since the pressure measurements are affected by slight shifts in wind tunnel velocity and temperature, pressure coefficients are used when the local and total tunnel pressures are compared and they are non-dimensionalized by the tunnel dynamic pressure. These coefficient are defined below :

$$C_{pt} = \frac{P_{tL} - P_t}{Q} \quad (18)$$

$$C_{ps} = \frac{P_{sL} - P_s}{Q} \quad (19)$$

where

- Q = Freestream dynamic pressure
- P_t = Freestream total pressure
- P_s = Freestream static pressure
- C_{pt} = Total pressure coefficient.
- C_{ps} = Static pressure coefficient.

e. Yaw Angle

Yaw angle is simply read from the traverse scale wheel when the pressures of the probe tip were nulled. This value is input to the program.

f. Temperature

Temperature is taken from the average of initial and final temperature. Runs are limited in time to allow for a maximum temperature excursion of 15°F.

$$T_{av} = \frac{T_{max} - T_{min}}{2}$$

g. Pressure

Pressure is read from the barometer and was recorded before and after each run.

4. REVX Program

This program is used to reverse the Y-coordinate of RESULT.DAT and to store the data in PLOT.DAT for the XPLANE program. The REVX program is shown in Appendix E.

5. XPLANE Program

The purpose of this program is to read the data of PLOT.DAT and convert those data into the crossflow direction and magnitude for the ARROW program. The XPLANE program is shown in Appendix F.

6. ARROW Program

This program plots the crossplane velocity vector plots. The ARROW program is shown in Appendix G.

C. EXPERIMENTAL CONDITIONS

To correlate the data with those of Rabang, all the experimental conditions were kept as much like Rabang's as experimental conditions would allow.

Reynolds number, test section dynamic pressure, test section velocity and nose geometry and roll angle are kept constant as possible.

Dynamic pressures were set to match those treated by Rabang, giving a subcritical Reynolds number of $Re = 1.1 \times 10^5$.

The angle of attack was fixed at 50° to get comparative data with that of Rabang for which maximum side force occurred at the no wing and no grid conditions. (See Figure 28.)

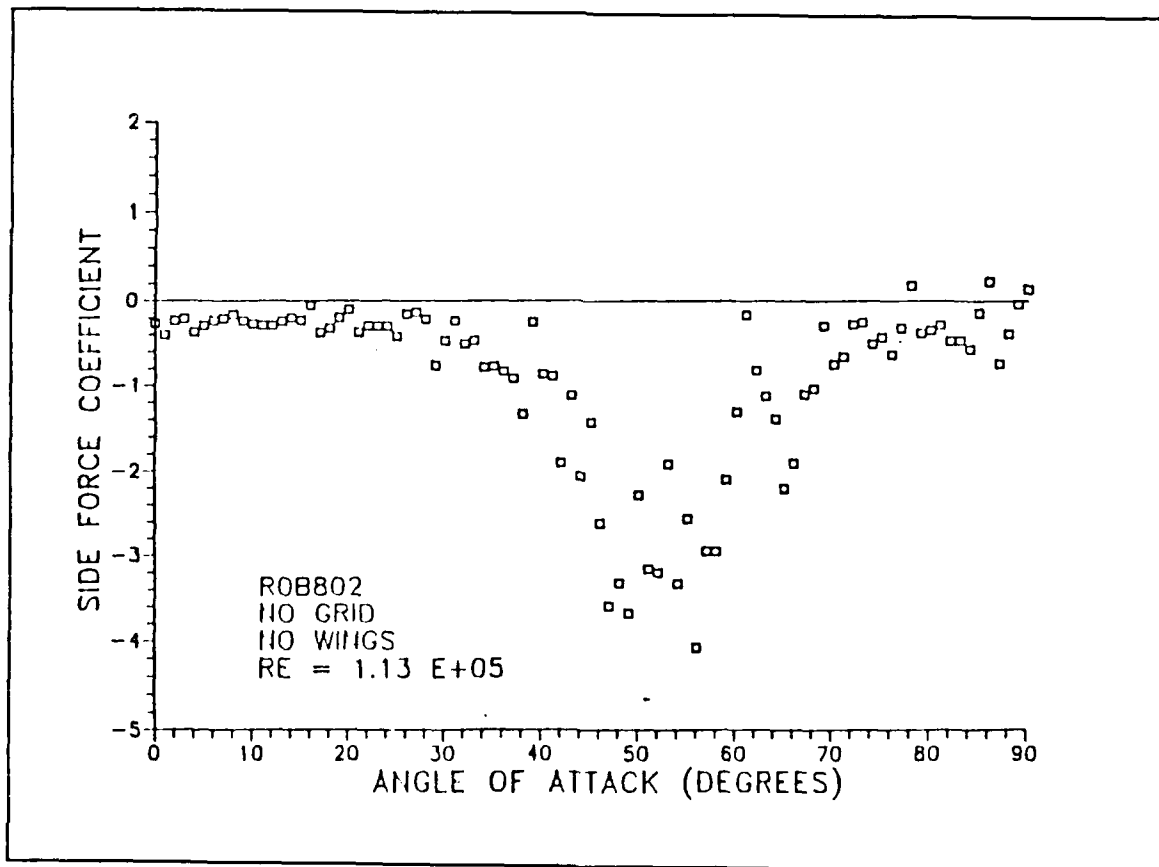


Figure 28. ROB802: Side Force Coefficient [Ref. 3]

For all cases of Rabang, the rose roll angle was held fixed. Afterbody roll angles of the reference system as shown in Figure 29 [Ref. 3].

- Body A: wings and tail at zero roll angle in a "+" configuration.
- Body B: no wings or tails, body roll angle set at $\phi_R = 45^\circ$.
- Body C: wings and tails at $\phi_R = 45^\circ$ roll angle in a "x" configuration.

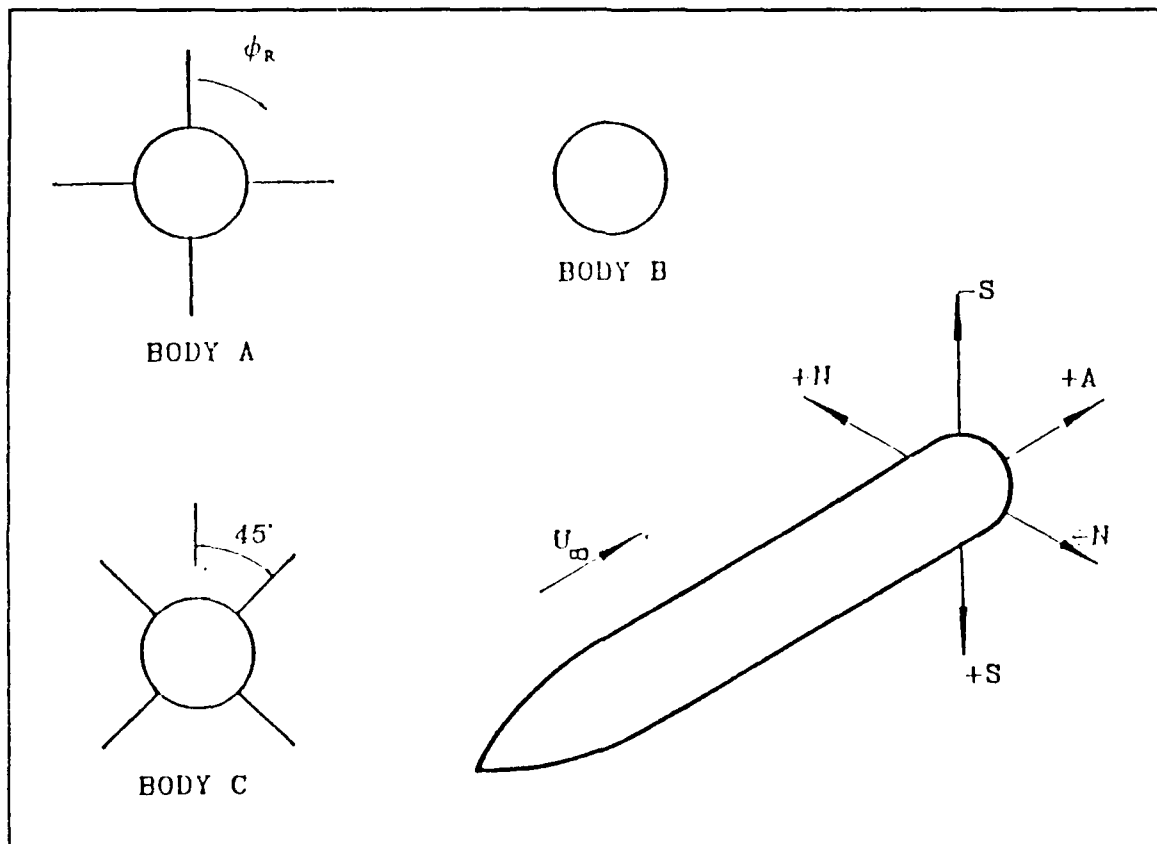


Figure 29. Body Configurations and Reference System [Ref. 3]

The longitudinal position for measurements was at a length/body diameter ratio of 6. This position equates to 10.5 inches from the nose of the missile model.

The goal of this experiment was to validate the pressure measurement system for flowfield variables with elevated levels of turbulence; to determine the location and intensity of the asymmetric vortices in the wake of the VLSAM model at a

raised level of freestream turbulence; and to display the asymmetric vortices by velocity mapping and pressure contours. The purpose is to correlate the results with the force measurements of Rabang to provide a greater understanding of the vortex flowfield.

D. EXPERIMENT PROCEDURE

1. Dynamic Pressure Calibration

For the purpose of continuing research, all of the turbulence grids were calibrated in the tunnel. Normally, the pressure difference between a set of static ports in the settling chamber and a set of static ports in the test section entrance is used to relate to the actual dynamic pressure in the test section. Because of the disturbance on the second set of static ports caused by the frames which support the grids, each grid must be tested for its own tunnel calibration constant. Readings from the tunnel calibration manometer and from a pitot-static tube inserted in the center of the test section were recorded over a speed range, and a calibration curve was generated for each grid. The calibration curves will be discussed in the Results section.

2. Scanivalve Transducer Calibration

The transducer voltage is first adjusted about zero in in milli voltage range, then the "CALP" program is run.

The scanivalve is calibrated by applying a known pressure source to the scanivalve transducer which is connected to the HP Digital Multimeter instrument. The known pressure source was provided by the calibration manometer. (See Figure 30.) The examination value of the calibration pressure is displayed on the Digital Panel Meter (DPM) (see Figure 31) and the readings are input to the

computer manually at the same time. Both transducers are referenced to an ambient pressure. A HP Digital Multimeter converts the analog voltage signal from the scanivalve transducer into a digital signal and stores the collected data into a calibration file. This procedure is performed before and after each run to measure any shifts between the initial and final readings.

These data were used to generate the calibration curve equation which relates the transducer voltage output to the wind tunnel dynamic pressure.

The calibration curve equation is used in the data reduction computation to transform voltage data into dynamic pressure data.

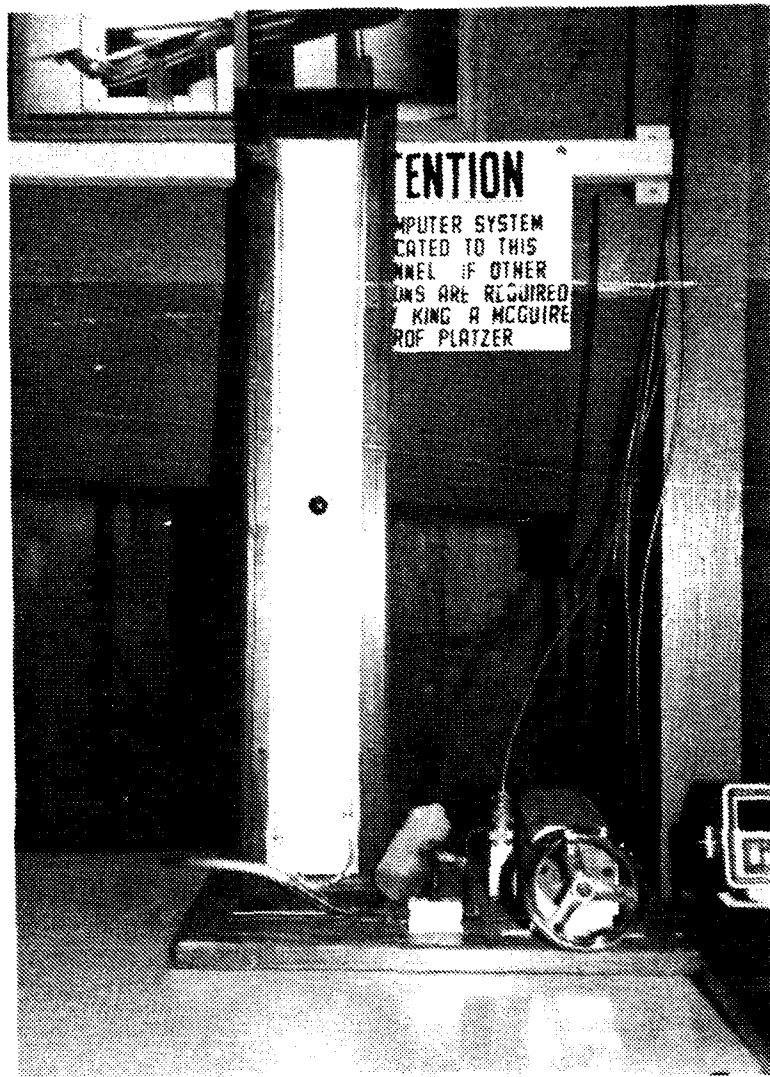


Figure 30. Calibration Manometer

3. Pressure Probe Calibration

The pressure probe was calibrated by the manufacturer prior to use in this experiment. The calibration chart is shown in Appendix D. The curves of velocity pressure coefficient, pitch angle, pressure coefficient and total pressure coefficient vs pitch angle have been transformed to polynomial equations by the author. This curve-fitting has been discussed in CONVERT program section. The 5-hole

pressure probe is rotated until opposing peripheral ports measure equal pressures. The corresponding angle rotation determines the yaw flow angle. For this reason, it is referred to as a nulling probe. Although the nulling procedure allows for analysis of large yaw angle flow, the procedure is mechanically complex and time consuming.

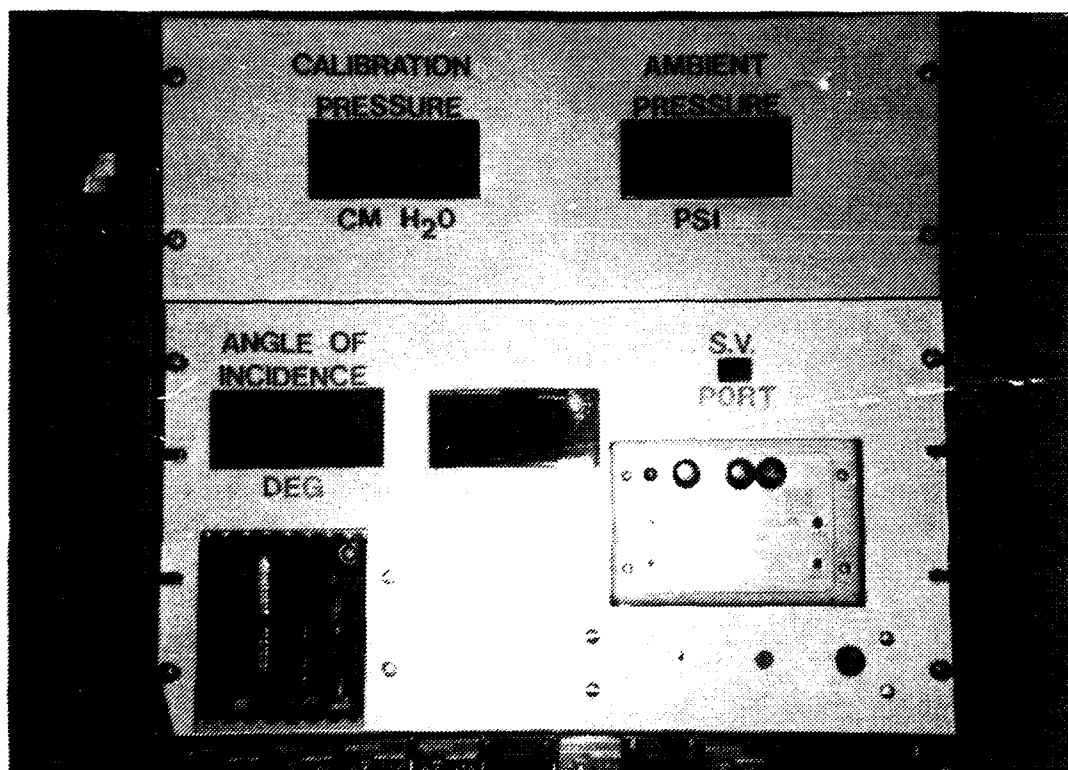


Figure 31. Digital Panel Meter (DPM)

4. Preliminary Run and Data Collection

The purpose of the preliminary run was to determine the location of the asymmetric vortices. The dimension of 6.5 by 8 inches and the step of 0.5 inch and the no grid condition were used in the preliminary run. Prior to each run, the initial settling chamber temperature and barometric pressure were recorded and the data acquisition system and traverser were fully energized and allowed to settle

out for about half an hour. During the settling period, the data acquisition system was cycled repeatedly by the program to bring the relay actuator, relay multiplex, digital multimeter, scanivalve amplifier and traverser to the operating temperature condition and to check the voltage output until all readings were consistent. Next, the wind tunnel was started and the flow was set at a different velocity for a small test measuring probe and the recorded data were checked for consistency. If they were not constant, the data acquisition system was re-calibrated again. The condition of each run is shown in Appendix H. The time of the preliminary run was about 6 hours. In order to keep the air density of test section as uniform as possible, the experimental procedure was interrupted when the settling chamber temperature rose 15°F above the operating temperature. The experiment was continued when the settling temperature had cooled down within 5°F of the operating temperature by the exchange of air. At the end of each run, the final settling chamber temperature and the barometric pressure were recorded again and the average value of them was used in the CONVERT program.

5. Actual Run

From the preliminary result, the dimension of 3 by 5.5 inches and a step of 0.25 inch were used through the experiment. This dimension covers the main portion of asymmetric vortices. Because the experiment requires considerable time for the nulling of the probe tip pressures before each measurement can be taken, and because the settling chamber temperature tended to rise quickly due the friction of the air flow through the turbulence generating grid, the time duration was about 10 ~11 hours for each run.

F. EXPERIMENTAL CORRECTIONS

Blockage factor corrections were made by Equations 20 and 21 from Ref. 26.

$$U = U_u(1+\epsilon) \quad (20)$$

$$q = q_u(1+2\epsilon) \quad (21)$$

where

- U : test section velocity (lb/ft²)
- U_u : Measured test section velocity (lb/ft²)
- q : dynamic pressure (lb/ft²)
- q_u : Measured dynamic pressure (lb/ft²)
- ϵ : blockage correction

The total blockage correction can be expressed as Equation 22.

$$\epsilon = \frac{1}{4} \frac{\text{model frontal area}}{\text{test section area}} \quad (22)$$

The blockage equation for each body configuration as a function of the model angle of attack has been investigated by Rabang as shown in Figure 32. The angle of attack was fixed for the experiments at 50°. The value of ϵ equals 0.0123. These equations are implemented into the data conversion program listed in Appendix B.

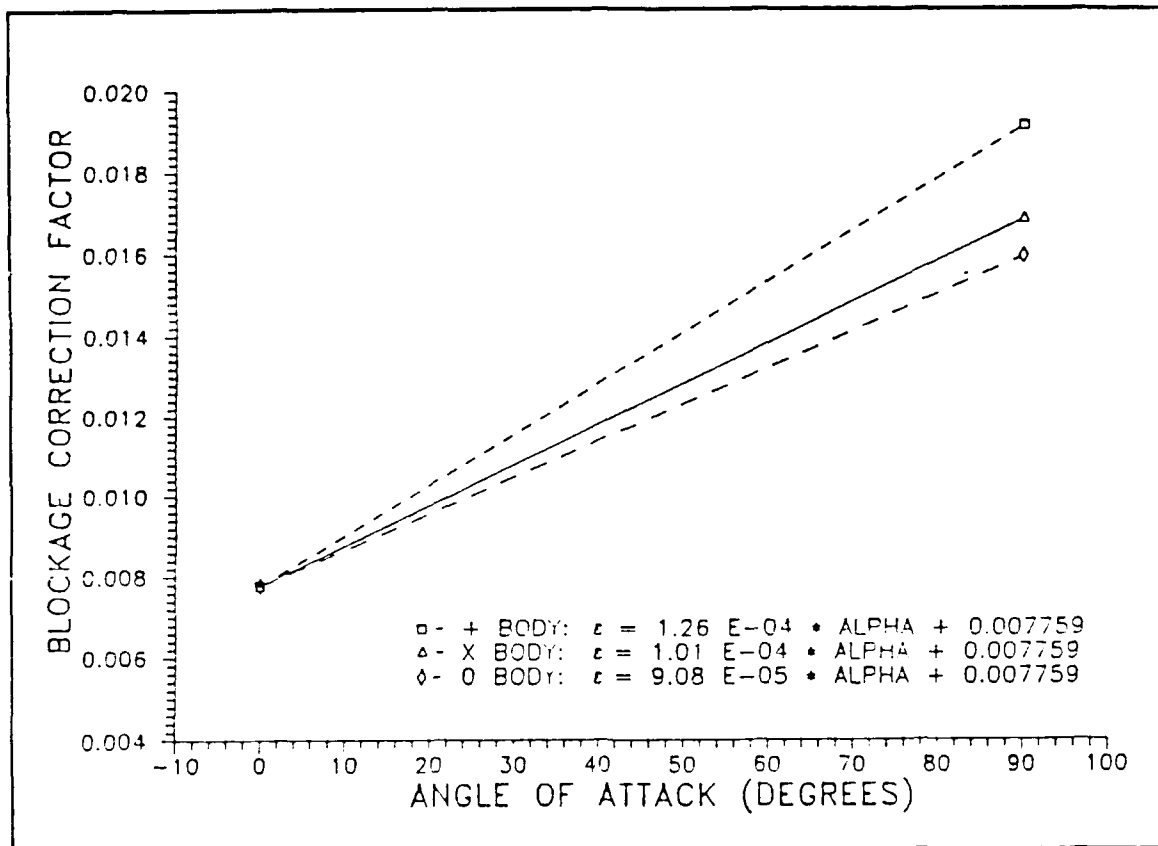


Figure 32. Blockage Factors [Ref. 3]

III. RESULTS

A DYNAMIC PRESSURE CALIBRATION

Wind tunnel dynamic pressure calibration was conducted prior to the experiment for each grid and no grid. From these data, the wind tunnel calibration factors were obtained. This reference dynamic pressure is used for adjusting the tunnel flow velocity to the expected experimental condition for the different grids. The calibration curves and equations for each run are shown in Table 3 in Fig. 33.

TABLE 3. WIND TUNNEL CALIBRATION RESULT

No Grid		Grid #1		Grid #2		Grid #3		Grid #4	
P_{TRUE}	P_{H_2O}	P_{TRUE}	P_{H_2O}	P_{TRUE}	P_{H_2O}	P_{TRUE}	P_{H_2O}	P_{TRUE}	P_{H_2O}
0	0	0	0	0	0	0	0.36	0	0.64
0.56	0.61	1.17	0.8	0.75	0.66	0.89	0.99	0.19	0.94
2.11	3.34	2.63	1.75	1.68	0.98	2.14	1.75	1.26	1.33
3.83	4.29	3.82	2.6	2.55	1.55	3.47	2.63	2.75	3.33
5.93	6.65	4.77	3.12	3.62	2.20	4.97	3.58	4.12	4.62
7.94	8.84	7.56	5.02	4.55	2.82	6.38	4.45	5.52	5.90
9.97	11.25	9.80	6.53	5.62	3.43	8.13	5.50	6.84	7.07
11.40	12.80	11.93	7.91	6.74	4.09	9.25	6.05	9.16	9.10
				8.13	4.95	10.08	6.45	11.0	10.37
				9.19	5.66				
				10.04	6.17				

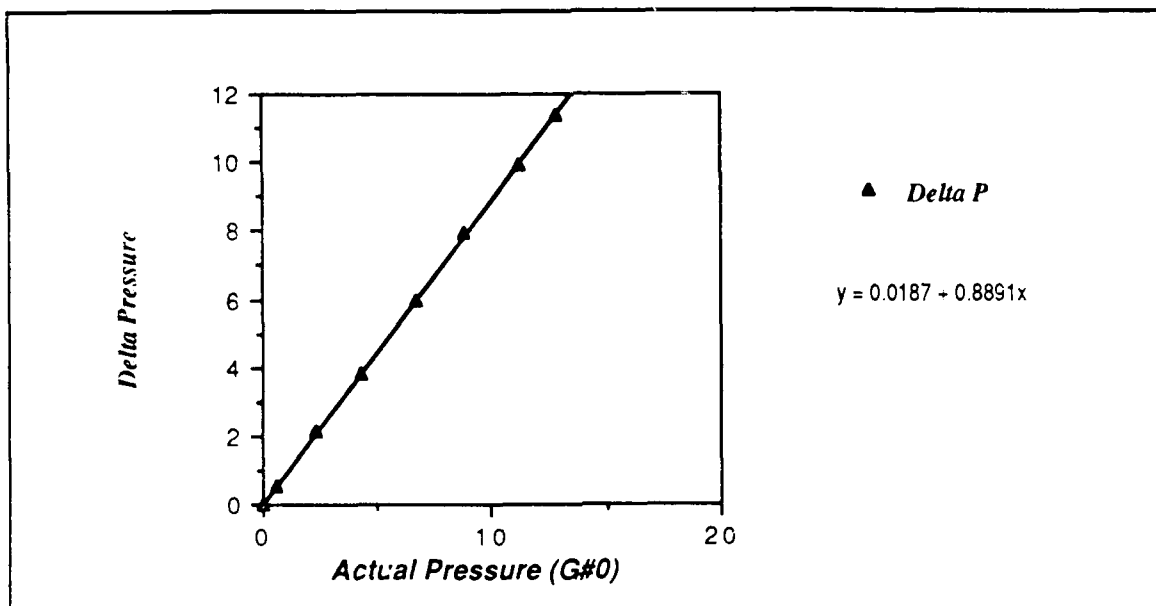


Figure 33(a). Dynamic Pressure Calibration at no Grid

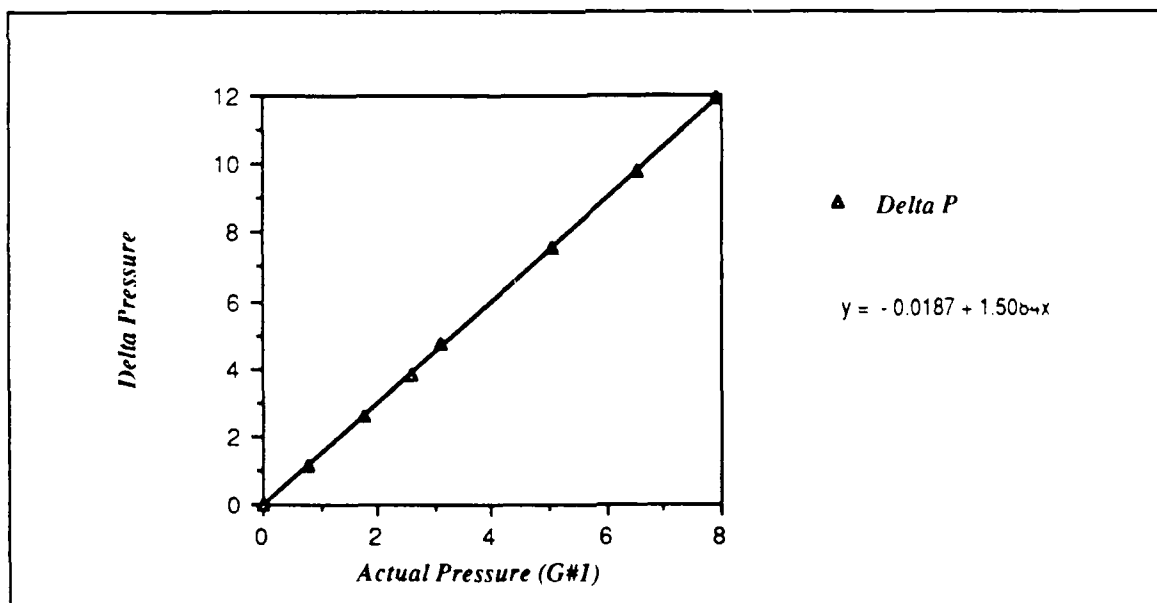


Figure 33(b). Dynamic Pressure Calibration at Grid #1

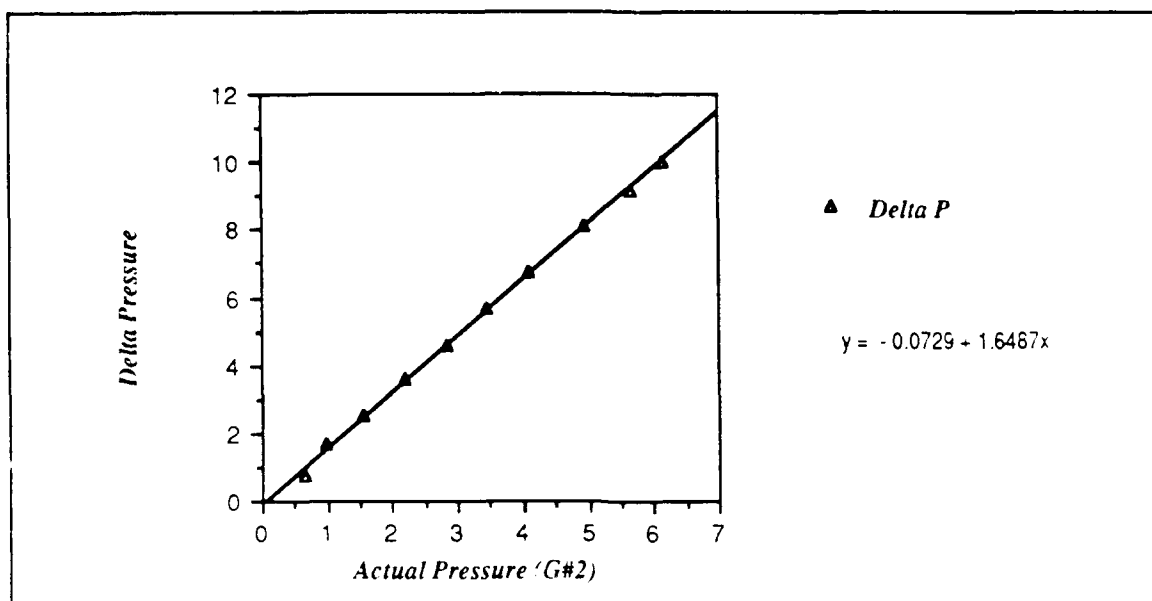


Figure 33(c). Dynamic Pressure Calibration at Grid #2

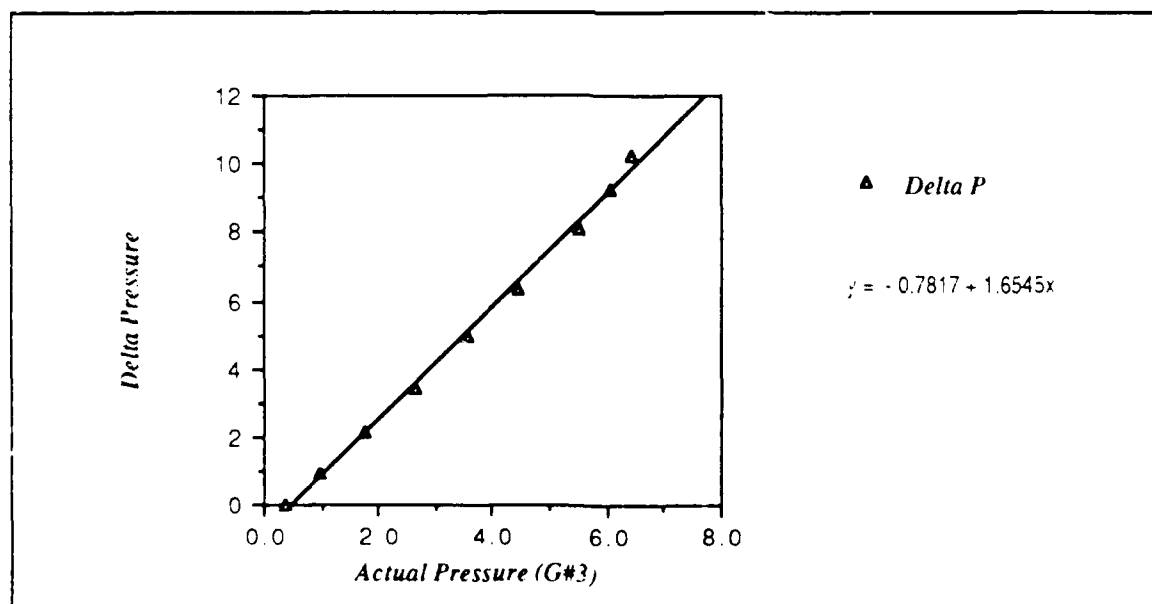


Figure 33(d). Dynamic Pressure Calibration for Grid #3

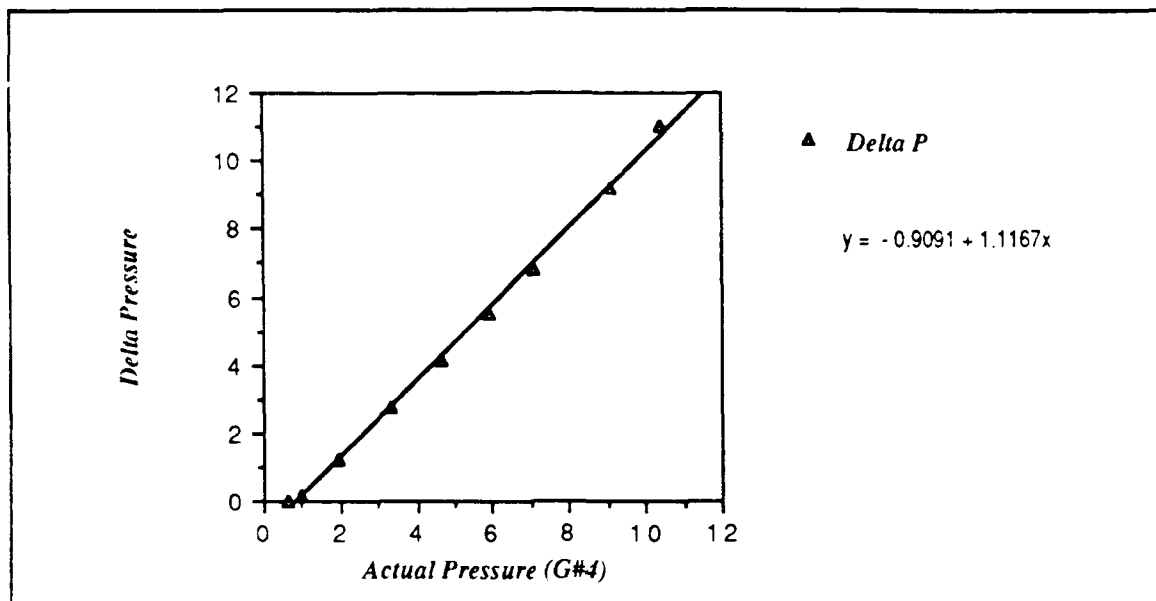


Figure 33(e). Dynamic Pressure Calibration at Grid #4

Figures 33 show the tunnel calibration factors k are 0.8891, 1.5084, 1.6487, 1.6545 and 1.1167 for no grid, grid 1, grid 2, grid 3 and grid 4 respectively. Due to the particular portable manometer, the curves were shifted to go through the origin. These values were used in the CONVERT program for calculating the pressure and velocity in the test section.

B. TRANSDUCER CALIBRATION

Transducer calibration was conducted both before and after each run. The results of the two calibrations for each run are presented in Table 4 and Figure 34 which shows a slight shift between initial and final runs. For a given voltage, the initial and final equations differed by approximately 5.16% for no grid and 0.03% for grid 1 for an experiment time duration of about 10 hours. An average of the two equations was used in the CONVERT program for all case runs to minimize the error. In each run, when the voltage difference between P_2 and P_3 is within 0.05, the data were recorded. The maximum relative error is 1.7% in pressure and

0.85% in velocity for Grid 1. For no grid condition, the maximum relative error is 3.23% in pressure and 1.5984% in velocity.

For this experiment, since the air flow Mach number was 0.1, the incompressible flow assumption was a reasonable approximation. In addition, it is assumed that the temperature and velocity gradients are negligible in a small region around the probe.

TABLE 4. TRANSDUCER CALIBRATION RESULT

	TEST RUN		G#0		G#1	
	pressure	voltage	pressure	voltage	pressure	voltage
Before	-8.91	-2.06663	-8.26	-1.9361	-8.22	-1.9152
	-4.37	-1.03319	-3.44	-0.8304	-3.92	-0.9304
	0.29	0.08565	0.55	0.1278	1.22	0.3017
	4.87	1.17548	3.24	0.7727	5.64	1.3487
	8.80	2.1055	6.18	1.4682	10.39	2.4762
			9.92	2.3514	13.52	3.2192
After	-8.81	-2.00795	-9.26	-2.1754	-7.77	-1.8257
	-4.46	-1.01094	-4.37	-1.0658	-3.53	-0.8461
	0.49	0.172168	-0.19	-0.0720	4.89	1.166
	4.74	1.17583	6.41	1.5074	9.16	2.1786
	9.52	2.3122	9.87	2.3242	12.32	2.9292

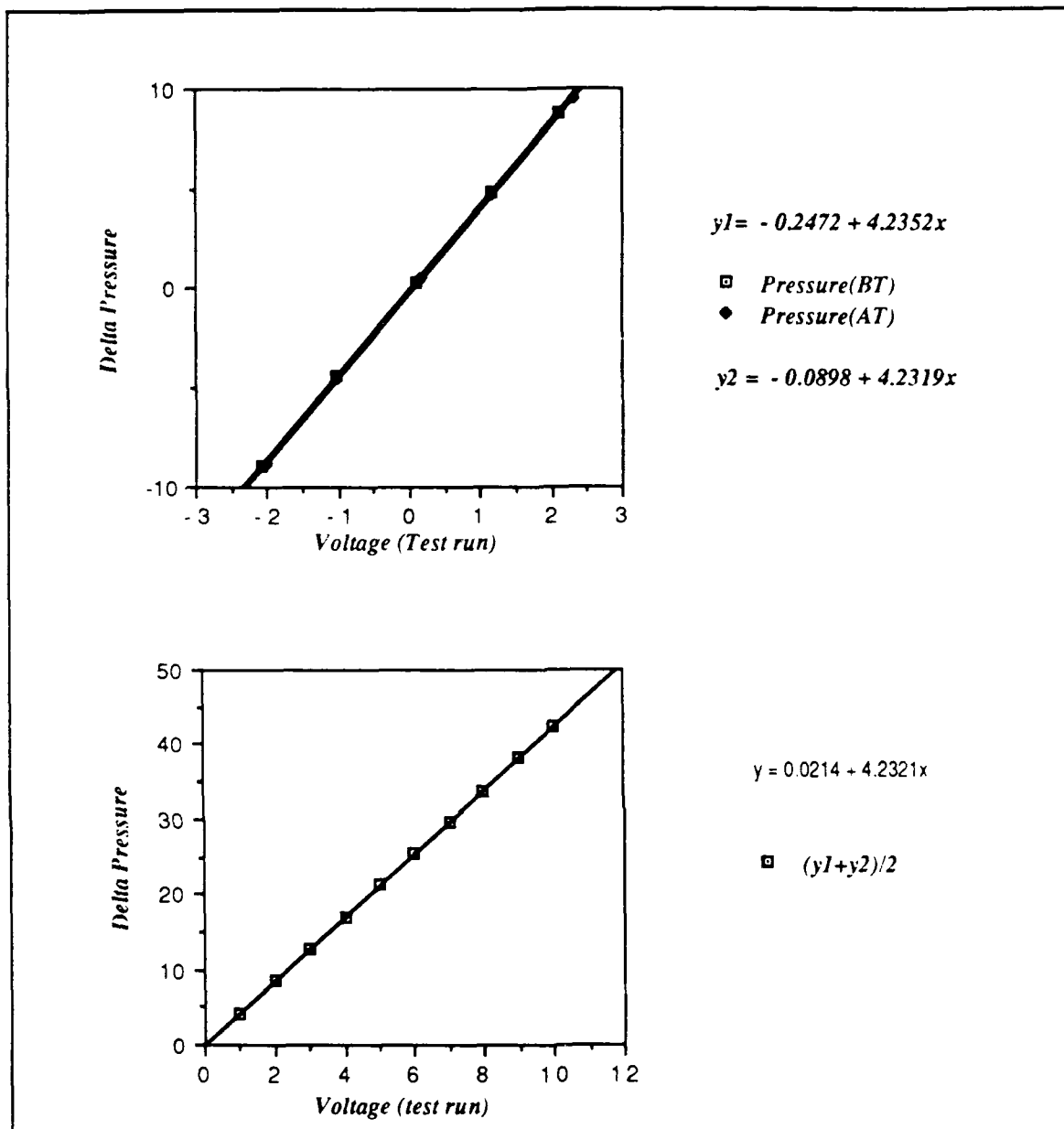


Figure 34(a). Transducer Calibration at no Grid Condition for the Preliminary Run

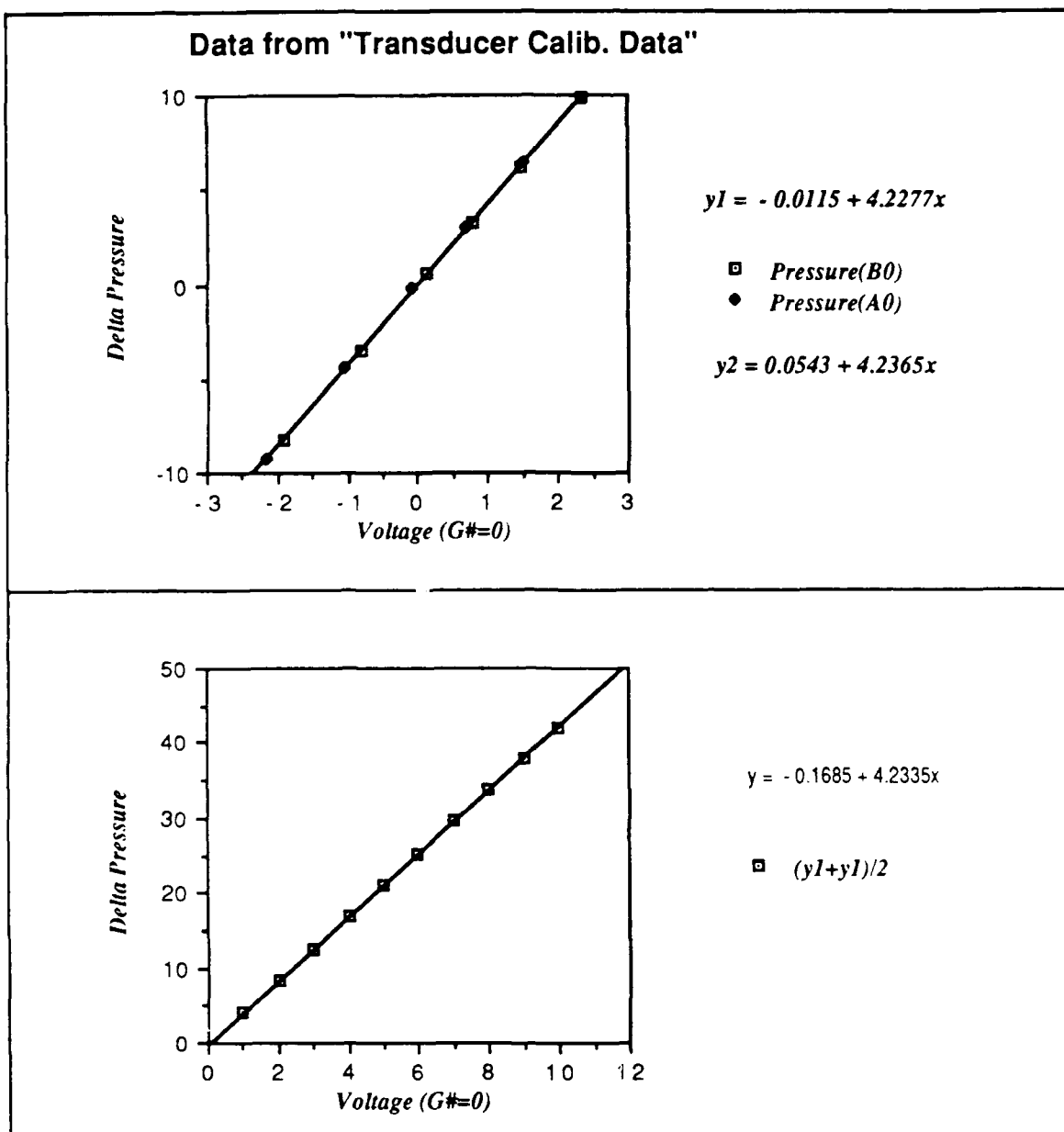


Figure 34(b). Transducer Calibration at no Grid Condition

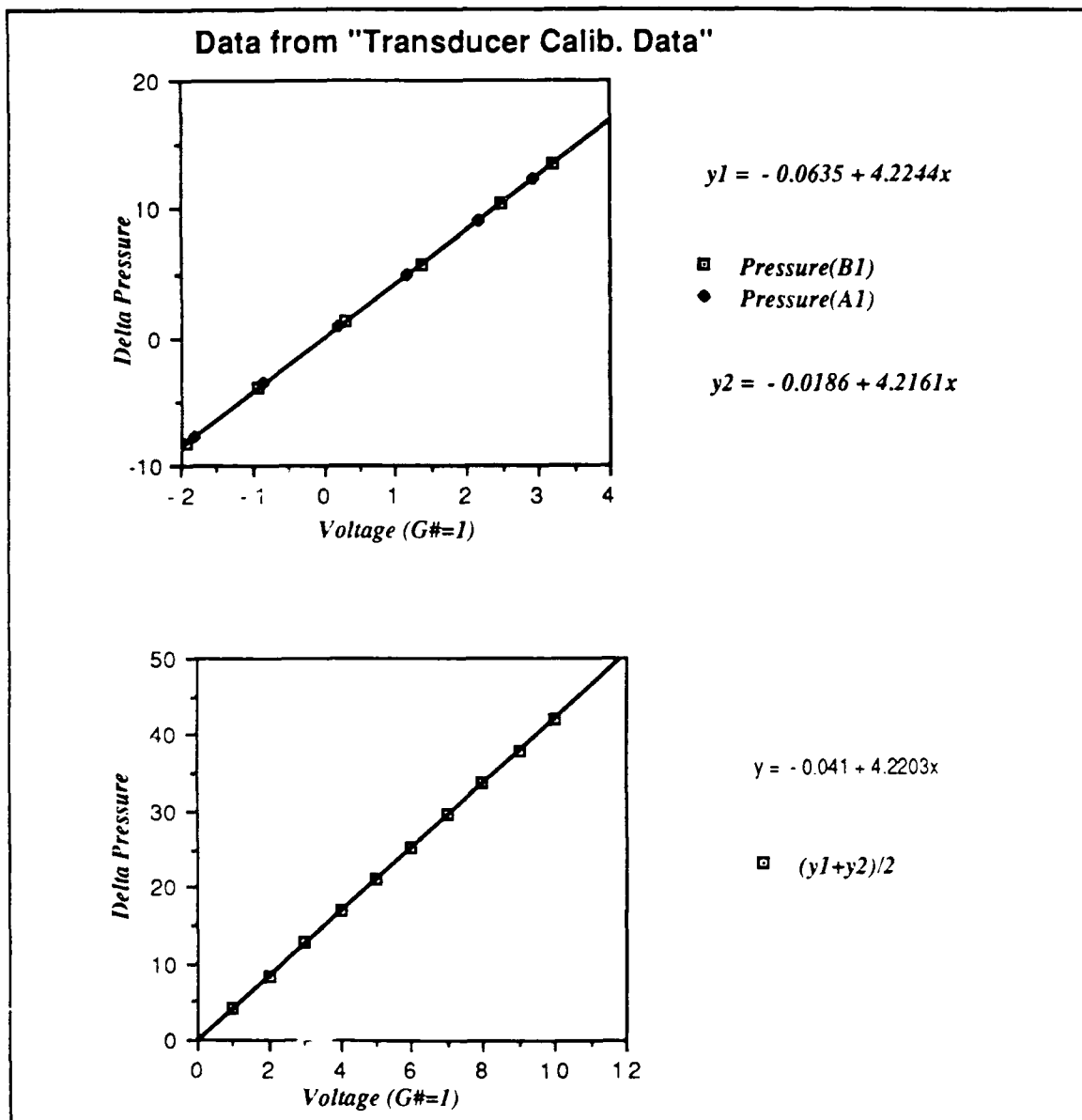


Figure 34(c). Transducer Calibration at Grid #1 Condition

C. PRELIMINARY RUN

The objective of the preliminary run was to determine the location of asymmetric vortices. This result was used to determine the size of the measured

plane and the step distance for the following runs, so that more accurate velocity and pressure data could be obtained. The preliminary run conducted 6d downstream of the nose of the missile in the plane normal to the freestream at ambient turbulence conditions, consisted of a 6.5- by 8-inch measured phase, a step distance of 0.5 inch, and the no grid condition. Figure 35 shows the velocity vectors superimposed on the measured grid which clearly shows the location of the vortex. The nose induced asymmetric vortices are marked by the swirling vectors. The velocities give a representation of an indirect flow visualization of the vortex. The crossflow is expected to reach zero at the freestream region. This inconsistency in arrow magnitude and direction are seen at the outer boundaries because of a possible misalignment of the traverser. Figures 36 and 37 show the 2D contour and 3D surface plots of local total pressure coefficient and local static pressure coefficient with the same data. The value between two contour lines is 0.15. From Figure 36, it is clear that the location of asymmetric vortices are 2.5 to 5.5 inches on the Z axis and 0 to 2 inches on the Y axis. Hence a small planar survey grid, 3 x 5.5 inches and with a step of 0.25 inch, was determined for further experiments.

Figures 36 and 37 show the total pressure coefficient to be uniform at the freestream and a high negative pressure gradient to exist in the core of the vortex. The static pressure coefficient has a positive value at the center of the measure planar and has a moderate negative pressure gradient in the vortex core. More accurate investigations in the vortex region are discussed in the following section.

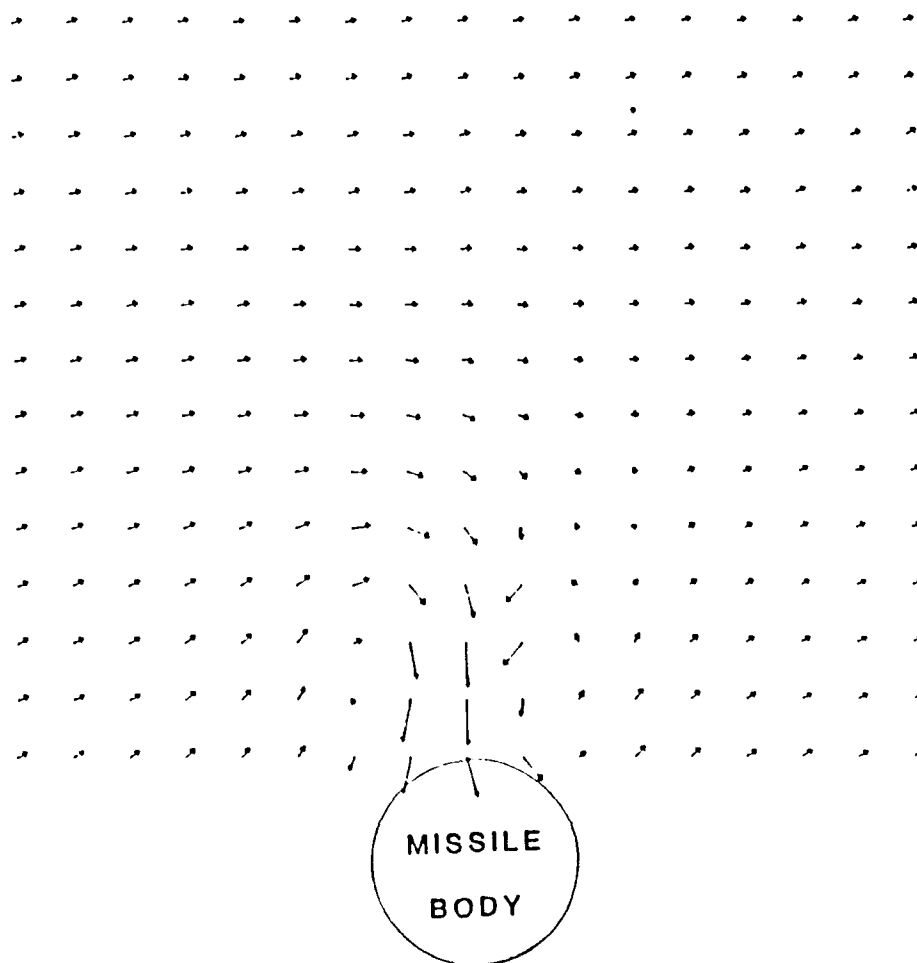


Figure 35. Preliminary Crossflow Velocity Vector Superimposed on the Grid.

TEST RUN, TOTAL PRESSURE COEFF.

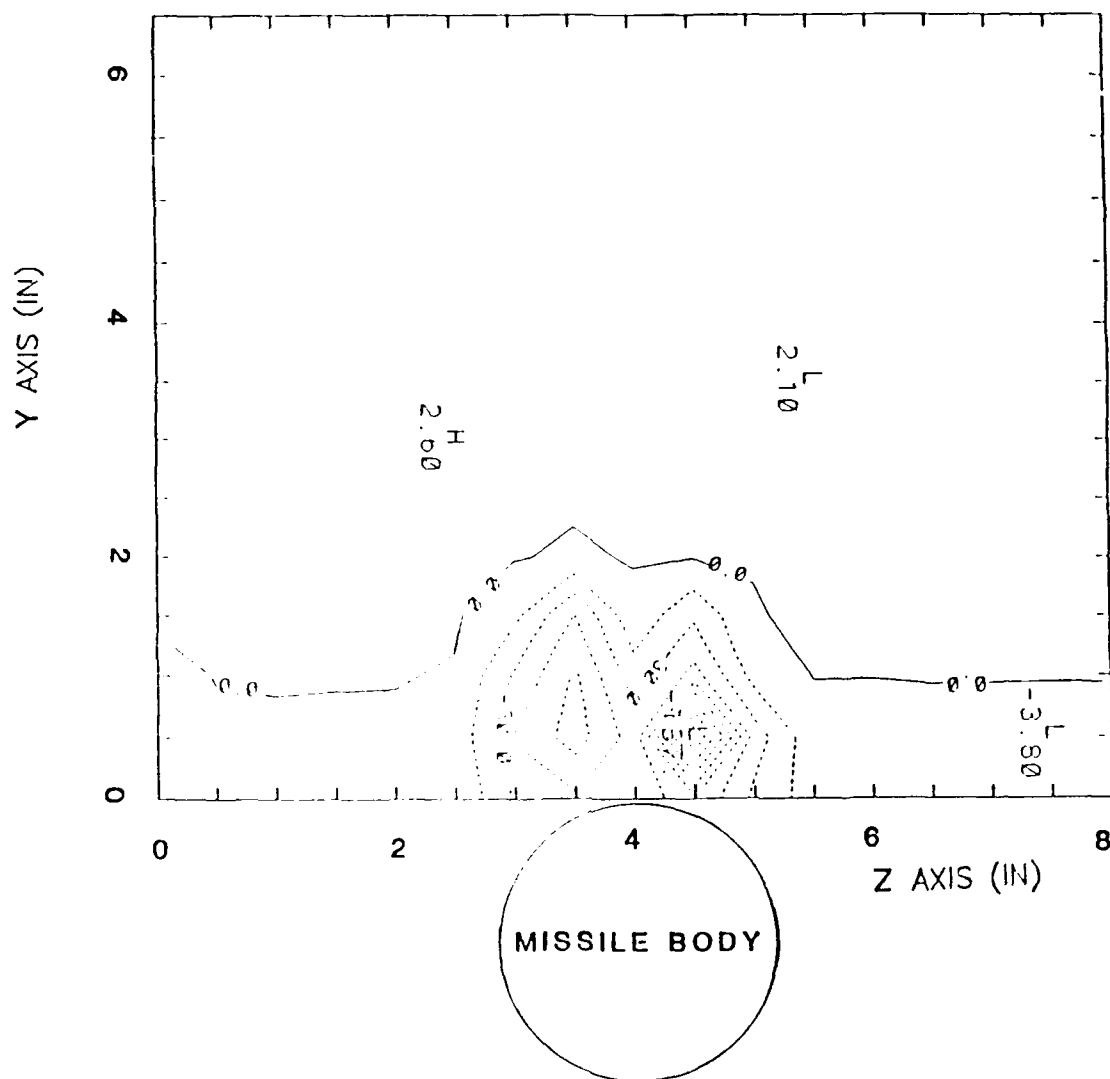


Figure 36(a). Total Pressure Coefficient Contour⁷

⁷Dashed line indicates the negative value. Note: data as plotted times 100. The distance between two isobars is 15.

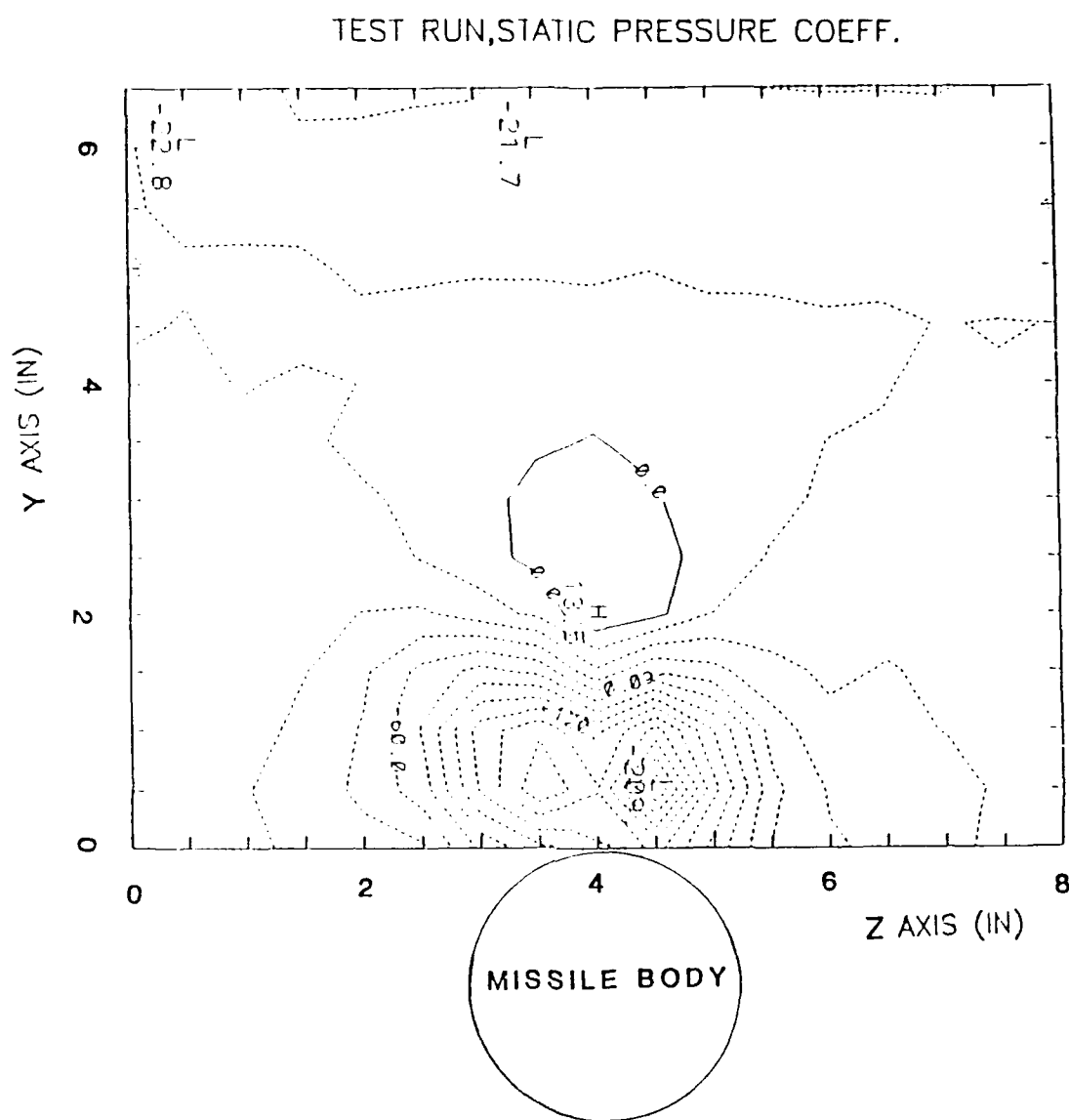


Figure 36(b). Local Static Pressure Coefficient Contour⁸

⁸Dashed line indicates the negative value. Note: data as plotted times 100. The distance between two isobars is 15.

TEST RUN, NO GRID

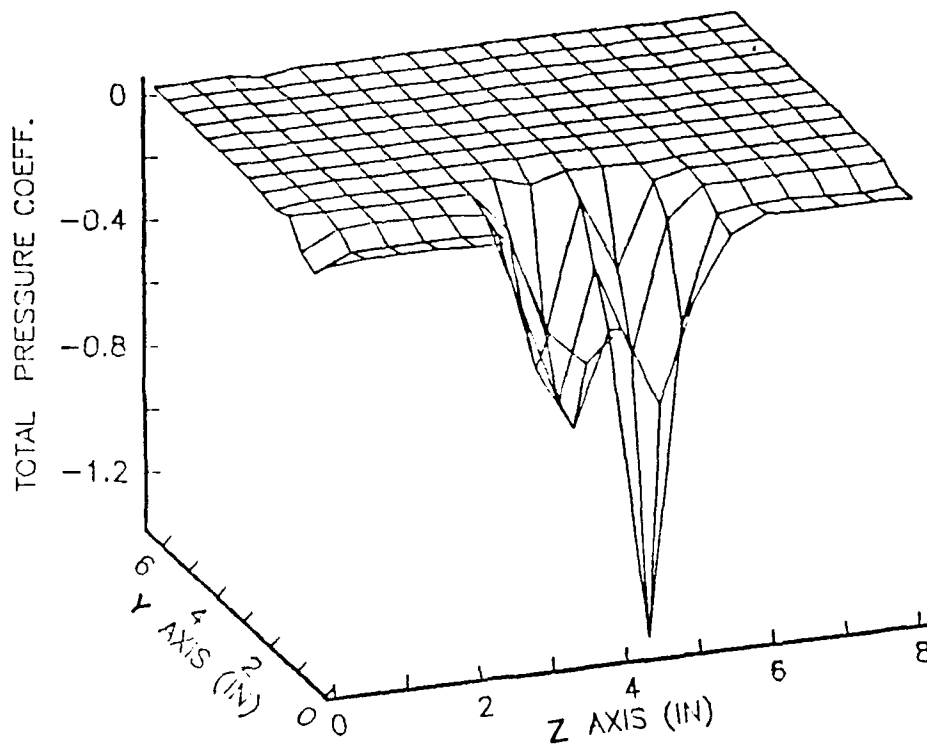


Figure 37 (a). 3D Surface Plot. Local Total Pressure Coefficient

TEST RUN, NO GRID

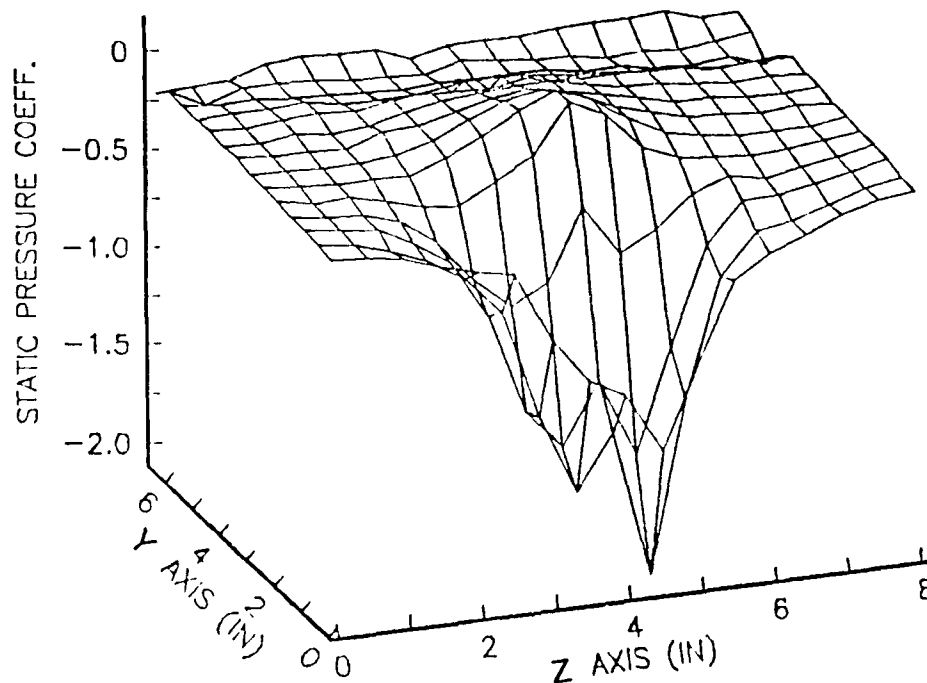


Figure 37 (b). 3D Surface Plot. Local Static Pressure Coefficient

D. BODY ONLY WITHOUT TURBULENCE

The results from Rabang show a maximum side force coefficient to be about -4.2 at 50° AOA for body-only and the no grid condition. [Ref. 3] (See Figure 28.)

As marked by the swirling vectors in Figure 38, two vortices form two circles and rotate in opposite directions. Represented by the velocity magnitude, the vortex strength reaches its maximum in the outer core of the two vortices. The

maximum side force is due to the relative strengths of the two vortices and the displaced location of the vortices from a symmetric configuration.

The total pressure coefficient is expected to be constant in the outer incompressible and inviscid portion of the vortex. The viscous forces found within the vortex core decrease the flow's fluid-mechanical energy; therefore the total pressure coefficient becomes negative. The vortex contour with a C_{pt} of -1.35 is approximately 0.57d above the missile surface. The other vortex with a C_{pt} of -1.43 is approximately 0.26d above the missile surface. It is clear to see from Figure 39(a) that the extent of each vortex is about 0.86d wide and the distance between vortex centers is about 0.86d. In a negative sense, closer isobars have a higher gradient which forms two inverted spike shaped vortices as shown in Figure 40(a). It is clear to see the shapes of vortex cores in this figure.

In the freestream condition, the static pressure coefficient is expected to be zero. [Ref. 32] While the static pressure coefficient progresses inward from the freestream conditions to the vortex core, the angular velocity increases, static pressure drops, and the static pressure coefficient itself decreases from zero to a negative value. The vortex contour with a C_{ps} of -1.8 vortex is approximately 0.37d above the missile surface. The other vortex contour with a C_{ps} of -2.22 is approximately 0.29d above the missile surface. Figure 39(b) shows 1.14d for the width of each vortex. The static pressure coefficient has a lower gradient inward to the vortex core. Figure 40(b) exhibits a fatter inverted spike shape, indicating a diffused and lesser strength. The vortex closer to the missile is stronger, as can be seen by the higher local gradients and the deeper peak.

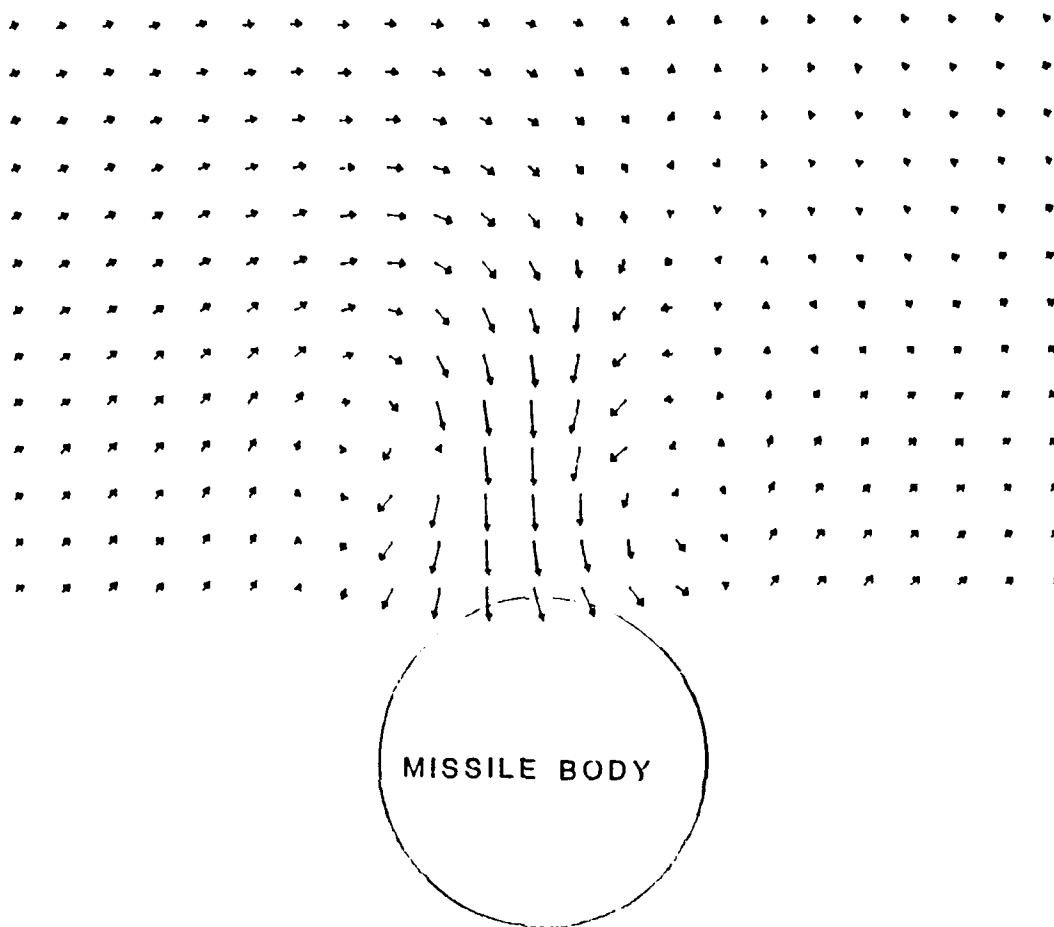


Figure 38. Crossflow Velocity Vector Superimposed on the Grid for
no Grid Condition

Figure 1 is a contour plot showing the variation of the magnetic field component H_z in Gauss (G) as a function of the Z-axis (in inches) and Y-axis (in inches). The Z-axis ranges from 0 to 5 inches, and the Y-axis ranges from 0 to 3 inches. The plot shows two main regions of high magnetic field strength, labeled -30.0 G and -14.0 G, centered around $Z=2.5$ and $Z=3.5$ respectively. The field strength decreases as the distance from these centers increases. A circular region labeled "MISSILE BODY" is shown at the bottom center, centered around $Z=2.5$ and $Y=0$.

⁹Dashed line indicates the negative value. Note: data as plotted times 100. The distance between two isobars is 15.

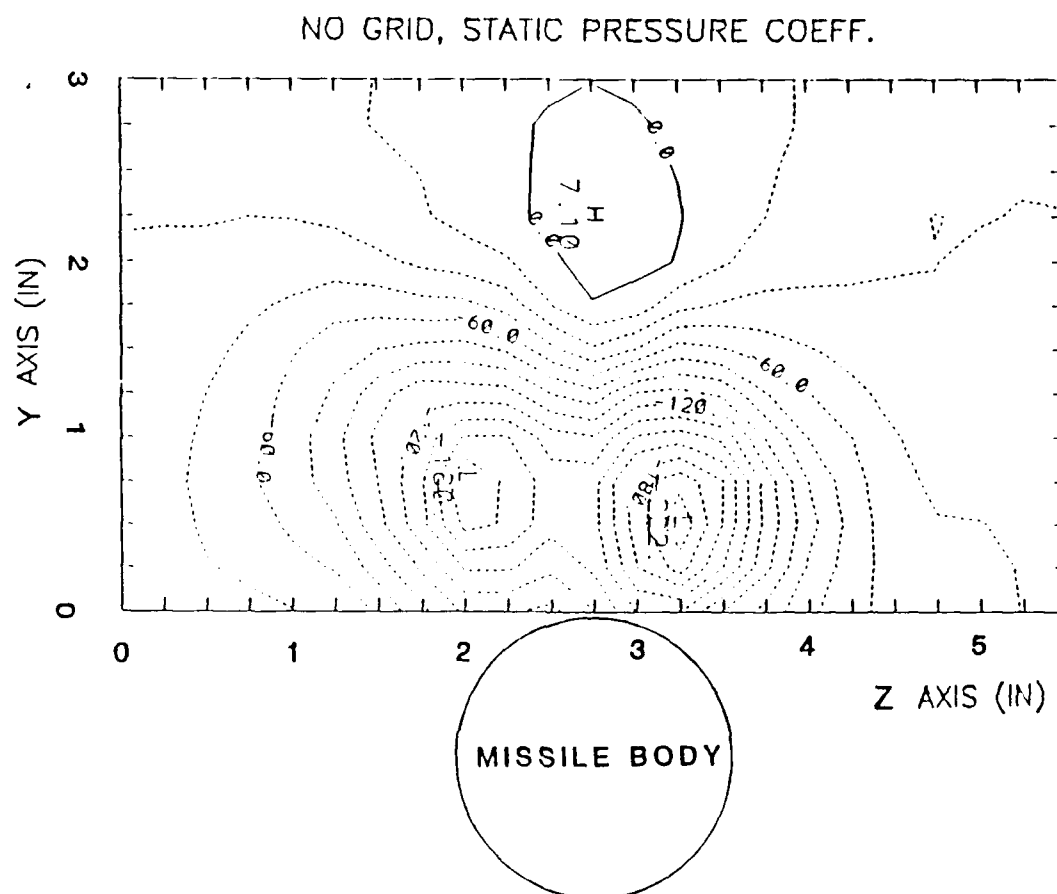


Figure 39(b). Local Static Pressure Coefficient Contour at no Grid Condition.¹⁰

¹⁰Dashed line indicates the negative value. Note: data as plotted times 100. The distance between two isobars is 15.

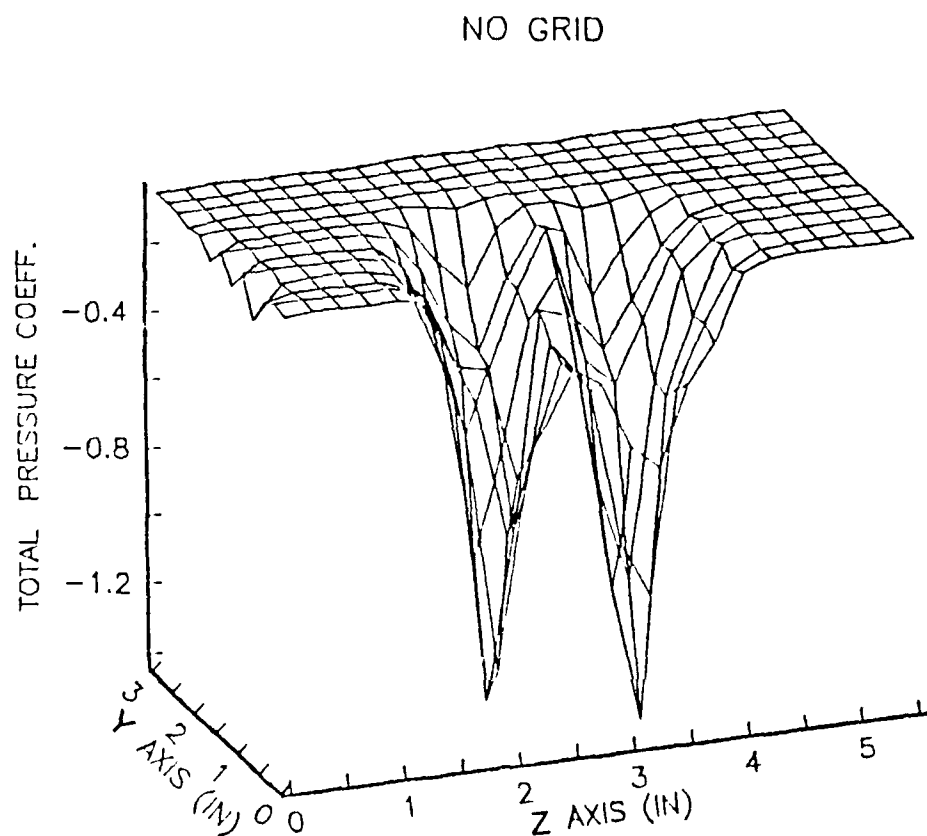


Figure 40(a). 3D Surface Plot. Local Total Pressure Coefficient at no Grid Condition.

NO GRID

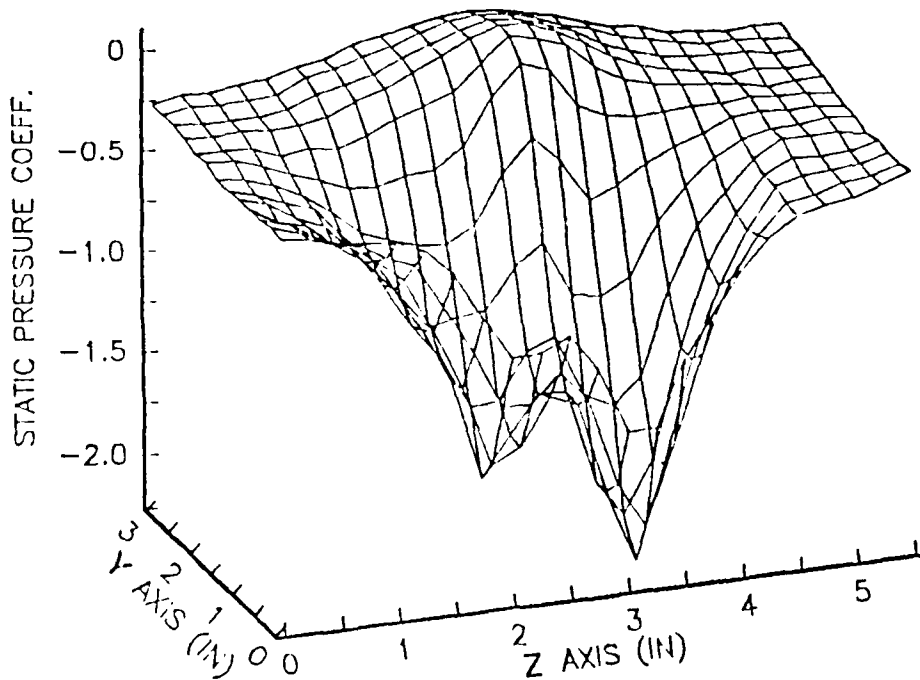


Figure 40(b). 3D Surface Plot. Local Static Pressure Coefficient at no Grid Condition.

E. BODY-ONLY WITH TURBULENCE

Rabang demonstrated that for the body-only case, an increase in turbulence intensity tends to reduce dramatically the maximum induced side force. [Ref. 3] (see Figure 41).

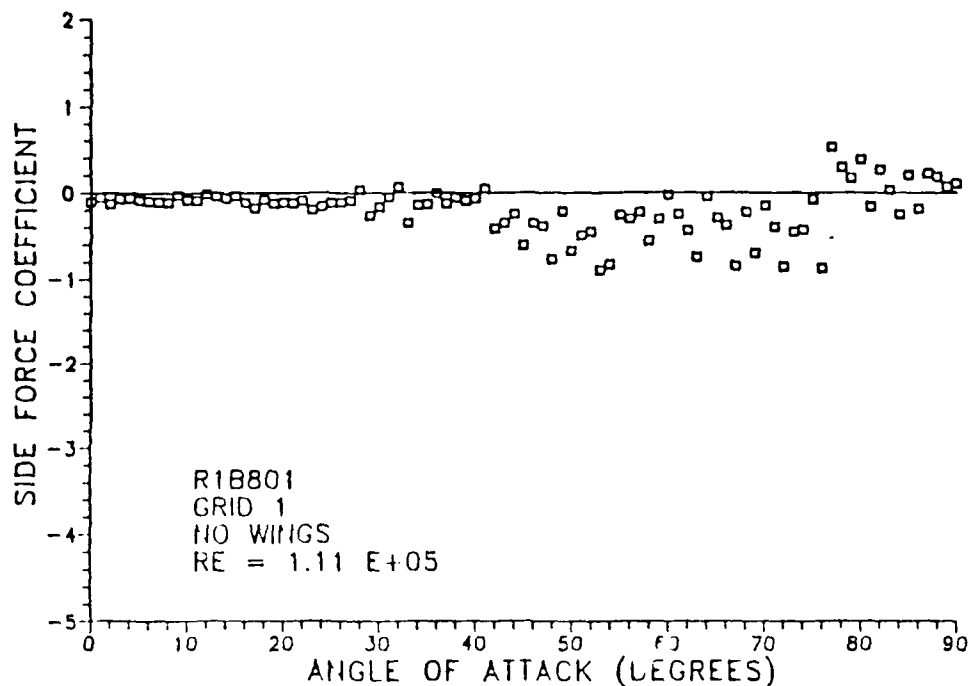


Figure 41 R1B801. Side Force Coefficient. [Ref. 3]

Figure 42 shows the crossflow velocity vectors and a slight shift in direction. Represented by the swirling vectors, the vortex has less strength than in the no turbulent condition. The asymmetry can still be seen in Figure 42.

The total pressure coefficient has a fatter spike shape and more of a plateau at the vortex core than in the no turbulent condition as shown in Figure 44(a). One vortex has a C_{pt} contour of -0.97 a distance of $0.43d$ above the missile surface and the other one has a C_{pt} contour of -1.16 a distance of $0.4d$ above the missile surface. The distance between the two vortices' cores is $0.71d$, which is $0.15d$ closer than the one in the no turbulent condition. (See Figure 43(a).) Each vortex has a larger extent than the one with no turbulence at the same isobars.

The static pressure coefficient, similar to the total pressure coefficient, has a more diffused shape than in the no turbulent condition. (See Figure 4(b).) The C_{ps}

contour of -0.45 for one vortex is more or less $0.36d$ above the missile surface and the C_{ps} contour of -0.72 for the other vortex is approximately $0.5d$ above the missile surface. The distance between these two vortices' cores is closer than that in no turbulent condition; each vortex has a width of about $1.14d$. (See Figure 43(b).)

Comparing the extents of the vortices with and without flowfield turbulence, a more tightly wrapped vortex (smaller diameter) has a greater strength. The result of the turbulence is to diffuse, but not to eliminate, the asymmetric vortices. With the additional turbulence, the vortex centers are closer to the missile surface and more symmetric. These facts agree with Rabang's results.

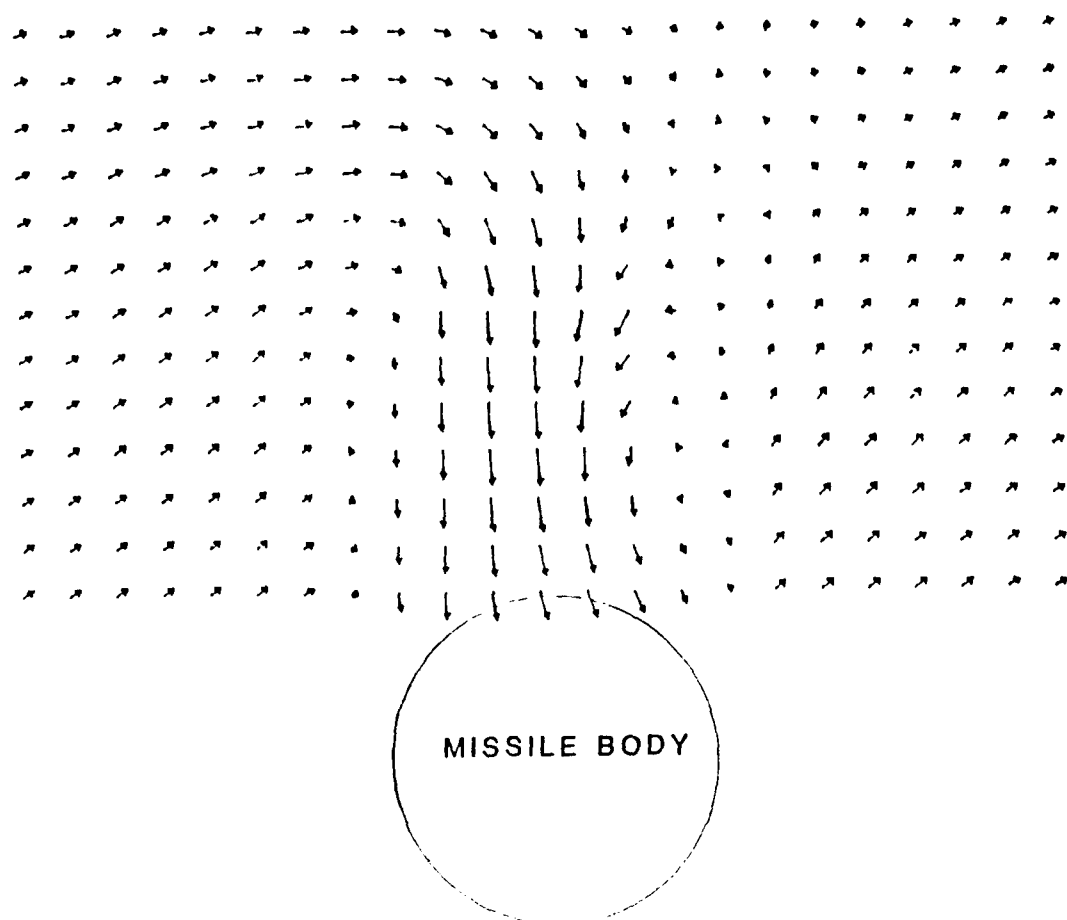


Figure 42. Crossflow Velocity Vector Superimposed on the Grid for Grid 1 Condition.

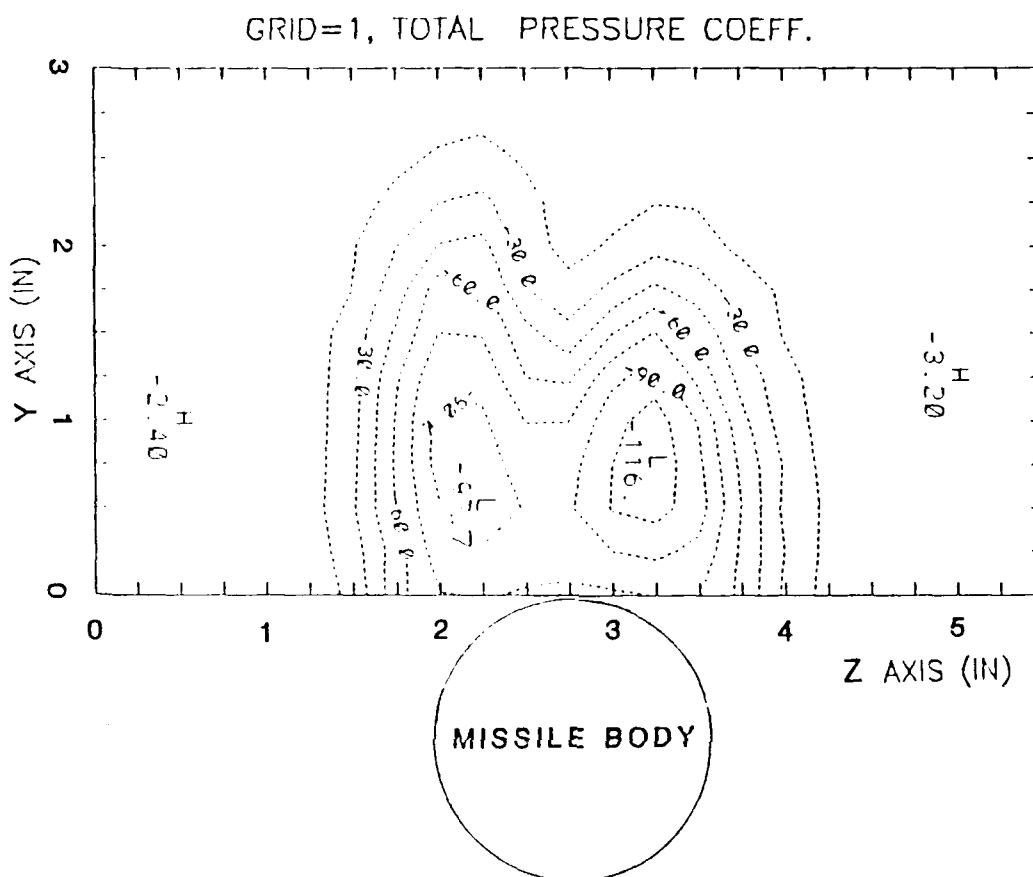


Figure 43(a). Total Pressure Coefficient Contour at Grid 1 Condition.¹¹

¹¹The dashed line indicates the negative value. Note: data as plotted times 100. The distance between two isobars is 15.

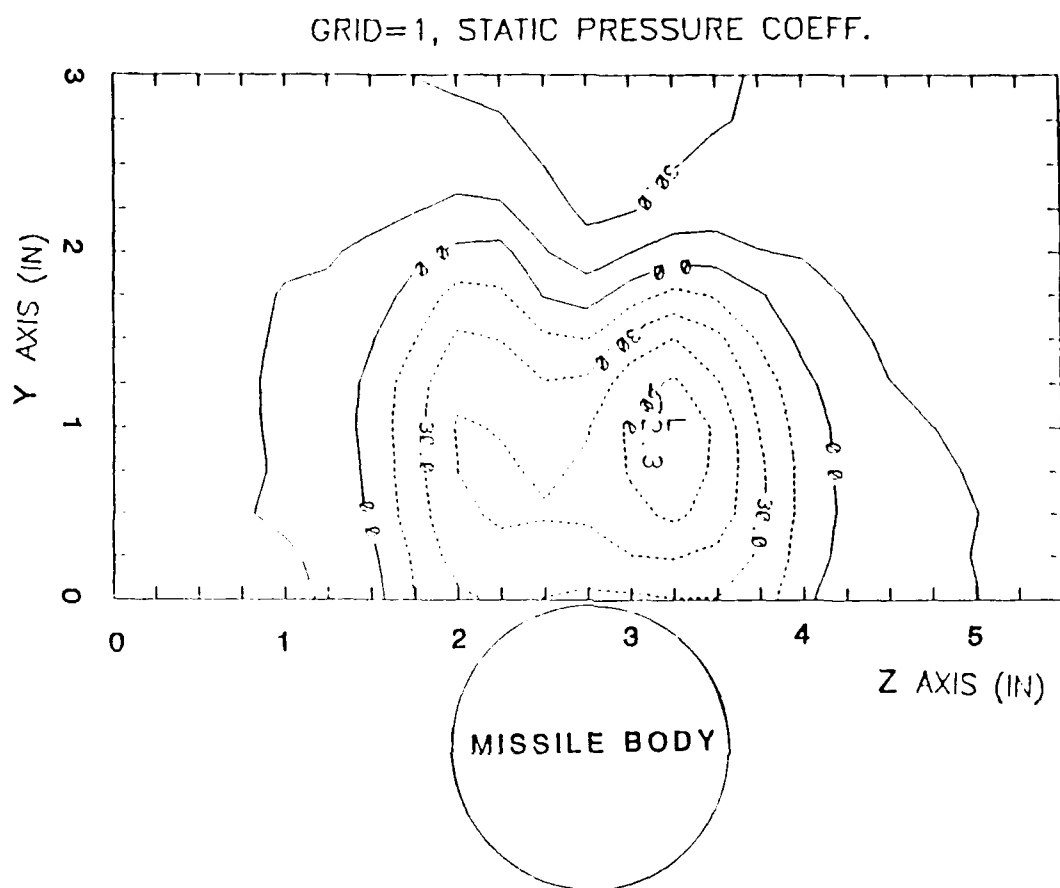


Figure 43(b). Local Static Pressure Coefficient Contour at Grid 1 Condition¹²

¹²Dashed line indicates the negative value. Note: data as plotted times 100. The distance between two isobars is 15.

GRID=1

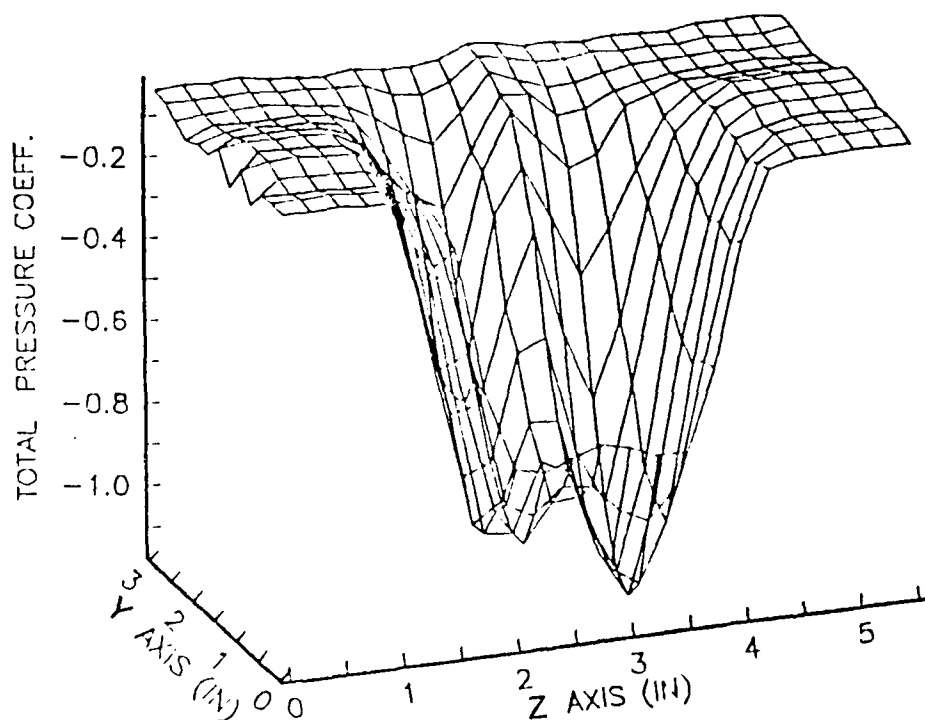


Figure 44(a). 3D Surface Plot. Local Total Pressure Coefficient at Grid 1 Condition.

GRID=1

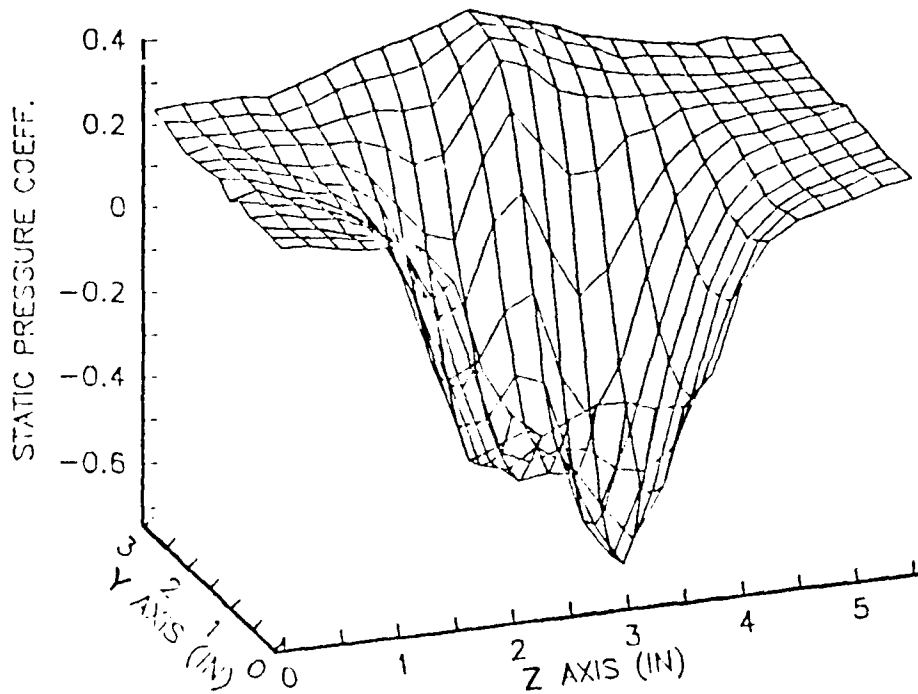


Figure 44(b). 3D Surface Plot. Local Static Pressure Coefficient at Grid 1 Condition.

IV. CONCLUSION AND RECOMMENDATIONS

The flowfield downstream of a vertically-launched surface-to-air missile model at an angle of attack of 50° and a Reynolds number of 1.1×10^5 was investigated in a wind tunnel of the Naval Postgraduate School. The body-only configuration was tested. Two flowfield conditions were treated: the nominal ambient wind tunnel condition, and a condition with grid-generated turbulence of 3.8% turbulence intensity and a dissipation length scale of 1.7 inches. The following conclusions were reached:

- 1) The relative strengths of the asymmetric vortices can be noted by the sharp spike shape in the ambient condition; this condition becomes diffused and becomes fatter in the turbulent condition;
- 2) The right side vortex has greater strength than the left side one as seen by the changes in the total pressure coefficient and static pressure coefficient contours with and without a turbulent condition;
- 3) An increase in turbulence intensity tends to reduce the strength of the asymmetric nose-generated vortices;
- 4) An increase in turbulence intensity also pushes two asymmetric vortices closer together;
- 5) Crossflow velocities were examined and were found to indicate the behavior denoted by the pressure contours.

To understand better the behavior of asymmetric vortices induced by the missile nose, a few recommendations are suggested as follows:

- 1) Examine the vortices at positions of length/diameter ratios of 3 and 9;

2) Investigate the interaction effects of wings and consider the effect of roll angle on asymmetric vortices;

3) Investigate the asymmetric vortex behavior affected by various angles of attack and turbulent conditions with varying intensities and length scales.

LIST OF REFERENCES

1. Friedman, N., "Naval Vertical Launch Missile System," *Military Technology*, pp. 24-31, May 1985.
2. Roane, D. P., *The Effect of a Turbulent Airstream on a Vertically-launched Missile at High Angles of Attack*, Master's Thesis, Naval Postgraduate School, Monterey, CA, December 1987.
3. Rabang, M. P., *Turbulence Effects on the High Angles of Attack Aerodynamics of a Vertically Launched Missile*, Master's Thesis, Naval Postgraduate School, Monterey, CA, June 1988.
4. Thomson, K. D. and Morrison, D. F., "The Spacing, Position and Strength of Vortices in the Wake of Slender Cylindrical at Large Incidence," *Fluid Mechanics*, pp. 751-783, v. 50, part 4, 1971.
5. Ericsson, L. E. and Reding, J. P., "Steady and Unsteady Vortex-Induced Asymmetric Load on Slender Vehicles," *Journal of Spacecraft*, v. 10, no. 2, March-April 1981.
6. Dahlem, V., Flaherty J. I., Shereda, D. E., *High Angle of Attack Missile Aerodynamics at Mach Numbers 0.3 to 1.5*, Technical report AFWAL-TR-80-3070, Rutgers, NJ, November 1980.
7. Jorgensen, L. H. and Nelson, E. R., *Experimental Aerodynamic Characteristic for a Cylindrical Body Revolution with Various Noses at AOA from 0 degree to 58 degrees and Mach Number from 0.6 to 2.0*, NASA TM-X-3130, Moffett Field, CA, March 1975.
8. Ericsson, L. E. and Reding, J. P., *Vortex-Induced Asymmetric Load on Slender Vehicles*, LMSC-D630807, Sunnyvale, CA, January 1979.
9. Reding, J. P. and Ericsson, L. E., "Re-examination of the Maximum Normalized Vortex-Induced Side Force," *Journal of Spacecraft*, v. 21., no. 5, September-October 1984.
10. Deffenbaugh, I. D. and Koerner, "Asymmetric Vortex Wake Development on Missiles at High Angle of Attack," *Journal of Spacecraft*, v. 14, no. 3, pp. 155-162, March 1977.

11. Wardlaw, A. B. Jr., and Morrison, A. M., *Induced Side Forces on Bodies of Revolution at High Angle of Attack*, NSWC/WOL/TR 75-176, Silver Springs, MD, November 1975.
12. Yongnian, Y., Xinzhi, Y. and Jianying, L., "Active Control of Asymmetric Forces at High Incidence," *Journal of Aircraft*, v. 25, no. 2, pp. 190-192, February 1988.
13. Ericsson, L., and Reding, J. P., "Asymmetric Vortex Shedding from Bodies of Revolution," *Tactical Missile Aerodynamics*, American Institute of Aeronautics and Astronautics, Inc., 1986.
14. Keener, E. R. and Chapman, G. T., *Onset of Aerodynamic Side Forces at Zero Sideslip on Symmetric Forebodies at High Angle of Attack*, AIAA paper 74-770, August 1974.
15. Keener, E. R. and others, *Side Force on Forebodies at High AOA and Mach Number from 0.1 to 0.7; Two Tangent Ogives, Paraboloid and Cone*, NASA-TM-X-3438, Moffett Field, CA, February 1977.
16. Keener, E. R. and others, *Side Forces on a Tangent Ogive Forebody with a Fineness Ratio of 3.5 at High AOA and Mach from 0.1 to 0.7*, NASA-TM-X-3437, Moffett Field, CA, February 1977.
17. Kruse, R.L., Keener, E. R., and Chapman, G. T., *Investigation of the Asymmetric Aerodynamic Characteristics of Cylindrical Bodies of Revolution with Various Variations in Nose Geometry and Rotational Orientation*, NASA-TM 78533, Moffett Field, CA, September 1979.
18. Gregoriou, G., "Modern Missile Design for High Angle of Attack," AGARD/VKI lecture series no. 121, *High Angle of Attack Aerodynamics*, March 1982.
19. Keener, E. R., and Chapman, G. T., "Similarity in Vortex Asymmetries over Slender Bodies and Wings," *AIAA Journal*, v. 15, no. 9., pp. 1370-1372, September 1977.
20. Tieleman, H. W., *A Survey of the Turbulence in the Marine Surface Layer for the Operation of Low-Reynolds Number Aircraft*, Virginia Polytechnic Institute Report, VPI-E-85-10, Blacksburg, VA, March 1985.
21. Bradshaw, P., *An Introduction to Turbulence and its Measurement*, Pergamon Press, 1971.

22. Deane, J. R., "Missile Body Vortices and Their Interaction with Lifting Surfaces," AGARD/VKI, Lecture Series, no. 121, *High Angle of Attack Aerodynamics*, March 1982.
23. Ericsson, L. E. and Reding, J. P., "Alleviation of Vortex-Induced Asymmetric Loads," *Journal of Spacecraft*, v. 17, no. 6, November-December 1980.
24. Healey, J. V., *Simulating the Helicopter-Ship Interface as an Alternative to Current Methods of Determining the Safe Operating Envelopes*, Naval Postgraduate School Report, NPS 67-86-003, Monterey, CA., September 1986.
25. Gregoriou, G. and Knoche, H. G., *High Incidence Aerodynamics of Missiles During Launch Phase*, MBB GMBH Report UA-523/80, Munich, West Germany, January 1980.
26. *Laboratory Manual for Slow-speed Wind Tunnel Testing*, Department of Aeronautics, Naval Postgraduate School, Monterey, CA, 1983.
27. Velmex, Inc., *User's Guide to 8300 Series Stepping Motor Controller/Drivers*, East Bloomfield, NY, January 1988.
28. Naik, D. A., *An Investigation of the Aerodynamic Characteristics of Planar and Non-planar Outboard Wing Planforms*, Doctoral Dissertation, Texas A&M University, College Station, TX, December 1987.
29. United Sensors, Inc., *5-hole Probes Calibration Manual*, Watertown, MA, June 1988.
30. Hewlett-Packard, Inc., *PC Instruments System Owner's Guide Using HP 610618 System Interface*, February 1986.
31. Kindelspire, D. W., *The Effects of Freestream Turbulence on Airfoil Boundary Layer Behavior at Low Reynolds Number*, Master's Thesis, Naval Postgraduate School, Monterey, CA, September 1988.
32. Reed, L., Mattigly, J. D., and Jonas, F. M., *The Seven-hole Pressure Probe*, USAFA-TN-84-9, United States Air Force Academy, Colorado Springs, CO, 1984.

APPENDIX A. PPROBE PROGRAM

```
1 DEF SEG: CLEAR , &HFE00: GOTO 4 'BEGIN PCIB PROGRAM SHELL
2 GOTO 1000 ' USER PROGRAM
3 GOTO 900 ' ERROR HANDLING
4 I=&HFE00 ' COPYRIGHT HEWLETT-PACKARD 1984,1985
5 PCIB.DIRS=ENVIRON$("PCIB")
6 IS=PCIB.DIRS+"PCIBILC.BLD"
7 BLOAD IS,I
8 CALL I(PCIB.DIRS,I%,J%): PCIB.SEG=I%
9 IF J%=0 THEN GOTO 13
10 PRINT "UNABLE TO LOAD.";
11 PRINT " (ERROR #";J%;")"
12 END
13 '
14 DEF SEG=PCIB.SEG: O.S=5: C.S=10: I.V=15
15 I.C=20: L.P=25: L.D.FILE=30
16 GET.MEM=35: L.S=40: PANELS=45: DEF.ERR=50
17 PCIB.ERRORS=STRING$(64,32): PCIB.NAMES=STRING$(16,32)
18 CALL DEF.ERR(PCIB.ERR,PCIB.ERRORS,PCIB.NAMES,PCIB.GLBERR): PCIB.BASERR=255
19 ON ERROR GOTO 3
20 J=-1
21 IS=PCIB.DIRS+"PCIB.SYN"
22 CALL O.S(IS)
23 IF PCIB.ERR<>0 THEN ERROR PCIB.BASERR
24 I=0
25 CALL I.V(I,READ.REGISTER,READ.SELFID,DEFINE,INITIALIZE.SYSTEM)
26 IF PCIB.ERR<>0 THEN ERROR PCIB.BASERR
27 CALL I.V(I,ENABLE.SYSTEM,DISABLE.SYSTEM,INITIALIZE.POWER.ON)
28 IF PCIB.ERR<>0 THEN ERROR PCIB.BASERR
29 CALL I.V(I,MEASURE,OUTPUT,START,HALT)
30 IF PCIB.ERR<>0 THEN ERROR PCIB.BASERR
31 CALL I.V(I,ENABLE.INT.TRIGGER,DISABLE.INT.TRIGGER,ENABLE.OUTPUT,DISABLE.OUTPUT)
32 IF PCIB.ERR<>0 THEN ERROR PCIB.BASERR
33 CALL I.V(I,CHECK.DONE,GET.STATUS,SET.FUNCTION,SET.RANGE)
34 IF PCIB.ERR<>0 THEN ERROR PCIB.BASERR
35 CALL I.V(I,SET.MODE,WRITE.CAL.READ.CAL,STORE.CAL)
36 IF PCIB.ERR<>0 THEN ERROR PCIB.BASERR
37 CALL I.V(I,DELAY,SAVE.SYSTEM,J,J)
38 IF PCIB.ERR<>0 THEN ERROR PCIB.BASERR
39 I=1
40 CALL I.V(I,SET.GATETIME,SET.SAMPLES,SET.SLOPE,SET.SOURCE)
41 IF PCIB.ERR<>0 THEN ERROR PCIB.BASERR
42 CALL I.C(I,FREQUENCY,AUTO.FREQ.PERIOD,AUTO.PER)
43 IF PCIB.ERR<>0 THEN ERROR PCIB.BASERR
44 CALL I.C(I,INTERVAL,RATIO,TOTALIZE,R100MILLI)
45 IF PCIB.ERR<>0 THEN ERROR PCIB.BASERR
46 CALL I.C(I,R1,R10,R100,R1KILO)
47 IF PCIB.ERR<>0 THEN ERROR PCIB.BASERR
48 CALL I.C(I,R10MEGA,R100MEGA,CHAN.A,CHAN.B)
49 IF PCIB.ERR<>0 THEN ERROR PCIB.BASERR
50 CALL I.C(I,POSITIVE,NEGATIVE,COMN,SEPARATE)
```

```

51 IF PCIB.ERR<>0 THEN ERROR PCIB.BASERR
52 I=2
53 I=3
54 CALL I.V(I,ZERO.OHMS,SET.SPEED,J,J)
55 IF PCIB.ERR<>0 THEN ERROR PCIB.BASERR
56 CALL I.C(I,DCVOLTS,ACVOLTS,OHMS,R200MILLI)
57 IF PCIB.ERR<>0 THEN ERROR PCIB.BASERR
58 CALL I.C(I,R2,R20,R200,R2KILO)
59 IF PCIB.ERR<>0 THEN ERROR PCIB.BASERR
60 CALL I.C(I,R20KILO,R200KILO,R2MEGA,R20MEGA)
61 IF PCIB.ERR<>0 THEN ERROR PCIB.BASERR
62 CALL I.C(I,AUTOM,R2.5,R12.5,J)
63 IF PCIB.ERR<>0 THEN ERROR PCIB.BASERR
64 I=4
65 CALL I.V(I,SET.COMPLEMENT,SET.DRIVER,OUTPUT.NO.WAIT,ENABLE.HANDSHAKE)
66 IF PCIB.ERR<>0 THEN ERROR PCIB.BASERR
67 CALL I.V(I,DISABLE.HANDSHAKE,SET.THRESHOLD,SET.START.BIT,SET.NUM.BITS)
68 IF PCIB.ERR<>0 THEN ERROR PCIB.BASERR
69 CALL I.V(I,SET.LOGIC.SENSE,J,J,J)
70 IF PCIB.ERR<>0 THEN ERROR PCIB.BASERR
71 CALL I.C(I,POSITIVE,NEGATIVE,TWOS,UNSIGNED)
72 IF PCIB.ERR<>0 THEN ERROR PCIB.BASERR
73 CALL I.C(I,OC,TTL,R0,R1)
74 IF PCIB.ERR<>0 THEN ERROR PCIB.BASERR
75 CALL I.C(I,R2,R3,R4,R5)
76 IF PCIB.ERR<>0 THEN ERROR PCIB.BASERR
77 CALL I.C(I,R6,R7,R8,R9)
78 IF PCIB.ERR<>0 THEN ERROR PCIB.BASERR
79 CALL I.C(I,R10,R11,R12,R13)
80 IF PCIB.ERR<>0 THEN ERROR PCIB.BASERR
81 CALL I.C(I,R14,R15,R16,J)
82 IF PCIB.ERR<>0 THEN ERROR PCIB.BASERR
83 I=6
84 CALL I.V(I,SET.FREQUENCY,SET.AMPLITUDE,SET.OFFSET,SET.SYMMETRY)
85 IF PCIB.ERR<>0 THEN ERROR PCIB.BASERR
86 CALL I.V(I,SET.BURST.COUNT,J,J,J)
87 IF PCIB.ERR<>0 THEN ERROR PCIB.BASERR
88 CALL I.C(I,SINE,SQUARE,TRIANGLE,CONTINUOUS)
89 IF PCIB.ERR<>0 THEN ERROR PCIB.BASERR
90 CALL I.C(I,GATED,BURST,J,J)
91 IF PCIB.ERR<>0 THEN ERROR PCIB.BASERR
92 I=7
93 CALL I.V(I,AUTOSCALE,CALIBRATE,SET.SENSITIVITY,SET.VERT.OFFSET)
94 IF PCIB.ERR<>0 THEN ERROR PCIB.BASERR
95 CALL I.V(I,SET.COUPLING,SET.POLARITY,SET.SWEEPSPEED,SET.DELAY)
96 IF PCIB.ERR<>0 THEN ERROR PCIB.BASERR
97 CALL I.V(I,SET.TRIG.SOURCE,SET.TRIG.SLOPE,SET.TRIG.LEVEL,SET.TRIG.MODE)
98 IF PCIB.ERR<>0 THEN ERROR PCIB.BASERR
99 CALL I.V(I,GET.SINGLE.WF,GET.TWO.WF,GET.VERT.INFO,GET.TIMEBASE.INFO)
100 IF PCIB.ERR<>0 THEN ERROR PCIB.BASERR
101 CALL I.V(I,GET.TRIG.INFO,CALC.WFVOLT,CALC.WFTIME,CALC.WF.STATS)
102 IF PCIB.ERR<>0 THEN ERROR PCIB.BASERR
103 CALL I.V(I,CALC.RISETIME,CALC.FALLTIME,CALC.PERIOD,CALC.FREQUENCY)
104 IF PCIB.ERR<>0 THEN ERROR PCIB.BASERR
105 CALL I.V(I,CALC.PLUSWIDTH,CALC.MINUSWIDTH,CALC.OVERSHOOT,CALC.PRESHOOT)

```

```

106 IF PCIB.ERR<>0 THEN ERROR PCIB.BASERR
107 CALL I.V(I,CALC.PK.TO.PK,SET.TIMEOUT,SCOPE.START,MEASURE.SINGLE.WF)
108 IF PCIB.ERR<>0 THEN ERROR PCIB.BASERR
109 CALL I.V(I,MEASURE.TWO.WF,J,J,J)
110 IF PCIB.ERR<>0 THEN ERROR PCIB.BASERR
111 CALL I.C(I,R10NANO,R100NANO,R1MICRO,R10MICRO)
112 IF PCIB.ERR<>0 THEN ERROR PCIB.BASERR
113 CALL I.C(I,R100MICRO,R1MILLI,R10MILLI,R100MILLI)
114 IF PCIB.ERR<>0 THEN ERROR PCIB.BASERR
115 CALL I.C(I,R1,R10,R20NANO,R200NANO)
116 IF PCIB.ERR<>0 THEN ERROR PCIB.BASERR
117 CALL I.C(I,R2MICRO,R20MICRO,R200MICRO,R2MILLI)
118 IF PCIB.ERR<>0 THEN ERROR PCIB.BASERR
119 CALL I.C(I,R20MILLI,R200MILLI,R2,R20)
120 IF PCIB.ERR<>0 THEN ERROR PCIB.BASERR
121 CALL I.C(I,R50NANO,R500NANO,R5MICRO,R50MICRO)
122 IF PCIB.ERR<>0 THEN ERROR PCIB.BASERR
123 CALL I.C(I,R500MICRO,R5MILLI,R50MILLI,R500MILLI)
124 IF PCIB.ERR<>0 THEN ERROR PCIB.BASERR
125 CALL I.C(I,R5,R50,CHAN.A,CHAN.B)
126 IF PCIB.ERR<>0 THEN ERROR PCIB.BASERR
127 CALL I.C(I,EXTERNAL,POSITIVE,NEGATIVE,AC)
128 IF PCIB.ERR<>0 THEN ERROR PCIB.BASERR
129 CALL I.C(I,DC,TRIGGERED,AUTO.TRIG,AUTO.LEVEL)
130 IF PCIB.ERR<>0 THEN ERROR PCIB.BASERR
131 CALL I.C(I,X1,X10,STANDARD,AVERAGE)
132 IF PCIB.ERR<>0 THEN ERROR PCIB.BASERR
133 I=8
134 CALL I.V(I,OPEN.CHANNEL,CLOSE.CHANNEL,J,J)
135 IF PCIB.ERR<>0 THEN ERROR PCIB.BASERR
136 CALL C.S
137 IF PCIB.ERR<>0 THEN ERROR PCIB.BASERR
138 IS=PCIB.DIRS+"PCIB.PLD"
139 CALL L.P(IS)
140 IF PCIB.ERR<>0 THEN ERROR PCIB.BASERR
141 IS="DMM.01":I=3:J=0:K=0:L=1
142 CALL DEFINE(DMM.01,IS,I,J,K,L)
143 IF PCIB.ERR<>0 THEN ERROR PCIB.BASERR
144 IS="FUNC.GEN.01":I=6:J=0:K=1:L=1
145 CALL DEFINE(FUNC.GEN.01,IS,I,J,K,L)
146 IF PCIB.ERR<>0 THEN ERROR PCIB.BASERR
147 IS="SCOPE.01":I=7:J=0:K=2:L=1
148 CALL DEFINE(SCOPE.01,IS,I,J,K,L)
149 IF PCIB.ERR<>0 THEN ERROR PCIB.BASERR
150 IS="COUNTER.01":I=1:J=0:K=3:L=1
151 CALL DEFINE(COUNTER.01,IS,I,J,K,L)
152 IF PCIB.ERR<>0 THEN ERROR PCIB.BASERR
153 IS="DIG.IN.01":I=4:J=0:K=4:L=1
154 CALL DEFINE(DIG.IN.01,IS,I,J,K,L)
155 IF PCIB.ERR<>0 THEN ERROR PCIB.BASERR
156 IS="DIG.OUT.01":I=4:J=1:K=4:L=1
157 CALL DEFINE(DIG.OUT.01,IS,I,J,K,L)
158 IF PCIB.ERR<>0 THEN ERROR PCIB.BASERR
159 IS="RELAY.ACT.01":I=8:J=0:K=5:L=1
160 CALL DEFINE(RELAY.ACT.01,IS,I,J,K,L)

```

```

161 IF PCIB.ERR<>0 THEN ERROR PCIB.BASERR
162 IS="RELAY.MUX.01":I=2:J=0:K=6:L=1
163 CALL DEFINE(RELAY.MUX.01,IS,I,J,K,L)
164 IF PCIB.ERR<>0 THEN ERROR PCIB.BASERR
800 IS=ENVIRON$("PANELS")+~PANELS.EXE"
801 CALL L.S(IS)
899 GOTO 2
900 IF ERR=PCIB.BASERR THEN GOTO 903
901 PRINT "BASIC ERROR #";ERR;" OCCURRED IN LINE ";ERL
902 STOP
903 TMPERR=PCIB.ERR:IF TMPERR=0 THEN TMPERR=PCIB.GLBERR
904 PRINT "PC INSTRUMENT ERROR #";TMPERR;" DETECTED AT LINE ";ERL
905 PRINT "ERROR: ";PCIB.ERRS
906 IF LEFT$(PCIB.NAMES,1)<>CHR$(32) THEN PRINT "INSTRUMENT: ";PCIB.NAMES
907 STOP
908 COMMON PCIB.DIRS,PCIB.SEG
909 COMMON LD.FILE,GET.MEM,PANELS,DEF.ERR
910 COMMON PCIB.BASERR,PCIB.ERR,PCIB.ERRS,PCIB.NAMES,PCIB.GLBERR
911 COMMON READ.REGISTER,READ.SELFID,DEFINE,INITIALIZE.SYSTEM,
    ENABLE.SYSTEM,DISABLE.SYSTEM,INITIALIZE.POWER.ON,MEASURE.OUTPUT,
    START,HALT,ENABLE.INT.TRIGGER,DISABLE.INT.TRIGGER,ENABLE.OUTPUT,
    DISABLE.OUTPUT,CHECK.DONE,GET.STATUS
912 COMMON SET.FUNCTION,SET.RANGE,SET.MODE,WRITE.CAL,READ.CAL,
    STORE.CAL,DELAY,SAVE.SYSTEM,SET.GATETIME,SET.SAMPLES,SET.SLOPE,
    SET.SOURCE,ZERO.OHMS,SET.SPEED,SET.COMPLEMENT,SET.DRIVER,
    OUTPUT.NO.WAIT,ENABLE.HANDSHAKE,DISABLE.HANDSHAKE
913 COMMON SET.THRESHOLD,SET.START.BIT,SET.NUM.BITS,SET.LOGIC.SENSE,
    SET.FREQUENCY,SET.AMPLITUDE,SET.OFFSET,SET.SYMMETRY,
    SET.BURST.COUNT,AUTOSCALE,CALIBRATE,SET.SENSITIVITY,
    SET.VERT.OFFSET,SET.COUPLING,SET.POLARITY,SET.SWEEPSPEED
914 COMMON SET.DELAY,SET.TRIG.SOURCE,SET.TRIG.SLOPE,SET.TRIG.LEVEL,
    SET.TRIG.MODE,GET.SINGLE.WF,GET.TWO.WF,GET.VERT.INFO,
    GET.TIMEBASE.INFO,GET.TRIG.INFO,CALC.WFVOLT,CALC.WFTIME,
    CALC.WF.STATS,CALC.RISETIME,CALC.FALLTIME,CALC.PERIOD
915 COMMON CALC.FREQUENCY,CALC.PLUSWIDTH,CALC.MINUSWIDTH,
    CALC.OVERSHOOT,CALC.PRESHOOT,CALC.PK.TO.PK,SET.TIMEOUT,
    SCOPE.START,MEASURE.SINGLE.WF,MEASURE.TWO.WF,OPEN.CHANNEL,
    CLOSE.CHANNEL
916 COMMON FREQUENCY,AUTO.FREQ,PERIOD,AUTO.PER,INTERVAL,RATIO,
    TOTALIZE,R100MILLI,R1,R10,R100,R1KILO,R10MEGA,R100MEGA,CHAN.A,
    CHAN.B,POSITIVE,NEGATIVE,COMN,SEPARATE,DCVOLTS,ACVOLTS,OHMS,
    R200MILLI,R2,R20,R200,R2KILO,R20KILO,R200KILO
917 COMMON R2MEGA,R20MEGA,AUTOM,R2.5,R12.5,POSITIVE,NEGATIVE,TWOS,
    UNSIGNED,OC,TTL,R0,R1,R2,R3,R4,R5,R6,R7,R8,R9,R10,R11,R12,R13,R14,R15,
    R16,SINE,SQUARE,TRIANGLE,CONTINUOUS,GATED,BURST,R10NANO,
    R100NANO,R1MICRO,R10MICRO,R100MICRO
918 COMMON R1MILLI,R10MILLI,R100MILLI,R1,R10,R20NANO,R200NANO,R2MICRO,
    R20MICRO,R200MICRO,R2MILLI,R20MILLI,R200MILLI,R2,R20,R50NANO,
    R500NANO,R5MICRO,R50MICRO,R500MICRO,R5MILLI,R50MILLI,R500MILLI,R5,
    R50,CHAN.A,CHAN.B,EXTERNAL,POSITIVE
919 COMMON NEGATIVE,AC,DC,TRIGGERED,AUTO.TRIG,AUTO.LEVEL,X1,X10,
    STANDARD,AVERAGE
920 COMMON DMM.01,FUNC.GEN.01,SCOPE.01,COUNTER.01,DIG.IN.01,DIG.OUT.01,
    RELAY.ACT.01,RELAY.MUX.01
999 END PCIB PROGRAM SHELL

```

```

1000 REM THIS STEP INITIALIZES THE HP SYSTEM
1010 CLS
1020 OPTION BASE 1
1030 DIM P(5),PA(50,5),PP(50,5),XPT(50),YPT(50),X(50),Y(50),YAW(50)
1040 REM
1050 CALL INITIALIZE.SYSTEM(PGMSHEL.HPC)
1060 REM
1070 REM SET FUNCTION ON THE 'DMM', 'RELAY MUX', 'RELAY ACTUATOR'
1080 REM
1090 CALL SET.FUNCTION(DMM.01,DCVOLTS)
1100 CALL SET.RANGE(DMM.01,AUTOM)
1110 CALL DISABLE.INT.TRIGGER(DMM.01)
1120 CALL ENABLE.OUTPUT(RELAY.MUX.01)
1130 CALL ENABLE.OUTPUT(RELAY.ACT.01)
1140 REM ***** PROGRAM TRAVERSE *****
1150 REM
1160 REM OPEN THE COM PORT AND INITIALIZE THE MOTOR SETTINGS
1170 OPEN "COM1:1200,N,8,1,RS,CS,DS,CD" AS #1
1180 REM SET MOTOR DEFAULT VALUES
1190 DATA 2000,2000,2000,2,2,2,0.000125,0.000125,0.000125
1200 READ V1,V2,V3,R1,R2,R3,C1,C2,C3
1210 REM DEFINE CHARACTERS FOR DATA REDUCTION ALGORITHM
1220 RN25="RENAME A:RAW.DAT "
1230 HEAD1S=" # X Y P1 P2 P3 P4 P5 YAW "
1240 FORMATS="## ##.## ##.## ###.### ###.### ###.### ###.### ###.### ###.###"
1250 PRINT
1260 PRINT "*****"
1270 PRINT "** USER MUST SELECT 'CAPS LOCK' FUNCTION **"
1280 PRINT "*****"
1290 REM DISPLAY MOTOR DEFAULT SETTINGS
1300 PRINT " *****"
1310 PRINT " INITIALIZED VALUES FOR ALL MOTOR SETTINGS:"
1320 PRINT " VELOCITY = 1000 STEPS/SEC"
1330 PRINT " RAMP(MOTOR ACCELERATION) = 2 (6000 STEPS/SEC^2)"
1340 PRINT " DEFAULT INCREMENTAL UNITS ARE INCHES"
1350 PRINT " *****"
1360 PRINT
1370 PRINT "NOTE!! USE MANUAL CONTROL TO INITIALIZE PROBE POSITION BEFORE"
1380 PRINT " SELECTING COMPUTER CONTROLLED MOVEMENT. "
1390 PRINT
1400 INPUT "MANUAL CONTROL OR COMPUTER CONTROL (ENTER 'MAN' OR 'CP')";CONS
1410 IF CONS="CP" THEN 3490
1420 REM OPTION TO CHANGE DEFAULT SETTINGS OF VELOCITY OR ACCELERATION
RAMP
1430 PRINT
1440 PRINT
1450 PRINT " DO YOU WANT TO CHANGE THE VELOCITY OR ACCELERATION RAMP"
1460 PRINT " DEFAULT SETTINGS? (Y OR N)"
1470 PRINT
1480 PRINT "IF 'NO', THIS PROGRAM WILL THEN LET YOU DEFINE THE"
1490 PRINT "DISTANCE YOU WANT TO MOVE (IN INCHES). IF 'YES',"
1500 PRINT "YOU CAN CHANGE ANY OR ALL OF THE DEFAULT SETTINGS FOR ANY
MOTOR."
1510 PRINT
1520 PRINT

```

```

1530 PRINT
1540 INPUT "DO YOU WANT TO CHANGE ANY OF THE DEFAULT SETTINGS? (Y OR N)";DS
1550 IF DS="Y" THEN 1590
1560 IF DS="N" THEN 2220
1570 REM
1580 REM ***** OPERATOR SELECTED MOTOR VARIABLES *****
1590 PRINT
1600 PRINT
1610 INPUT "WHICH DEFAULT VALUE? (ENTER '1' FOR VELOC OR '2' FOR ACCEL RAMP)";L
1620 ON L GOTO 1690,1930
1630 PRINT "DO YOU WANT TO CHANGE THE DEFAULT VELOCITY? (Y OR N)"
1640 INPUT VS
1650 IF VS="Y" THEN 1690
1660 PRINT "DO YOU WANT TO CHANGE THE DEFAULT ACCELERATION RAMP? (Y OR N)"
1670 IF RS="Y" THEN 1990
1680 IF RS="N" THEN 1450
1690 PRINT
1700 PRINT
1710 INPUT "WHICH MOTOR VELOCITY DO YOU WISH TO CHANGE? (1,2, OR 3)";J
1720 ON J GOTO 1730,1830,1880
1730 PRINT
1740 PRINT
1750 INPUT "ENTER DESIRED VELOCITY OF MOTOR #1";V1
1760 PRINT
1770 PRINT
1780 PRINT
1790 PRINT "DO YOU WANT TO CHANGE VELOCITY OF ANOTHER MOTOR? (Y OR N)"
1800 INPUT VS
1810 IF VS="Y" THEN 1690
1820 IF VS="N" THEN 1430
1830 PRINT
1840 PRINT
1850 INPUT "ENTER DESIRED VELOCITY OF MOTOR 2";V2
1860 PRINT
1870 GOTO 1780
1880 PRINT
1890 PRINT
1900 INPUT "ENTER DESIRED VELOCITY OF MOTOR #3";V3
1910 PRINT
1920 GOTO 1780
1930 PRINT
1940 PRINT
1950 INPUT "WHICH MOTOR ACCEL RAMP DO YOU WANT TO CHANGE? (1, 2, OR 3)";K
1960 ON K GOTO 1970,2060,2120
1970 PRINT
1980 PRINT
1990 INPUT "ENTER DESIRED ACCELERATION RAMP OF MOTOR #1";R1
2000 PRINT
2010 PRINT
2020 PRINT "DO YOU WANT TO CHANGE THE ACCEL RAMP OF ANOTHER MOTOR? (Y OR N)?"
2030 INPUT RMS
2040 IF RMS="Y" THEN 1930
2050 IF RMS="N" THEN 1450
2060 PRINT

```

```

2070 PRINT
2080 INPUT "ENTER DESIRED ACCELERATION RAMP OF MOTOR #2";R2
2090 PRINT
2100 PRINT
2110 GOTO 2000
2120 PRINT
2130 PRINT
2140 INPUT "ENTER DESIRED ACCELERATION RAMP OF MOTOR #3";R3
2150 PRINT
2160 PRINT
2170 GOTO 2000
2180 REM
2190 REM DEFINE DISTANCE TO MOVE MOTOR
2200 PRINT
2210 PRINT
2220 PRINT
2230 REM INITIALIZE MOTOR INCREMENTS TO ZERO
2240 I1=0
2250 I2=0
2260 I3=0
2270 PRINT
2280 PRINT " *****"
2290 PRINT " **      DEFINE WHICH MOTOR YOU WANT TO MOVE      **"
2300 PRINT " **                                                    **"
2310 PRINT " **      NOTE!!! A POSITIVE (+) INCREMENT TO A MOTOR      **"
2320 PRINT " **      MOVES TRAVERSER AWAY FROM THAT PARTICULAR MOTOR **"
2330 PRINT " **                                                    **"
2340 PRINT " ** -- MOTOR #1 MOVES THE PROBE UPSTREAM AGAINST THE FLOW **"
2350 PRINT " ** -- MOTOR #2 MOVES THE PROBE TOWARD THE ACCESS WINDOW **"
2360 PRINT " ** -- MOTOR #3 MOVES THE PROBE VERTICALLY DOWNWARD      **"
2370 PRINT " *****"
2380 PRINT
2390 PRINT
2400 INPUT "WHICH MOTOR DO YOU WANT TO MOVE? (1,2, OR 3)";L
2410 ON L GOTO 2420,2680,2970
2420 PRINT
2430 PRINT
2440 PRINT "HOW FAR DO YOU WANT TO MOVE MOTOR #1?"
2450 PRINT " ***** (ENTER DISTANCE IN INCHES) *****"
2460 INPUT I1
2470 PRINT
2480 PRINT " *****"
2490 PRINT
2500 PRINT "SUMMARY OF OPERATOR INPUTS:"
2510 PRINT "      MOTOR #1  VELOCITY = ";V1
2520 PRINT "              ACCELERATION RAMP = ";R1
2530 PRINT "              INCREMENTAL DISTANCE = ";I1;"INCHES"
2540 PRINT " *****"
2550 PRINT "DO YOU WANT TO CHANGE ANY OF THESE VALUES? (Y OR N)"
2560 PRINT
2570 PRINT "ENTER 'N' TO START MOTOR MOVEMENT.  ENTER 'Y' TO RETURN"
2580 PRINT "TO VARIABLE SELECTION SUBROUTINE."
2590 INPUT VS
2600 IF VS="Y" THEN 1430
2610 GOSUB 3410

```

```

2620 PRINT
2630 PRINT "DO YOU WANT TO MOVE ANOTHER MOTOR ALSO? (Y OR N)?"
2640 INPUT CS
2650 IF CS="Y" THEN 2220
2660 IF CS="N" THEN 3260
2670 PRINT
2680 PRINT
2690 PRINT "HOW FAR DO YOU WANT TO MOVE MOTOR #2?"
2700 PRINT " ***** (ENTER DISTANCE IN INCHES) *****"
2710 INPUT I2
2720 PRINT
2730 PRINT
2740 REM DISPLAY OPERATOR SELECTED MOTOR VARIABLES
2750 PRINT" *****"
2760 PRINT
2770 PRINT "SUMMARY OF OPERATOR INPUTS:"
2780 PRINT "      MOTOR #2  VELOCITY = ";V2
2790 PRINT "      ACCELERATION RAMP = ";R2
2800 PRINT "      INCREMENTAL DISTANCE = ";I2;"INCHES"
2810 PRINT" *****"
2820 PRINT
2830 PRINT
2840 PRINT "DO YOU WANT TO CHANGE ANY OF THESE VALUES? (Y OR N)"
2850 PRINT
2860 PRINT "ENTER 'N' TO START MOTOR MOVEMENT. ENTER 'Y' TO RETURN"
2870 PRINT "TO VARIABLE SELECTION SUBROUTINE."
2880 INPUT VS
2890 IF VS="Y" THEN 1430
2900 GOSUB 3410
2910 PRINT
2920 PRINT "DO YOU WANT TO MOVE ANOTHER MOTOR ALSO? (Y OR N)?"
2930 INPUT CS
2940 IF CS="Y" THEN 2220
2950 IF CS="N" THEN 3260
2960 PRINT
2970 PRINT
2980 PRINT "HOW FAR DO YOU WANT TO MOVE MOTOR #3?"
2990 PRINT " ***** (ENTER DISTANCE IN INCHES) *****"
3000 INPUT I3
3010 PRINT
3020 PRINT
3030 REM DISPLAY OPERATOR SELECTED MOTOR VARIABLES
3040 PRINT" *****"
3050 PRINT
3060 PRINT "SUMMARY OF OPERATOR INPUTS:"
3070 PRINT "      MOTOR #3  VELOCITY = ";V3
3080 PRINT "      ACCELERATION RAMP = ";R3
3090 PRINT "      INCREMENTAL DISTANCE = ";I3;"INCHES"
3100 PRINT
3110 PRINT" *****"
3120 PRINT
3130 PRINT
3140 PRINT "DO YOU WANT TO CHANGE ANY OF THESE VALUES? (Y OR N)"
3150 PRINT
3160 PRINT "ENTER 'N' TO START MOTOR MOVEMENT. ENTER 'Y' TO RETURN"

```



```

3170 PRINT "TO VARIABLE SELECTION SUBROUTINE."
3180 INPUT VS
3190 IF VS="Y" THEN 1430
3200 GOSUB 3410
3210 PRINT
3220 PRINT
3230 INPUT "DO YOU WANT TO INPUT ANOTHER MANUAL MOTOR MOVEMENT (Y OR
N)";MS
3240 IF MS="Y" THEN 2210
3250 PRINT
3260 PRINT "DO YOU WANT TO INPUT COMPUTER CONTROLLED MOTOR MOVEMENT?"
3270 PRINT " ***** NOTE!!! ***** "
3280 PRINT " ALL PREVIOUS MOTOR INCREMENT INPUTS HAVE BEEN ZEROIZED."
3290 PRINT "PROGRAM WILL LET YOU CHOOSE MANUAL OR CP-CONTROLLED MOVEMENT."
3300 PRINT "***** (IF NO, THE PROGRAM WILL END). *****"
3310 PRINT
3320 INPUT "DO YOU WANT COMPUTER CONTROLLED MOTOR MOVEMENT (Y OR N)";NS
3330 IF NS="Y" THEN 3500
3340 PRINT
3350 PRINT
3360 PRINT
3370 PRINT " *****"
3380 PRINT " THE PROGRAM HAS ENDED."
3390 PRINT " *****"
3400 END
3410 REM ***** MOTOR MOVEMENT SUBROUTINE *****
3420 PRINT #1, "&" :PRINT #1, "E";C1="";C1="";C2="";C2="";C3="";C3
3430 PRINT #1, "I1=";I1="";V1="";V1="";R1="";R1;
3440 PRINT #1, "I2=";I2="";V2="";V2="";R2="";R2
3450 PRINT #1, "I3=";I3="";V3="";V3="";R3="";R3;"@"
3460 RETURN
3470 REM *****
3480 REM *****
3490 PRINT
3500 REM ***** COMPUTER CONTROLLED MOVEMENT *****
3510 PRINT
3520 PRINT "THE PRESSURE DATA WILL BE WRITTEN TO FILES ON DRIVE 'A' "
3530 PRINT
3540 PRINT "YOU WILL BE ASKED TO INPUT FILE NAMES FOR THESE."
3550 PRINT
3560 INPUT "IS A FORMATTED DISK IN DRIVE 'A'? PRESS 'ENTER' TO CONTINUE";DS
3570 PRINT
3580 PRINT
3590 PRINT
3600 PRINT " *****"
3610 PRINT " ** NOTE !!! **"
3620 PRINT " ** COMPUTER CONTROLLED MOVEMENT **"
3630 PRINT " ** IS PROGRAMMED WITH A **"
3640 PRINT " ** DEFAULTED NEGATIVE MOTOR INCREMENT **"
3650 PRINT " ** (I.E. MOTOR #3 WILL MOVE UPWARD **"
3660 PRINT " ** BY ENTERING A (+) DISTANCE). **"
3670 PRINT " *****"
3680 PRINT
3690 REM SET INITIAL MOVEMENT DISTANCE AND NUMBER OF DATA POINTS TO ZERO
3700 HT=0

```

```

3710 WD=0
3720 DIST=0
3730 XPT=0
3740 YPT=0
3750 N=0
3760 PRINT
3770 PRINT
3780 INPUT "WHAT IS THE DIMENSION ( X , Y ) (IN INCHES) THAT YOU WANT TO
      MEASURE." ;WD,HT
3790 PRINT
3800 INPUT "WHAT IS THE STEP (IN INCHES) THAT YOU WANT TO MOVE.";DIST
3810 YPT=INT(HT /DIST) + 1
3820 XPT=INT(WD /DIST)+ 1
3830 N=XPT*YPT
3840 PRINT
3850 PRINT "THERE ARE ";XPT;" * ";YPT;" = ";N;" POINTS TO BE MEASURED "
3860 PRINT
3870 INPUT "ARE THE NUMBER OF POINTS IS OK.(Y OR N)";CS
3880 IF CS="N" THEN 3780
3890 CLS
3900 N=XPT
3910 IF (N < 1) OR (N > 99) GOTO 3780
3920 REM *** GENERATING STRING STRING SEGMENTS FOR DATA FILE NAMES
3930 BS = MIDS(STR$(1), 2): REM ** STRING NUMBER "1"
3940 ES = MIDS(STR$(N), 2): REM ** ENDING STRING NUMBER "N"
3950 XS = "XXXXXX"
3960 EXS = ".DAT"
3970 CLS
3980 PRINT "DATA FILES WILL BE INCREMENTED FROM:"
3990 PRINT
4000 PRINT (XS + BS + EXS); " TO "; (XS + ES + EXS)
4010 PRINT
4020 PRINT
4030 INPUT "ENTER DATA FILE NAME (6 CHARACTERS MAX -- NO EXTENSION)";F2S
4040 PRINT
4050 PRINT
4060 IF LEN(F2S) > 6 OR LEN(F2S) < 1 GOTO 4030
4070 CLS
4080 PRINT N; "DATA FILES WILL BE GENERATED AND INCREMENTED AS FOLLOWS:"
4090 PRINT
4100 PRINT
4110 PRINT (F2S + BS + EXS); " TO "; (F2S + ES + EXS)
4120 PRINT
4130 PRINT
4140 INPUT "ARE THE NUMBER OF POINTS AND FILE NAMES OK.(Y OR N)"; CS
4150 IF CS = "N" GOTO 3780
4160 IF CS = "Y" GOTO 4180
4170 GOTO 4140
4180 CLS
4190 PRINT
4200 PRINT
4210 REM SET INITIAL POSITION DATA
4220 X(1)=-DIST
4230 Y(1)=-DIST
4240 FOR IX=2 TO XPT+1

```

```

4250 X(IX)=0
4260 NEXT IX
4270 FOR JY=2 TO YPT+1
4280 Y(JY)=0
4290 NEXT JY
4300 FOR I=1 TO XPT
4302 I1=0
4304 I2=0
4306 I3=0
4310 FOR J=1 TO YPT
4320 REM MOTOR CP-CONTROLLED MOTOR MOVEMENT
4330 I1=0
4340 I2=0
4350 I3=0
4360 REM EACH POINT TAKE 10 TIMES READINGS
4370 X(I+1)=X(I)+DIST
4380 XPT(J)=X(I+1)
4390 Y(J+1)=Y(J)+DIST
4400 YPT(J)=Y(J+1)
4405 INPUT " ADJUST THE WHEEL TO MAKE THE P2 =P3,INPUT THE YAW ANGLE";YAW(J)
4408 PRINT
4410 INPUT " PRESS 'ENTER' TO START THE MEASUREMENT";MOVES
4420 REM
4430 REM READ FIVE CHANNELS AND DISPLAY THE DATA
4440 REM
4450 STEPPER=4
4460 SWITCH = 3
4470 HOMER=8
4480 DELAY1 = .1
4490 DELAY2 = 1
4500 REM SET THE S.V PORT TO #4
4510 FOR IL=1 TO 3
4520 THYME = TIMER
4530 CALL OUTPUT(RELAY.ACT.01,STEPPER)
4540 CHKTIME = TIMER
4550 IF CHKTIME < (THYME + DELAY1) GOTO 4540
4560 CALL OPEN.CHANNEL(RELAY.ACT.01,SWITCH)
4570 CLS
4580 NEXT IL
4590 PRINT
4600 PRINT " NOW IS "J;" POINT "
4610 REM START MEASURE FROM PORT 4 TO PORT 8
4620 FOR JJ=1 TO 5
4630 CALL OUTPUT(RELAY.ACT.01,STEPPER)
4640 CHKTIME = TIMER
4650 IF CHKTIME < (THYME + DELAY2) GOTO 4640
4660 REM EACH PORT SAMPLE 10 TIMES
4670 FOR II=1 TO 10
4680 ROUT=1
4690 CALL OUTPUT(RELAY.MUX.01,ROUT)
4700 CALL MEASURE(DMM.01,VOLTS)
4710 PA(II,JJ)=VOLTS
4720 NEXT II
4730 CALL OPEN.CHANNEL(RELAY.ACT.01,SWITCH)
4740 IF JJ=5 THEN 4760

```

```

4750 NEXT JJ
4760 REM HOME THE S.V PORT TO #48
4770 CALL OUTPUT(RELAY.ACT.01,HOMER)
4780 CALL OPEN.CHANNEL(RELAY.ACT.01,HOMER)
4790 REM
4800 REM DISPLAY THE SAMPLE DATA
4810 REM
4820 PRINT HEAD1$
4830 FOR IS= 1 TO 10
4840 PRINT USING FORMATS;IS,XPT(J),YPT(J),PA(IS,1),PA(IS,2),PA(IS,3),PA(IS,4),
      PA(IS,5),YAW(J)
4850 NEXT IS
4860 REM
4870 REM AVERAGE THE DATA
4880 REM
4890 FOR JA = 1 TO 5
4900 TOTAL = 0
4910 FOR IA = 1 TO 10
4920 TOTAL = TOTAL + PA(IA,JA)
4930 NEXT IA
4940 AVERAGE = TOTAL /10
4950 P(JA)=AVERAGE
4960 NEXT JA
4970 PRINT
4980 PRINT "THE AVERAGE ARE: "
4990 PRINT
5000 PRINT HEAD1$
5010 FOR JD=1 TO 5
5020 PP(J,JD)=P(JD)
5030 NEXT JD
5040 PRINT USING FORMATS;J,XPT(J),YPT(J),PP(J,1),PP(J,2),PP(J,3),PP(J,4),PP(J,5),YAW(J)
5045 PRINT
5050 PRINT "DO YOU WANT RE-MEASURE AGAIN (Y / N)"
5060 PRINT
5062 PRINT "IF 'Y' WILL RE-SAMPLE AGAIN."
5064 PRINT
5070 INPUT "IF 'N' WILL MOVE THE TRAVERSER STEP UPWARD (WAIT 7 SEC )";CS
5075 PRINT
5080 IF CS="Y" THEN 4405
5082 IF CS="N" THEN 5090
5084 GO TO 5070
5090 IF J=YPT THEN 5160
5100 REM
5110 REM MOVE THE TRAVERSER STEP UPWARD.
5120 REM
5130 I3=-DIST
5140 GOSUB 3410
5150 NEXT J
5160 REM*** STORE DATA BEFORE NEXT SAMPLE***
5170 OPEN "A:\RAW.DAT" FOR OUTPUT AS #2
5180 PRINT #2 ,HEAD1$
5190 FOR ID=1 TO YPT
5200 PRINT #2 ,USING FORMATS;ID,XPT(ID),YPT(ID),PP(ID,1),PP(ID,2),PP(ID,3), PP(ID,4),
      PP(ID,5),YAW(ID)
5210 NEXT ID

```

```

5220 CLOSE #2
5230 REM *** GENERATING INCREMENTED DATA FILE NAME
5240 IF (I > 10) OR (I = 10) THEN IS = MIDS(STR$(I), 2)
5250 IF (I < 10) THEN IS = (MIDS(STR$(0), 2) + MIDS(STR$(I), 2))
5260 FI2$ = (F2$ + IS + EX$)
5270 PRINT
5280 PRINT " WRITING DATA FILE "; FI2$
5290 DF2$=RN2$+FI2$
5300 REM ** RENAME DATA FILE
5310 SHELL DF2$
5320 REM
5330 REM MOVE THE TRAVERSER TO THE NEXT SAMPLE POSITION
5340 REM
5350 PRINT
5360 IF I=XPT THEN 5430
5370 INPUT "THEN PRESS 'ENTER' FOR NEXT COLUMN SAMPLE( 90 SEC) ";MOVES
5390 I2=-DIST
5400 I3=HT
5410 GOSUB 3410
5420 NEXT I
5430 CLS
5440 PRINT "ALL MOVEMENTS COMPLETE"
5450 PRINT
5460 PRINT
5470 PRINT "YOU WANT TO REPOSITION TRAVERSER FOR ANOTHER MOVEMENT(YOR N)?"
5480 PRINT
5490 PRINT "IF 'Y', THE PROGRAM WILL TAKE YOU TO MANUAL CONTROL SUBROUTINE."
5500 PRINT "IF 'N', THE PROGRAM WILL END."
5510 PRINT
5520 INPUT "ANOTHER MOVEMENT";RS
5530 IF RS = "Y" THEN 1370
5540 IF RS = "N" THEN 3370

```

APPENDIX B. CALP PROGRAM

```
1 DEF SEG: CLEAR , &HFE00: GOTO 4 'BEGIN PCIB PROGRAM SHELL
2 GOTO 1000 ' USER PROGRAM
3 GOTO 900 ' ERROR HANDLING
4 I=&HFE00 ' COPYRIGHT HEWLETT-PACKARD 1984,1985
5 PCIB.DIRS=ENVIRONS("PCIB")
6 IS=PCIB.DIRS+"PCIBILC.BLD"
7 BLOAD IS,I
8 CALL I(PCIB.DIRS,I%,J%):PCIB.SEG=I%
9 IF J%=0 THEN GOTO 13
10 PRINT "UNABLE TO LOAD.";
11 PRINT " (ERROR #";J%;" )"
12 END
13 '
14 DEF SEG=PCIB.SEG: O.S=5: C.S=10: I.V=15
15 I.C=20: L.P=25: LD.FILE=30
16 GET.MEM=35: L.S=40: PANELS=45: DEF.ERR=50
17 PCIB.ERRS=STRINGS(64,32): PCIB.NAMES=STRINGS(16,32)
18 CALL DEF.ERR(PCIB.ERR,PCIB.ERRS,PCIB.NAMES,PCIB.GLBERR): PCIB.BASERR=255
19 ON ERROR GOTO 3
20 J=-1
21 IS=PCIB.DIRS+"PCIB.SYN"
22 CALL O.S(IS)
23 IF PCIB.ERR<>0 THEN ERROR PCIB.BASERR
24 I=0
25 CALL I.V(I,READ.REGISTER,READ.SELFID,DEFINE,INITIALIZE.SYSTEM)
26 IF PCIB.ERR<>0 THEN ERROR PCIB.BASERR
27 CALL I.V(I,ENABLE.SYSTEM,DISABLE.SYSTEM,INITIALIZE,POWER.ON)
28 IF PCIB.ERR<>0 THEN ERROR PCIB.BASERR
29 CALL I.V(I,MEASURE,OUTPUT,START,HALT)
30 IF PCIB.ERR<>0 THEN ERROR PCIB.BASERR
31 CALL I.V(I,ENABLE.INT.TRIGGER,DISABLE.INT.TRIGGER,ENABLE.OUTPUT,DISABLE.OUTT)
32 IF PCIB.ERR<>0 THEN ERROR PCIB.BASERR
33 CALL I.V(I,CHECK.DONE,GET.STATUS,SET.FUNCTION,SET.RANGE)
34 IF PCIB.ERR<>0 THEN ERROR PCIB.BASERR
35 CALL I.V(I,SET.MODE,WRITE.CAL,READ.CAL,STORE.CAL)
36 IF PCIB.ERR<>0 THEN ERROR PCIB.BASERR
37 CALL I.V(I,DELAY,SAVE.SYSTEM,J,J)
38 IF PCIB.ERR<>0 THEN ERROR PCIB.BASERR
39 I=1
40 CALL I.V(I,SET.GATETIME,SET.SAMPLES,SET.SLOPE,SET.SOURCE)
41 IF PCIB.ERR<>0 THEN ERROR PCIB.BASERR
42 CALL I.C(I,FREQUENCY,AUTO.FREQ.PERIOD,AUTO.PER)
43 IF PCIB.ERR<>0 THEN ERROR PCIB.BASERR
44 CALL I.C(I,INTERVAL,RATIO,TOTALIZE,R100MILLI)
45 IF PCIB.ERR<>0 THEN ERROR PCIB.BASERR
46 CALL I.C(I,R1,R10,R100,R1KILO)
47 IF PCIB.ERR<>0 THEN ERROR PCIB.BASERR
48 CALL I.C(I,R10MEGA,R100MEGA,CHAN.A,CHAN.B)
49 IF PCIB.ERR<>0 THEN ERROR PCIB.BASERR
50 CALL I.C(I,POSITIVE,NEGATIVE,COMN,SEPARATE)
```

```

51 IF PCIB.ERR<>0 THEN ERROR PCIB.BASERR
52 I=2
53 I=3
54 CALL I.V(I,ZERO.OHMS,SET.SPEED,J,J)
55 IF PCIB.ERR<>0 THEN ERROR PCIB.BASERR
56 CALL I.C(I,DCVOLTS,ACVOLTS,OHMS,R200MILLI)
57 IF PCIB.ERR<>0 THEN ERROR PCIB.BASERR
58 CALL I.C(I,R2,R20,R200,R2KILO)
59 IF PCIB.ERR<>0 THEN ERROR PCIB.BASERR
60 CALL I.C(I,R20KILO,R200KILO,R2MEGA,R20MEGA)
61 IF PCIB.ERR<>0 THEN ERROR PCIB.BASERR
62 CALL I.C(I,AUTOM,R2.5,R12.5,J)
63 IF PCIB.ERR<>0 THEN ERROR PCIB.BASERR
64 I=4
65 CALL I.V(I,SET.COMPLEMENT,SET.DRIVER,OUTPUT.NO.WAIT,ENABLE.HANDSHAKE)
66 IF PCIB.ERR<>0 THEN ERROR PCIB.BASERR
67 CALL I.V(I,DISABLE.HANDSHAKE,SET.THRESHOLD,SET.START.BIT,SET.NUM.BITS)
68 IF PCIB.ERR<>0 THEN ERROR PCIB.BASERR
69 CALL I.V(I,SET.LOGIC.SENSE,J,J,J)
70 IF PCIB.ERR<>0 THEN ERROR PCIB.BASERR
71 CALL I.C(I,POSITIVE,NEGATIVE,TWOS,UNSIGNED)
72 IF PCIB.ERR<>0 THEN ERROR PCIB.BASERR
73 CALL I.C(I,OC,TTL,R0,R1)
74 IF PCIB.ERR<>0 THEN ERROR PCIB.BASERR
75 CALL I.C(I,R2,R3,R4,R5)
76 IF PCIB.ERR<>0 THEN ERROR PCIB.BASERR
77 CALL I.C(I,R6,R7,R8,R9)
78 IF PCIB.ERR<>0 THEN ERROR PCIB.BASERR
79 CALL I.C(I,R10,R11,R12,R13)
80 IF PCIB.ERR<>0 THEN ERROR PCIB.BASERR
81 CALL I.C(I,R14,R15,R16,J)
82 IF PCIB.ERR<>0 THEN ERROR PCIB.BASERR
83 I=6
84 CALL I.V(I,SET.FREQUENCY,SET.AMPLITUDE,SET.OFFSET,SET.SYMMETRY)
85 IF PCIB.ERR<>0 THEN ERROR PCIB.BASERR
86 CALL I.V(I,SET.BURST.COUNT,J,J,J)
87 IF PCIB.ERR<>0 THEN ERROR PCIB.BASERR
88 CALL I.C(I,SINE,SQUARE,TRIANGLE,CONTINUOUS)
89 IF PCIB.ERR<>0 THEN ERROR PCIB.BASERR
90 CALL I.C(I,GATED,BURST,J,J)
91 IF PCIB.ERR<>0 THEN ERROR PCIB.BASERR
92 I=7
93 CALL I.V(I,AUTOSCALE,CALIBRATE,SET.SENSITIVITY,SET.VERT.OFFSET)
94 IF PCIB.ERR<>0 THEN ERROR PCIB.BASERR
95 CALL I.V(I,SET.COUPLING,SET.POLARITY,SET.SWEEPSPEED,SET.DELAY)
96 IF PCIB.ERR<>0 THEN ERROR PCIB.BASERR
97 CALL I.V(I,SET.TRIG.SOURCE,SET.TRIG.SLOPE,SET.TRIG.LEVEL,SET.TRIG.MODE)
98 IF PCIB.ERR<>0 THEN ERROR PCIB.BASERR
99 CALL I.V(I,GET.SINGLE.WF,GET.TWO.WF,GET.VERT.INFO,GET.TIMEBASE.INFO)
100 IF PCIB.ERR<>0 THEN ERROR PCIB.BASERR
101 CALL I.V(I,GET.TRIG.INFO,CALC.WFVOLT,CALC.WFTIME,CALC.WF.STATS)
102 IF PCIB.ERR<>0 THEN ERROR PCIB.BASERR
103 CALL I.V(I,CALC.RISETIME,CALC.FALLTIME,CALC.PERIOD,CALC.FREQUENCY)
104 IF PCIB.ERR<>0 THEN ERROR PCIB.BASERR
105 CALL I.V(I,CALC.PLUSWIDTH,CALC.MINUSWIDTH,CALC.OVERSHOOT,CALC.PRESHOOT)

```

```

106 IF PCIB.ERR<>0 THEN ERROR PCIB.BASERR
107 CALL I.V(I,CALC.PK.TO.PK.SET.TIMEOUT,SCOPE.START,MEASURE.SINGLE.WF)
108 IF PCIB.ERR<>0 THEN ERROR PCIB.BASERR
109 CALL I.V(I,MEASURE.TWO.WF,J,J)
110 IF PCIB.ERR<>0 THEN ERROR PCIB.BASERR
111 CALL I.C(I,R10NANO,R100NANO,R1MICRO,R10MICRO)
112 IF PCIB.ERR<>0 THEN ERROR PCIB.BASERR
113 CALL I.C(I,R100MICRO,R1MILLI,R10MILLI,R100MILLI)
114 IF PCIB.ERR<>0 THEN ERROR PCIB.BASERR
115 CALL I.C(I,R1,R10,R20NANO,R200NANO)
116 IF PCIB.ERR<>0 THEN ERROR PCIB.BASERR
117 CALL I.C(I,R2MICRO,R20MICRO,R200MICRO,R2MILLI)
118 IF PCIB.ERR<>0 THEN ERROR PCIB.BASERR
119 CALL I.C(I,R20MILLI,R200MILLI,R2,R20)
120 IF PCIB.ERR<>0 THEN ERROR PCIB.BASERR
121 CALL I.C(I,R50NANO,R500NANO,R5MICRO,R50MICRO)
122 IF PCIB.ERR<>0 THEN ERROR PCIB.BASERR
123 CALL I.C(I,R500MICRO,R5MILLI,R50MILLI,R500MILLI)
124 IF PCIB.ERR<>0 THEN ERROR PCIB.BASERR
125 CALL I.C(I,R5,R50,CHAN.A,CHAN.B)
126 IF PCIB.ERR<>0 THEN ERROR PCIB.BASERR
127 CALL I.C(I,EXTERNAL,POSITIVE,NEGATIVE,AC)
128 IF PCIB.ERR<>0 THEN ERROR PCIB.BASERR
129 CALL I.C(I,DC,TRIGGERED,AUTO.TRIG,AUTO.LEVEL)
130 IF PCIB.ERR<>0 THEN ERROR PCIB.BASERR
131 CALL I.C(I,X1,X10,STANDARD,AVERAGE)
132 IF PCIB.ERR<>0 THEN ERROR PCIB.BASERR
133 I=8
134 CALL I.V(I,OPEN.CHANNEL,CLOSE.CHANNEL,J,J)
135 IF PCIB.ERR<>0 THEN ERROR PCIB.BASERR
136 CALL C.S
137 IF PCIB.ERR<>0 THEN ERROR PCIB.BASERR
138 IS=PCIB.DIR5+"PCIB.PLD"
139 CALL L.P(IS)
140 IF PCIB.ERR<>0 THEN ERROR PCIB.BASERR
141 IS="DMM.01":I=3:J=0:K=0:L=1
142 CALL DEFINE(DMM.01,IS,I,J,K,L)
143 IF PCIB.ERR<>0 THEN ERROR PCIB.BASERR
144 IS="FUNC.GEN.01":I=6:J=0:K=1:L=1
145 CALL DEFINE(FUNC.GEN.01,IS,I,J,K,L)
146 IF PCIB.ERR<>0 THEN ERROR PCIB.BASERR
147 IS="SCOPE.01":I=7:J=0:K=2:L=1
148 CALL DEFINE(SCOPE.01,IS,I,J,K,L)
149 IF PCIB.ERR<>0 THEN ERROR PCIB.BASERR
150 IS="COUNTER.01":I=1:J=0:K=3:L=1
151 CALL DEFINE(COUNTER.01,IS,I,J,K,L)
152 IF PCIB.ERR<>0 THEN ERROR PCIB.BASERR
153 IS="DIG.IN.01":I=4:J=0:K=4:L=1
154 CALL DEFINE(DIG.IN.01,IS,I,J,K,L)
155 IF PCIB.ERR<>0 THEN ERROR PCIB.BASERR
156 IS="DIG.OUT.01":I=4:J=1:K=4:L=1
157 CALL DEFINE(DIG.OUT.01,IS,I,J,K,L)
158 IF PCIB.ERR<>0 THEN ERROR PCIB.BASERR
159 IS="RELAY.ACT.01":I=8:J=0:K=5:L=1
160 CALL DEFINE(RELAY.ACT.01,IS,I,J,K,L)

```



```

161 IF PCIB.ERR<>0 THEN ERROR PCIB.BASERR
162 IS="RELAY.MUX.01":I=2:J=0:K=6:L=1
163 CALL DEFINE(RELAY.MUX.01,IS,I,J,K,L)
164 IF PCIB.ERR<>0 THEN ERROR PCIB.BASERR
800 IS=ENVIRONS("PANELS")+ "\PANELS.EXE"
801 CALL L.S(IS)
899 GOTO 2
900 IF ERR=PCIB.BASERR THEN GOTO 903
901 PRINT "BASIC ERROR #";ERR;" OCCURRED IN LINE ";ERL
902 STOP
903 TMPERR=PCIB.ERR:IF TMPERR=0 THEN TMPERR=PCIB.GLBERR
904 PRINT "PC INSTRUMENT ERROR #";TMPERR;" DETECTED AT LINE ";ERL
905 PRINT "ERROR: ";PCIB.ERRS
906 IF LEFTS(PCIB.NAMES,1)<>CHRS(32) THEN PRINT "INSTRUMENT: ";PCIB.NAMES
907 STOP
908 COMMON PCIB.DIRS,PCIB.SEG
909 COMMON LD.FILE,GET.MEM,PANELS,DEF.ERR
910 COMMON PCIB.BASERR,PCIB.ERR,PCIB.ERRS,PCIB.NAMES,PCIB.GLBERR
911 COMMON READ.REGISTER,READ.SELFID,DEFINE,INITIALIZE.SYSTEM,
    ENABLE.SYSTEM,DISABLE.SYSTEM,INITIALIZE.POWER.ON,MEASURE,OUTPUT,
    START,HALT,ENABLE.INT.TRIGGER,DISABLE.INT.TRIGGER,ENABLE.OUTPUT,
    DISABLE.OUTPUT,CHECK.DONE,GET.STATUS
912 COMMON SET.FUNCTION,SET.RANGE,SET.MODE,WRITE.CAL,READ.CAL,
    STORE.CAL,DELAY,SAVE.SYSTEM,SET.GATETIME,SET.SAMPLES,SET.SLOPE,
    SET.SOURCE,ZERO.OHMS,SET.SPEED,SET.COMPLEMENT,SET.DRIVER,
    OUTPUT.NO.WAIT,ENABLE.HANDSHAKE,DISABLE.HANDSHAKE
913 COMMON SET.THRESHOLD,SET.START.BIT,SET.NUM.BITS,SET.LOGIC.SENSE,
    SET.FREQUENCY,SET.AMPLITUDE,SET.OFFSET,SET.SYMMETRY,
    SET.BURST.COUNT,AUTOSCALE,CALIBRATE,SET.SENSITIVITY,
    SET.VERT.OFFSET,SET.COUPLING,SET.POLARITY,SET.SWEEPSPEED
914 COMMON SET.DELAY,SET.TRIG.SOURCE,SET.TRIG.SLOPE,SET.TRIG.LEVEL,
    SET.TRIG.MODE,GET.SINGLE.WF,GET.TWO.WF,GET.VERT.INFO,
    GET.TIMEBASE.INFO,GET.TRIG.INFO,CALC.WFVOLT,CALC.WFTIME,
    CALC.WF.STATS,CALC.RISETIME,CALC.FALLTIME,CALC.PERIOD
915 COMMON CALC.FREQUENCY,CALC.PLUSWIDTH,CALC.MINUSWIDTH,
    CALC.OVERSHOOT,CALC.PRESHOOT,CALC.PK.TO.PK,SET.TIMEOUT,
    SCOPE.START,MEASURE.SINGLE.WF,MEASURE.TWO.WF,OPEN.CHANNEL,
    CLOSE.CHANNEL
916 COMMON FREQUENCY,AUTO.FREQ,PERIOD,AUTO.PER.INTERVAL,RATIO,
    TOTALIZE,R100MILLI,R1,R10,R100,R1KILO,R10MEGA,R100MEGA,CHAN.A,
    CHAN.B,POSITIVE,NEGATIVE,COMN,SEPARATE,DCVOLTS,ACVOLTS,OHMS,
    R200MILLI,R2,R20,R200,R2KILO,R20KILO,R200KILO
917 COMMON R2MEGA,R20MEGA,AUTOM,R2.5,R12.5,POSITIVE,NEGATIVE,TWOS,
    UNSIGNED,OC,TTL,R0,R1,R2,R3,R4,R5,R6,R7,R8,R9,R10,R11,R12,R13,R14,R15,
    R16,SINE,SQUARE,TRIANGLE,CONTINUOUS,GATED,BURST,R10NANO,
    R100NANO,R1MICRO,R10MICRO,R100MICRO
918 COMMON R1MILLI,R10MILLI,R100MILLI,R1,R10,R20NANO,R200NANO,R2MICRO,
    R20MICRO,R200MICRO,R2MILLI,R20MILLI,R200MILLI,R2,R20,R50NANO,
    R500NANO,R5MICRO,R50MICRO,R500MICRO,R5MILLI,R50MILLI,R500MILLI,R5,
    R50,CHAN.A,CHAN.B,EXTERNAL,POSITIVE
919 COMMON NEGATIVE,AC,DC,TRIGGERED,AUTO.TRIG,AUTO.LEVEL,X1,X10,
    STANDARD,AVERAGE
920 COMMON DMM.01,FUNC.GEN.01,SCOPE.01,COUNTER.01,DIG.IN.01,DIG.OUT.01,
    RELAY.ACT.01,RELAY.MUX.01
999 END PCIB PROGRAM SHELL

```

```

1000 REM THIS STEP INITIALIZES THE HP SYSTEM
1010 REM THIS STEP INITIALIZES THE HP SYSTEM
1020 CLS
1030 OPTION BASE 1
1040 DIM P(10),PA(50,6),PP(50,6),XPT(40),CAL(40)
1050 CALL INITIALIZE.SYSTEM(PGMSHEL.HPC)
1060 REM
1070 REM ALL PC DEVICES NOW HAVE AN INITIAL STATE
1080 REM SET FUNCTION ON THE DMM AND RELAY MUX
1090 REM
1100 CALL SET.FUNCTION(DMM.01,DCVOLTS)
1110 CALL SET.RANGE(DMM.01,AUTOM)
1120 CALL DISABLE.INT.TRIGGER(DMM.01)
1130 CALL ENABLE.OUTPUT(RELAY.MUX.01)
1140 FORMATS="## ##.#### ##.#### ##.#### ##.#### ##.#### ##.####"
1200 FOR I=1 TO 10
1210 CAL(I)=0.0
1220 NEXT I
1510 REM
1520 REM READ THE VOLTAGE OF 48TH CHANNEL AND DISPLAY THE DATA
1530 REM
1540 PRINT " CHOOSE 6 POINTS"
1550 PRINT
1550 PRINT "THE CALIBRATION WILL BE STORES IN 'CAL.DAT'"
1560 REM
1570 REM BEGIN SAMPLING LOOP
1580 REM
1600 FOR J=1 TO 1
1610 PRINT
1630 FOR JJ=1 TO 6
1631 INPUT "INPUT THE CALIBRATION PRESSURE";CAL(JJ)
1632 INPUT "PRESS 'ENTER' TO START MEASUREMENT";MOVES
1640 FOR II=1 TO 10
1650 ROUT=1
1660 CALL OUTPUT(RELAY.MUX.01,ROUT)
1670 CALL MEASURE(DMM.01,VOLTS)
1680 PA(II,JJ)=VOLTS
1690 NEXT II
1700 IF JJ=6 THEN 1740
1730 NEXT JJ
1740 REM
1750 REM DISPLAY THE SAMPLE DATA
1760 REM
1780 FOR IS= 1 TO 10
1790 PRINT USING FORMATS;IS,PA(IS,1),PA(IS,2),PA(IS,3),PA(IS,4),PA(IS,5),PA(IS,6)
1800 NEXT IS
1810 REM
1820 REM AVERAGE THE DATA
1830 REM
1840 FOR JA = 1 TO 6
1850 TOTAL = 0
1860 FOR IA = 1 TO 10
1870 TOTAL = TOTAL + PA(IA,JA)
1880 NEXT IA
1890 AVERAGE = TOTAL /10

```

```
1900 P(JA)=AVERAGE
1920 NEXT JA
1930 PRINT
1940 PRINT "THE AVERAGE ARE: "
2000 FOR JD=1 TO 6
2010 PP(J,JD)=P(JD)
2020 NEXT JD
2055 PRINT USING FORMATS;J,PP(J,1),PP(J,2),PP(J,3),PP(J,4),PP(J,5),PP(J,6)
2070 PRINT
2080 INPUT "DO YOU WANT RE-MEASURE AGAIN ? (Y / N)";CS
2090 IF CS="Y" THEN 1580
2101 REM*** STORE DATA BEFORE NEXT SAMPLE***
2102 OPEN "A:\CAL.DAT" FOR OUTPUT AS #2
2106 FOR ID=1 TO 6
2107 PRINT #2,USING FORMATS;ID,PP(J,ID),CAL(ID)
2108 NEXT ID
2109 CLOSE #2
2210 NEXT J
```

APPENDIX C. CONVERT PROGRAM

```
*****
THIS PROGRAM CONVERTS THE VOLTAGE OF TRANSDUCER INTO PHYSICAL
PRESSURE, VELOCITY, YAW ANGLE, PITCH ANGLE, TOTAL PRESSURE, TOTAL PRESSURE
COEFFICIENT, STATIC PRESSURE AND STATIC PRESSURE COEFFICIENT. THOSE DATA ARE
USED TO PLOT VELOCITY MAPPING AND PRESSURE CONTOUR.
*****
```

```
CHARACTER*12 FNAME
CHARACTER*12 NAME
CHARACTER*2 A(13)
CHARACTER*80 ST
REAL LO, PI, PF, TI, TF, K, E
DATA A/'01','02','03','04','05','06','07','08','09',
*      '10','11','12','13'/
NAME='R0B1A100.DAT'
* CONVERT THE PRESSURE UNIT FROM INHG TO PSF
  PI=29.81
  PF=29.89
  PATM=(PI+PF)*2.54*27.845/2.
  K=0.889
  E=0.0123
  R=1718
  TI=62
  TF=68
  T=(TI+TF)/2.+460
  LO=PATM/(R*T)
* OPEN A NEW FILE TO STORE THE REDUCED DATA
  OPEN(2, FILE='RESULT0.DAT', STATUS='NEW')
* OPEN A SEQUENTIAL OF DATA FILE
  DO 20 I=1,13
    NAME(7:8)=A(I)
    FNAME=NAME
    OPEN(1, FILE=FNAME)
    READ(1,100)ST
100  FORMAT(A65)
15  READ(1,1000,END=30)NO,X,Y,V1,V2,V3,V4,V5,BETA
1000 FORMAT(I2,F7.2,F6.2,5F9.3,F8.2)
* CONVERT THE VOLTAGE TO PRESSURE IN LBF/FT**2
  P1=DELTAP(V1)*2.0475+PATM
  P2=DELTAP(V2)*2.0475+PATM
  P3=DELTAP(V3)*2.0475+PATM
  P4=DELTAP(V4)*2.0475+PATM
  P5=DELTAP(V5)*2.0475+PATM
* CALCULATE THE PITCH ANGLE IN DEGREE
  P=(P4-P5)/(P1-P2)
  ALPHA=FPITCH(P)
* CALCULATE THE VELOCITY IN FT/SEC
  YSLOP=FYSLOP(ALPHA)
  VELM=SQRT((2*YSLOP*(P1-P2))/(LO*K))
  VEL=VELM*(1+E)
* CALCULATE THE FREE STREAM AND LOCAL DYNAMIC PRESSURE
```

```

      QM1=7.2*2.0475/K
      QM=LO*VEL**2/2.
      Q1=QM1*(1+2*E)
      Q=QM*(1+2*E)
*   CALCULATE THE YAW ANGLE IN DEGREE
      YAW=FYAW(BETA)
*   CALCULATE THE LOCAL TOTAL PRESSURE COEFFICIENT
      PTC=FPT(ALPHA)
      PT1=P1-Q*PTC
      PT=PT1/144
      CPT=(PT1-PATM-Q1)/Q1
*   CALCULATE THE LOCAL STATIC PRESSURE COEFFICIENT
      PS1=PT1-Q
      PS=PS1/144
      CPS=(PS1-PATM)/Q1
      WRITE(2,2000)NO,X,Y,VEL,YAW,ALPHA,PT,CPT,PS,CPS
2000  FORMAT(I5,9F10.3)
      GO TO 15
30   CLOSE(1)
20   CONTINUE
      CLOSE(2)
      STOP
      END
*****
* THIS FUNCTION CONVERT THE VOLTAGE TO PHYSICAL PRESSURE
      FUNCTION DELTAP(X)
      REAL DELTAP,X
      DELTAP=0.0214+4.2321*X
      END
*****
* THIS FUNCTION CALCULATES THE PITCH ANGLE
      FUNCTION FPITCH(X)
      REAL FPITCH,X
      FPITCH=3.759+53.7568*X-1.3085*X**2-1.6583*X**3
      *   -0.8061*X**4+16.5115*X**5
      END
*****
* THIS FUNCTION CALCULATES THE VELOCITY PRESSURE COEFFICIENT
      FUNCTION FYSLOP(X)
      REAL FYSLOP,X
      IF(X.LT.-10)THEN
        FYSLOP=0.981-0.0102*X-3.000E-4*X**2-2.500E-6*X**3
      ELSE IF((X.GE.-10).AND.(X.LE.10))THEN
        FYSLOP=0.98-0.006*X+2.000E-4*X**2
      ELSE
        FYSLOP=0.9801-0.0035*X-1.143E-4*X**2+5.833E-6*X**3
      END IF
      END
*****
* THIS FUNCTION CALCULATES THE YAW ANGLE
      FUNCTION FYAW(X)
      REAL FYAW,X
      IF((X.GE.0).AND.(X.LE.180)) THEN
        FYAW=-X
      ELSE

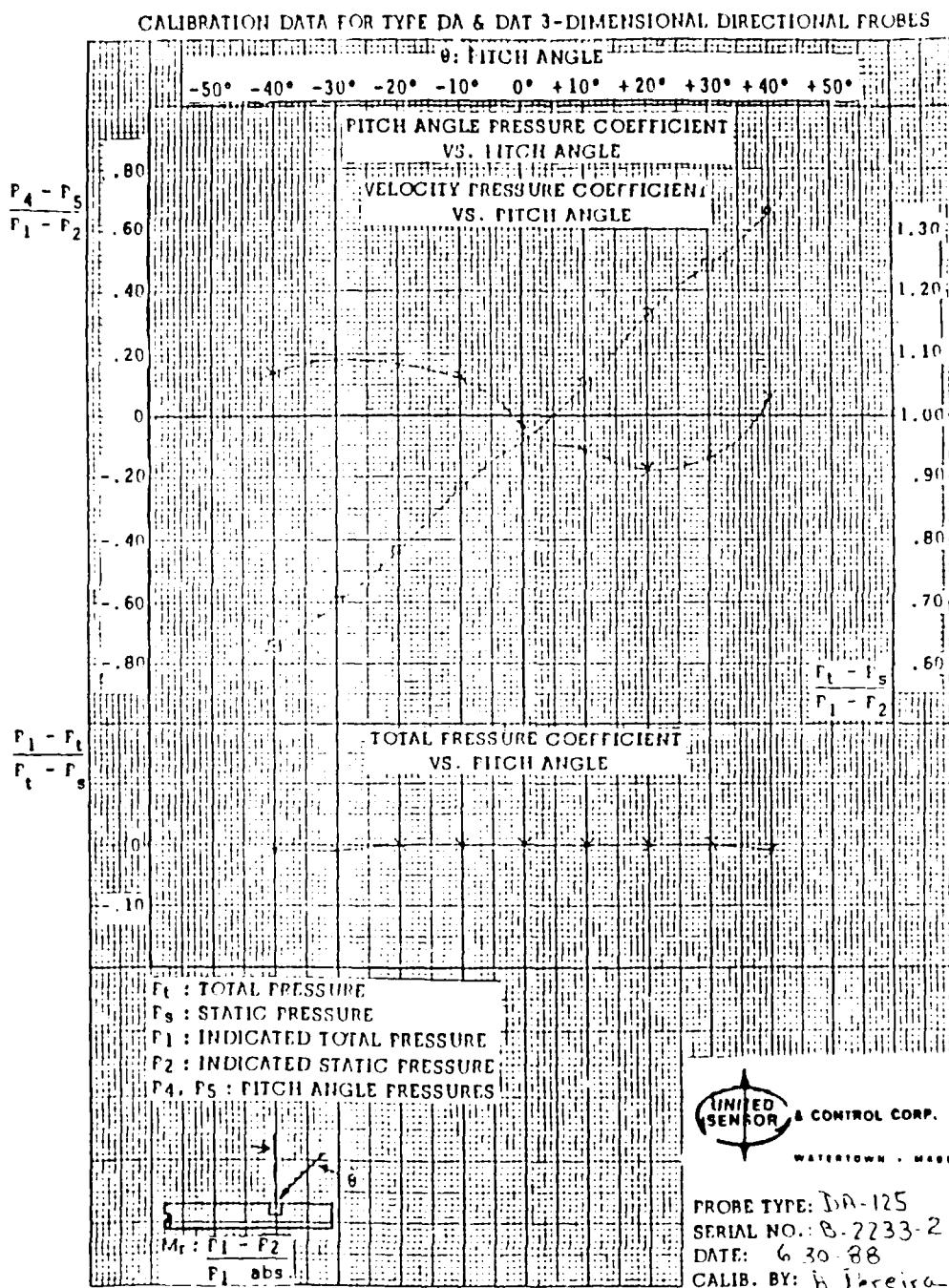
```

```

      FYAW=360-X
    END IF
  END
*****
* THIS FUNCTION CALCULATES THE TOTAL PRESSURE COEFFICIENT
  FUNCTION FPT(X)
    REAL FPT,X
    IF(X.LE.-30) THEN
      FPT=-0.01
    ELSE IF((X.GT.-30).AND.(X.LT.-20)) THEN
      FPT=0.02+1.00E-3*X
    ELSE IF((X.GE.-20).AND.(X.LE.30)) THEN
      FPT=0
    ELSE
      FPT=0.03-1.00E-3*X
    END IF
  END

```

APPENDIX D. PRESSURE PROBE CALIBRATION CHART



APPENDIX E. REVX PROGRAM

```
* OPEN A OLD FILE TO REVERSE THE X COORDINATE
  INTEGER A(300)
  REAL B(300),C(300),D(300),TEMP(500)
  REAL E(300),F(300),G(300),H(300),P(300),Q(300)
  OPEN(1,FILE='RESULT0.DAT')
  OPEN(2,FILE='P1.DAT',STATUS='NEW')
  DO 40 K=1,299
    READ(1,1000) NO,X,Y,VEL,YAW,ALPHA,PT,CPT,PS,CPS
1000  FORMAT(15,9F10.3)
    A(K)=NO
    B(K)=X
    C(K)=Y
    D(K)=VEL
    E(K)=YAW
    F(K)=ALPHA
    G(K)=PT
    H(K)=CPT
    P(K)=PS
    Q(K)=CPS
  40  CONTINUE
    CLOSE(1)
    N=299
    ICOUNT=N
    DO 10 I=1,N
      TEMP(I)=B(ICOUNT)
      ICOUNT=ICOUNT-1
  10  CONTINUE
    DO 20 I=1,N
      B(I)=TEMP(I)
  20  CONTINUE
    DO 50 J=1,N
      WRITE(2,2000) J,B(J),C(J),D(J),E(J),F(J),H(J),Q(J)
2000  FORMAT(15,7F10.3)
  50  CONTINUE
    CLOSE(2)
  END
```


APPENDIX F. XPLANE PROGRAM

```

CHARACTER*14 FNAME
REAL Y(500),Z(500),YN(500),ZN(500),V(500),VXP(500),
      BETA(500),ALPHA(500),VX1(500),VY(500),VZ(500)

C
  PI = 4.*ATAN(1.)
  WRITE(*, '(A)') ' INPUT DATA FILE? (D:FILENAME.EXT): '
  READ(*, '(A14)') FNAME
  OPEN(5, FILE=FNAME, STATUS='OLD')
  WRITE(*, '(A)') ' OUTPUT FILE NAME? (D:FILENAME.EXT): '
  READ(*, '(A14)') FNAME
  OPEN(6, FILE=FNAME, STATUS='NEW')

C
  READ(5, 100) NDATA
  VXMAX = 0.0

C
  DO 500 I=1, NDATA
    READ(5, 101) I, Y(I), Z(I), V(I), BETA(I), ALPHA(I)
C----- FIND CROSSPLANE VELOCITY COMPONENT, VXP
C----- CONVERT DEGREES TO RADIANS
    BETA(I) = BETA(I)*PI/180.
    ALPHA(I) = ALPHA(I)*PI/180.
    SB = SIN(BETA(I))
    SA = SIN(ALPHA(I))
    VZ(I) = V(I)*SA
    VY(I) = SQRT(V(I)**2 - VZ(I)**2)*SB
    VX1(I) = SQRT(VY(I)**2 + VZ(I)**2)
    VXP(I) = VX1(I)
C----- FIND THE LARGEST CROSSPLANE VELOCITY COMPONENT
    IF(VXP(I).GT.VXMAX) VXMAX = VXP(I)
  500 CONTINUE

C
C----- NORMALIZE CROSSPLANE COMPONENTS TO A MAXIMUM VALUE OF 1
  DO 510 I=1, NDATA
    VXP(I) = VXP(I)/VXMAX
  510 CONTINUE

C
C----- NORMALIZE CROSSPLANE VELOCITY TO A SPECIFIED FRACTION OF ONE
C----- GRID STEP FOR PLOTTING. ASSUME CONSTANT SIZE STEP.
C
  WRITE(*, '(A)') ' WHAT IS THE PROBE GRID STEP SIZE (IN.): '
  READ(*, *) STEP
  WRITE(*, '(A)') ' WHAT FRACTION OF GRID STEP IS MAX VELOCITY FOR '
  WRITE(*, '(A)') ' PLOTTING? (LIKE 0.5, ETC.): '
  READ(*, *) FRAC
  DO 520 I=1, NDATA
    VXP(I) = FRAC*STEP*VXP(I)
  520 CONTINUE
C----- DIVIDE PLOTTING VELOCITY INTO COMPONENTS FOR COORDINATES
  DO 530 I=1, NDATA
    YN(I) = Y(I) + VY(I)/VX1(I)*VXP(I)

```

```

      ZN(I) = Z(I)+VZ(I)/VX1(I)*VXP(I)
530 CONTINUE
C----- STORE OUTPUT FOR PLOTTING BY "ARROW"
      WRITE(6,100)NDATA
      DO 540 I=1,NDATA
      WRITE(6,101)I,Y(I),Z(I),YN(I),ZN(I)
540 CONTINUE
100 FORMAT(I5)
101 FORMAT(I5,5F10.3)
      CLOSE(5)
      CLOSE(6)
      STOP
      END

```

APPENDIX G. ARROW PROGRAM

```

C*****
C
C  THIS PROGRAM PLOTS DATA IN THE FORM OF VELOCITY VECTORS.
C  INPUT Y-Z POSITION, VELOCITIES, AND YAW AND PITCH ANGLES.
C
C*****
C  CHARACTER*14 NAME,FNAME
C----- SF IS THE PHYSICAL SCALE FACTOR BETWEEN DATA AND PAPER.
C----- 0.025 MM = ONE PLOTTER UNIT.
C  WRITE(*, '(A)') 'THE SCALE FACTOR SCALES THE PHYSICAL DIMENSIONS'
C  WRITE(*, '(A)') 'TO FIT THE PAGE.'
C  WRITE(*, '(A)') 'DESIRED SCALE FACTOR? (FOR EXAMPLE, 0.5): '
C  READ(*, *) SF
C  FACT = 25.4 * SF / 0.025
C  WRITE (*,60)
60  FORMAT (' ARROW HEAD LENGTH = ? (0.075 IS A TYPICAL VALUE)')
C  READ (*, *) HEAD
C  HEAD = 25.4 * HEAD / 0.025
C  WRITE (*,70)
70  FORMAT (' ARROW HEAD WEDGE ANGLE = ? (30 DEG IS TYPICAL)')
C  PI = 4.0 * ATAN(1.0)
C  READ (*, *) ANGLE
C  ANGLE = ANGLE * PI / 180.0
C----- "YREF,ZREF" IS THE INITIAL (REFERENCE) POINT RELATIVE TO WHICH
C----- ALL DATA ARE PLOTTED. (0,0) IS ASSUMED.
C  WRITE(*, '(A)') 'COORDINATES ARE ASSUMED TO BEGIN WITH 0,0 IN THE'
C  WRITE(*, '(A)') 'FAR LOWER LEFT CORNER. IF THIS OK, TYPE 1. IF'
C  WRITE(*, '(A)') 'AN OFFSET IS DESIRED, TYPE 0: '
C  READ(*, *) NCOORD
C  IF(NCOORD.EQ.1) GO TO 150
C  WRITE(*, '(A)') 'DESIRED SHIFTED ZERO REFERENCE? (IE, -2.,-2.): '
C  READ (*, *) YREF,ZREF
C  GO TO 151
150 YREF = 0.0
C  ZREF = 0.0
151 CONTINUE
C  WRITE (*,200)
C200 FORMAT (' OUTPUT DATA FILE?: ')
C  READ (*, *) NAME
C  CALL ZINIT (IPLOT,IPORT,NAME)
C  NAME = 'B:PLOT.DAT'
C  CALL ZINIT (1,1,NAME)
C  CALL ZVS(12.0)
300 WRITE (*, '(A)') 'INPUT DATA FILE? (D:FILENAME.EXT): '
C  READ (*, '(A14)') FNAME
C  OPEN (5,FILE=FNAME,STATUS='OLD')
C
C  THIS IS THE PROGRAM PROPER
C
C  READ(5,102) NDATA

```

```

DO 400 I = 1, NDATA
  READ (5,102) I, Y, Z, YN, ZN
102 FORMAT(15,4F10.0)
C
C   THIS SECTION PLOTS THE TAIL OF THE ARROW (PEN UP)
  CALL ZPU
  IX = NINT((Y + YREF) * FACT)
  IY = NINT((Z + ZREF) * FACT)
  CALL ZPA (IX,IY)
C   THIS SECTION PLOTS THE SHAFT OF THE ARROW (PEN DOWN)
  CALL ZPD
  IX = NINT((YN + YREF) * FACT)
  IY = NINT((ZN + ZREF) * FACT)
  CALL ZPA (IX,IY)
C   THIS SECTION PLOTS THE HEAD OF THE ARROW
  CALL ZPD
  IF (ABS(YN - Y).GT.0.0001) GO TO 250
  ALPHA = -PI/2.
  IF (ZN.GT.Z) ALPHA = PI/2.
  GO TO 251
250 ALPHA = ATAN( (ZN - Z)/(YN - Y) )
251 IF ( (YN - Y).GE.0.0 ) THEN
  IXU = IX - NINT(HEAD * COS(ALPHA - ANGLE))
  IYU = IY - NINT(HEAD * SIN(ALPHA - ANGLE))
  ELSE
  IXU = IX + NINT(HEAD * COS(ALPHA - ANGLE))
  IYU = IY + NINT(HEAD * SIN(ALPHA - ANGLE))
  ENDIF
  CALL ZPA (IXU,IYU)
C   -----
  CALL ZPU
  CALL ZPA (IX,IY)
  CALL ZPD
  IF ( (YN - Y).GE.0.0 ) THEN
  IXU = IX - NINT(HEAD * COS(ALPHA + ANGLE))
  IYU = IY - NINT(HEAD * SIN(ALPHA + ANGLE))
  ELSE
  IXU = IX + NINT(HEAD * COS(ALPHA + ANGLE))
  IYU = IY + NINT(HEAD * SIN(ALPHA + ANGLE))
  ENDIF
  CALL ZPA (IXU,IYU)
C
400 CONTINUE
C----- CLOSE UP SHOP
  CALL ZPU
  CALL ZFINIS
  CLOSE (5)
  STOP
  END

```

APPENDIX H. RUN MATRIX

		Test Run	Grid #0	Grid #1
1	Date	Nov. 18, 1988	Nov. 25, 1988	Nov. 26, 1988
2	Start/End Time	1526/2148	0830/1821	0143/1115
3	T_{wi}/T_{wf}	62/66	62/68	62/78
4	p_o (in Hg)	30.14/30.19	29.81/29.89	29.97/30.06
5	PH_2O (cm)	7.2	7.2	10
6	Grid #	0	0	1
7	Missile configuration	B	B	B
8	AoA	50°	50°	50°
9	Measured dimension	6.5"x8"	3"x5.5"	3"x5.5"
10	Step distance	0.5"	0.25"	0.25"
11	Data file name	R0B1B201.DAT to R0B1B214.DAT	R0B1A101.DAT to R0B1A113.DAT	R1B1A101.DAT to R1B1A113.DAT
12	Calibration file name	CALDATT1.DAT CALDATT2.DAT	CAL0B.DAT CAL0A.DAT	CAL1B.DAT CAL1A.DAT

INITIAL DISTRIBUTION LIST

	No. Copies
1. Defense Technical Information Center..... Cameron Station Alexandria, VA 22304-6145	2
2. Library, Code 0142..... Naval Postgraduate School Monterey, CA 93943-5002	2
3. Chairman, Code 67..... Department of Aeronautics and Astronautics Naval Postgraduate School Monterey, CA 93943	1
4. Commander..... Naval Weapons Center Code 406 China Lake, CA 93555	1
5. Commander..... Naval Surface Weapons Center Silver Spring, MD 20903-5000	1
6. NASA-Ames Research Center..... Technical Library Moffett Field, CA 93555	1
7. Commander..... Naval Surface Warfare Center Attn: G205 Dahlgren, VA 22448-5000	1
8. Commander..... Pacific Missile Test Center Point Mugu, CA 93041	1

9. Library of Chinese Naval Academy2
P.O. Box 8494 Tso-Ying,
Kaohsiung, Taiwan
Republic of China

10. Library of Chung-Cheng Institute of Technology.....2
Tashih, Tao-Yuan, Taiwan
Republic of China

11. Prof. R.M. Howard, Code 67HO7
Department of Aeronautics and Astronautics
Naval Postgraduate School
Monterey, CA 93943

12. LT. Lung, Ming-Hung2
No. 114-5 Chung-Ching Rd.
Taichung, Taiwan 400
Republic of China